Optical sum frequency spectroscopy and microscopy of flat and vicinal H-Si(111) surfaces

KHUAT THI THU HIEN

Japan Advanced Institute of Science and Technology

Optical sum frequency spectroscopy and microscopy of flat and vicinal H-Si(111) surfaces

By

KHUAT THI THU HIEN

Submitted to

Japan Advanced Institute of Science and Technology

In partial fulfillment of the requirements for the degree of Doctor of Philosophy

Supervisor: Professor Goro Mizutani

School of Materials Science

Japan Advanced Institute of Science and Technology

September 2013

ACKNOWLEDGEMENTS

It seems like yesterday when I started this adventure, which marks an important chapter in my life. While, I alone, initiated this journey, my successful completion is far from being my own accomplishment, but rather that of all the people that have assisted, encouraged and supported me along the way.

First and foremost, I would like to thank my thesis supervisor and committee chairman, Professor Goro Mizutani, who gave me the freedom and flexibility to be creative, in and outside of research, while also providing support as a great mental help. I am really honored to have been a member of his research group and to have worked with him. His advice and encouragement regarding this research are invaluable to me.

I would like to thank my internal committee members, Prof. Masahiko Tomitori, Prof. Mikio Koyano, Prof. Yukiko Yamada-Takamura from School of Materials Science, JAIST. My special thanks go to Prof. Tsuneo Yasue from Osaka Electro-Communication University as an external committee member. I thank all of them for their time and consideration in serving on my thesis committee.

My special thank goes to Assistant Prof. Yoshihiro Miyauchi for welcoming and mentoring me. It is a tremendous honor to work alongside such distinguished and dedicated scientist. Through the past five years including my master course, I have gone through twists and turns as well as faced trials and tribulations. I was fortunate to have met a wonderful senior that have listened, advised, tutored, supported and encouraged me. I would like to express my thanks to Prof. H. Sano, Prof. Tadaoki Mitani for their fruitful comments and discussion throughout this work.

I would like to give my thanks and appreciation to Prof. Nobuo Otsuka and Prof. Masahiko Tomitori who gave me many kind supports during my PhD course.

Many thanks go to my lab members, Mr. Takahashi, Mr. Hieu, Mr. Quang, Mr. Ono Ms. Li, Ms. Matsui, Ms. Siti…, and so on for their camaraderie throughout my graduate school experience, especially for all of the hours of fun we have shared. I also thank all of the Vietnamese students I had a wonderful time to work and play with while in JAIST. I cannot imagine a better group of friends with whom to have endured and challenges of the last 5 years; they have made the bad times better and the good time unforgettable. I will always

look back to my time in graduate school with fond memories because of them and to them I express my most sincere and heartfelt gratitude.

Finally, and most importantly, I express my deepest gratitude to my family for their undying love and encouragement. I especially thank my husband and my little daughter, for their support and trust that have given me great self-confidence. If not for their help, I would never have ended up at JAIST.

JAIST, August 2013

Khuat Thi Thu Hien

Abstract

Silicon wafer is one of the most important substrates for thin film fabrication which is employed for industrial applications such as biological sensor and solar cell. In order to grow a high quality thin film on the Si wafer, chemical vapor deposition (CVD) is an efficient method. Before loaded into a CVD chamber, the Si atoms are terminated by hydrogen (chemical treatment) to protect the surface from oxidization. In the CVD process, the qualities of the grown thin film layer on Si surfaces depend not only on the radical reaction in the vapor phase but also on an early reaction with the Si surface. Therefore, removal of the hydrogen layer from this Si surface is the central issue in the CVD growth.

In this study, I will investigate the hydrogen desorption from H-Si(111) 1x1 surfaces by performing sum frequency generation (SFG) spectroscopy and microscopy. SFG is a sensitive method for surface analysis. Furthermore, in the previous work of my group, hydrogen desorption on H-Si(111) surfaces irradiated by desorption-inducer IR light pulses was investigated by observing SFG intensity images. The interesting point which I stress here is the unidentified bonding state of H-Si bonds at a boundary between the areas with and without the irradiation. The dynamics of the electrons and phonons on the edges of the light pulse spot become complicated because the IR light pulse not only raises the surface temperature but also simultaneously excites the electron-hole (e-h) plasma. In order to clarify the dynamics at a particular part of this region, picosecond-order snapshots of the hydride on a Si surface have to be taken after the pump light irradiation. Therefore, the pump-probe technique must be applied to the SFG microscope. SFG is forbidden for centrosymmetric bulk. Thus, it is considered as a sensitive method for monolayer of adsorbate on the surface.

On the other hand, the unidentified bonding state of H-Si bonds at boundary is considered as due to a phase transition between the areas with and without the irradiation. Beside the disorder of molecular orientation of monohydride, the

dihydride maybe appeared in this boundary because of IR irradiation. Similarly to this model, a regular step Si(111) with 9.5^{o} miscut angle toward $[\bar{1}\bar{1}2]$ direction has dihydride on the step. Thus, observing SFG images of dihydride on step surfaces is comparable with SFG images of the boundary. However, in this study, I will terminate hydrogen on the regular step surface by dosing hydrogen molecules in a UHV chamber, and investigate the SFG vibrational spectra as the first step before observing SFG images. Furthermore, nowadays stepped Si(111) surfaces have been considered as natural templates for ordered growth of quantum dots and nanowires due to their active sites. Therefore, understanding of the behavior of steps is very important for these applications.

In this study, I constructed a pump-probe SFG microscopy system for the first time. By using this system, dynamics of H-Si species on flat H-Si(111)1x1 surfaces were investigated by observing the time-resolved *ppp*-SFG spectra and microscopic images in a UHV chamber. The SFG intensity images showed consistent results with the time resolved SFG spectroscopy. After visible pump light irradiation the non-resonant SFG signal increased, and then decreased with the life time of ~1 ns. Inversely, the resonant SFG signal decreased and then recovered in ~1 ns. The candidate origin of this change of the non-resonant SFG signal is suggested to be excitation and relaxation of e-h pairs after the pump light irradiation. Especially, at 930 ps after pump light irradiation, the Si-H peak had a remarkably asymmetric lineshape. The vibration of H-Si bonds could be modified by the pump light irradiation.

Also the reduction of hydrogen coverage of the H-Si(111)1x1 surface due to high surface temperatures was observed directly for the first time. I obtained isothermal desorption spectra of the H-Si(111) 1×1 surface at temperatures of ~711, 732, 752 and 771 K by probing directly the vibrationally resonant optical SFG spectra. The desorption order of hydrogen was consistent with the second order scheme. The dipole-dipole coupling among the H-Si bonds could be considered during the hydrogen

desorption process. I have calculated modulation of the Si-H vibrational mode on a Si(111) 1×1 surface by a partial absence of Si-H bonds using CPA method, and made a comparison between modulations in the experimental and theoretical SFG spectra of the surface. As the first time of discovery, a theoretical peak shift reproduced the experiment quantitatively, and thus the peak shift was due to the modulation of average polarizability of the Si-H oscillators via dipole coupling. On the other hand, inhomogeneous broadenings of the theoretical peaks in the SFG spectra at lower coverages were much larger than those of the calculated peaks. Thus, it should be explained by other origins than dipole coupling.

On the other hand, I also investigated the hydrogen desorption from regular step H-Si(111) surfaces with 9.5° miscut toward $[\bar{1}\bar{1}2]$ direction. The hydrogen was terminated on the regular Si(111) surface by dosing hydrogen molecules in the UHV chamber. When the visible and IR lights reach the surface in step up direction, the SFG signal is called the upstair SFG. Inversely, when they reach the surface in step down direction, the SFG signal is called the downstair SFG. After hydrogen termination process on the vicinal Si surface, the upstair and downstair SFG spectra with *ppp* and *ssp* polarization combination were taken. In all the cases, the terrace mode A (2082cm^{-1}), and step modes C_1 (2094 cm^{-1}) peaks were clearly observed, while step modes C_2 (2101 cm^{-1}) and C_3 (2134 cm^{-1}) were not. The A mode is readily attributed to the in-phase terrace vibration of the monohydride. From LEED patterns, about 5 ~ 7 steps were bunched when the Si surface was flashed at 1200 °C. Thus, the step C_2, C_3 modes cannot be detected on this surface because of the decrease in the step mode intensities.

The regular step H-Si(111)1x1 surface with 9.5° miscut toward $[\bar{1}\bar{1}2]$ direction was heated at several high temperatures, and time dependence of the upstair SFG spectra with *ppp* and *ssp* polarization combinations were observed. The peak intensity of both terrace and step modes was reduced when the heating time was increased, but the step mode reduction was faster. The reduction is the best fit with the 2nd order of hydrogen desorption. The step mode C_1 was shifted by ~2 cm^{-1}. I

suggest that it may be related to the dipole-dipole interaction among the H-Si species. However, the theoretical calculation is required to clarify this point.

In conclusion, the pump-probe SFG microscopy system was successfully constructed. It contributes to surface science as a new analysis systems, and opens new opportunity for directly observing two dimensional images of particular adsorbate species. Isothermal hydrogen desorption on flat Si(111) was investigated by observing the time-resolved SFG spectra and SFG intensity images. Understanding the effect of surface temperature and excited e-h pairs on behavior of H-Si bonds is very important for growth of organic and inorganic thin film which is utilized for silicon based devices. Isothermal hydrogen desorption on the step Si(111) was investigated for the first time by observing the time-resolved SFG spectra. It reveals the existence of a new configuration of step hydrogen orientation. Intensity transfers from the terrace peak to the step one and the step mode shifted to the lower frequency via dipole interaction effect. This study about hydrogen desorption on the step Si surface will contribute to fundamental science and open a new research topic.

Chapter 1 : Introduction and research motivation

1.1 Literature of hydrogenated silicon surfaces and research motivation.

Silicon was discovered by Berzelius in 1824 and isolated as amorphous brown powder. Crystalline silicon was first prepared in 1854 as a grey material with metallic luster. Normally, silicon is prepared by reduction of silica, using different reducing agents. Silicon has a crystal structure similar to diamond. Cleavage of a silicon crystal results in a large variety of surfaces. The surfaces are characterized by their Miller indices, which refer to the plane thorough which the crystal was originally cleaved. The most common Si surface orientations used for industry are Si(100), Si(110) and Si(111). Each orientation has its own advantage which depends on the tasks and applications. In this research, I am interested in a Si(111) surface because its surface structure is isotropic and uniform. Thus, it is the best substrate for new hybrid organic monolayer silicon devices [1, 2].

For example, chemical hydrogenated Si(111) surfaces are used as effective substrates of silicon-based bioelectrical sensors and devices [1, 2]. Ideal thin film platforms on silicon substrates should allow specific binding of biological targets. To block nonspecific binding, the silicon substrates are commonly modified with organosiloxane films presenting oligo- or poly(ethylene glycol) on the oxide surface of the substrates [3]. However, the protein resistance and stability of these films are not satisfactory, probably due to the relatively low packing density of the films and the high density of defects resulting from the interaction of silanols with the hydrophilic oligo ethylene glycol chains [3, 4]. Thus, non-oxidized silicon substrates via Si-C bonds was developed [3-5]. Formation of the Si-C bonds is via surface hydrosilylation on hydrogen-terminated silicon surfaces [6, 7]. Figure 1.1.1 shows an example of an organic monolayer growth on the H-Si surface [8]. On the other hand, Si(111) substrates are also

good substrates for depositing DNA [9]. The chemical and dipole interactions between the DNA and the reactive semiconductor substrate seem to play an important role in folding and pinning. M. Tomitori *et al.* [9] succeeded in depositing DNA on a Si(111) surface and these results can open a new biotechnology combined with reactive semiconductor surfaces to assemble biomolecules on the surface intentionally. Therefore, the performance and stability of H-Si bonds on the Si substrates are very important for quality of ultrathin organic films. In this research, I will concentrate on the study of dynamics of H-Si bonds on a H-Si(111) surface. Especially, hydrogen desorption due to laser light irradiation and due to high temperature will be investigated.

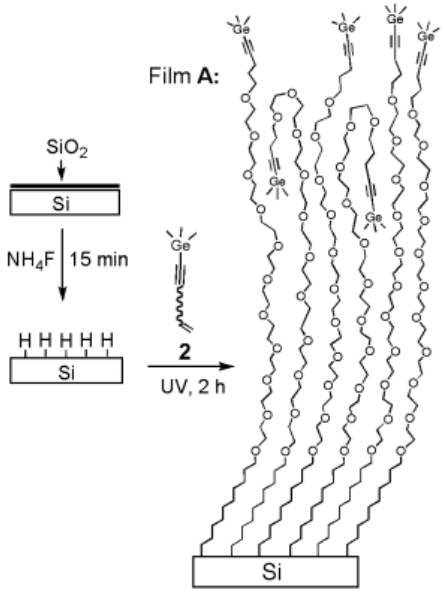

Fig. 1.1.1: An example of an organic monolayer growth on the H-Si surface [8]

In addition, chemical hydrogen termination on a Si surface is commonly used to protect the surface from oxidization before the CVD process. The hydrogen layer is

removed from this Si surface in the initial process of the CVD growth. Spatial uniformity of coverage and the orientation of H-Si bonds are important. Therefore, the hydrogen termination and desorption from Si surfaces should be understood well.

Recombinative hydrogen desorption processes from H-Si(100)3×1, H-Si(100)2×1, H-Si(111)7×7 surfaces have been vigorously studied by several techniques, including temperature programmed desorption (TPD) [10, 11], laser-induced thermal desorption (LITD) [12-15], scanning tunneling microscopy (STM) [16, 17], optical second harmonic generation (SHG) [18, 19] and Fourier transform infrared spectroscopy (FT-IR) [20, 21]. However, there is lack of reports about hydrogen desorption process from a H-Si(111)1×1 surface [22-29] and there are many retained problems. The process on the H-Si(111)1×1 surface is complicated, and still not well understood, since the termination itself influences the structure and the chemical reactions. Renzi and his colleagues studied the dynamics on a 1×1 surface by using low energy electron diffraction (LEED), ultra-violet photoemission spectroscopy (UPS), and high resolution electron energy loss spectroscopy (HREELS) [25]. Below 738 K, they found upward band bending due to the creation of a small number of dangling bonds but they observed no structural change from 1×1. When the temperature increased from 773 to 973 K all hydrogen was desorbed, and the surface began to reconstruct. Above 873 K, the band bending decreased, the 7×7 reconstruction became predominant, and an adatom state was progressively formed. Vinh et al., who used reflection high energy electron diffraction (RHEED) patterns, also observed no intrinsic structural change of the surface below 823 K [23]. These studies indicate the electronic and structural change via thermal hydrogen desorption. However, it is still unclear how the changes of the structure and the electronic states give feedback to the bonding states of the monohydride. On the other hand, Becker *et al.* [22] observed

scanning tunneling microscopy (STM) of a H-Si(111)1×1 surface after electron bombardment with an energy of 2~10 eV. The results are consistent with the typical complexity of the desorption process. Namely, the bombardment induced hydrogen atomic desorption, and then the resulting 1×1 structure changed into quasi-stable 2×1 due to the free energy of the dangling bonds created at the vacancy site. Hence the electron-stimulated desorption (ESD) directly broke the Si-H bonds. The direct breaking process induced the change of the electronic states and the surface reconstruction. Therefore, I will study the dynamics of H-Si bonds and how their effect on the surface structure by investigating isothermal hydrogen desorption from a H-Si(111)1×1 surface. In my study, I will terminate the Si(111)1x1 surface by hydrogen, and then observe the vibrational spectroscopy of H-Si bonds after heating the surface at high temperature.

In the hydrogen desorption process, the spatial distribution of the coverage and the orientation of the H-Si bonds on the Si surface are complicated and should be understood well. However, there are not so many reports on the spatial distribution of hydrogen coverage on a Si surface [30-32], and none concerning the spatial distribution of the orientation and vibrational mode of the H-Si bonds. As mentioned previously, some methods such as TPD, LITD, or FT-IR were used to study the hydrogen desorption on the Si surface. But those are almost indirect measurement so that they could not observe direct images of the Si surface during the desorption process. Therefore, the new techniques for directly monitoring a two-dimensional distribution image of hydrogen on a Si surface are required. In order to establish a technique for such observations, we have developed a visible–IR sum frequency generation (SFG) microscope operating in ultra-high vacuum (UHV) conditions. The SFG microscopy enables me to observe a resonant vibrational image on a Si(111) surface. It is expected to be useful for detecting

the spatial variation of the orientation and the vibrational mode of the Si–H bonds. The peak wavenumber of the SFG response reflects the species of the hydrides.

In summary, from these literature, I will concentrate on the study of dynamics of H-Si bonds on a H-Si(111) surface. Especially, hydrogen desorption due to laser light irradiation and due to high temperature will be investigated. I will also observe the two-dimensional images of a H-Si(111) surface by using the SFG microscope. The spatial variation of the orientation and the vibrational mode of the Si–H bonds will be understood. In the next section, I will introduce previous work of my group and I will explain more about my targets in this research.

1.2 Previous works and research motivation

1.2.1 SFG intensity images of a H-Si(111)1x1 surface after IR light pulse irradiation

In previous works, Miyauchi and his coworkers [33] have studied the hydrogen desorption on H-Si(111) surfaces irradiated by desorption-inducer IR light pulses. SFG intensity images of a H-Si(111) surface were observed directly by using a long distance microscope.

The H-Si(111) surface was prepared in a clean room by a few cycles of etching in a hot solution of 97%H_2SO_4:30%H_2O_2 = 4:1, then in hydrofluoric acid, and finally in NH_4F solutions. By this wet etching method, a monohydride terminated Si(111) surface with one monolayer was formed in well order [34]. After that, it was introduced immediately into an ultrahigh vacuum chamber (UHV) with the pressure of $5x10^{-8}$ Pa. Before irradiating the sample with IR light, a SFG intensity spectrum was taken and a sharp peak at 2080 cm^{-1} attributed to the stretching vibration of the monohydride species appeared. I note that Higashi and his coworkers performed and ATR-IR measurement of

a H-Si(111) surface (with a resolution of ~0.5 cm^{-1}), and determined that the peak at 2083.7 cm^{-1} was due to the Si-H stretching vibration [34]. The probe light in our work had bandwidth of ~6 cm^{-1}, so we could not measure peaks with resolution better than ~6 cm^{-1}. Within this spectral resolution, therefore, the peak observed at 2080 cm^{-1} in this work should be considered to have been caused by the same H-Si stretching vibration as that observed by Higashi *et al.* The Si surface was irradiated with desorption-inducer IR light pulses from a Nd^{+3}:YAG laser with some parameters such as: wavelength 1064 nm; pulse duration ~6 μs; repetition rate 10 Hz; pulse energy 6-12 mJ/pulse; focus size ~0.1 mm; total irradiation time for drawing a circle pattern ~32s; irradiating time/one point ~2s.

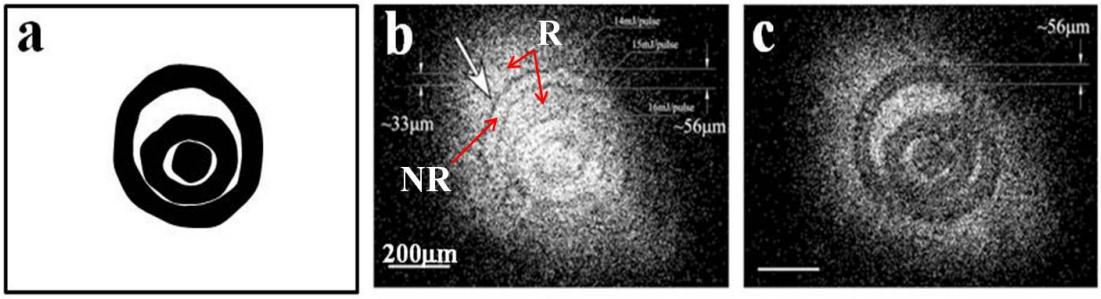

Fig. 1.2.1.1: SFG intensity images of a H-Si(111) surface after irradiation with IR light pulses inducing hydrogen desorption. (a) Dark circles schematically show the areas irradiated by the IR laser beam for desorption with the pulse energies indicated in the figure. (b) and (c) The SFG intensity images for the probe infrared wavenumber 2080 cm^{-1} 10 min and 22 h after the IR pulse irradiation for desorption, respectively. The white arrow in (b) shows the dark boundary area between the areas with resonant and non-resonant SFG signals.

The irradiated areas by IR light with different pulse energies were drawn in three concentric circular patterns, as they are shown schematically in Fig. 1.2.1.1(a). Each circular pattern was drawn in about 32s. Figure 1.2.1.1(b-c) show the SFG intensity images of the H-Si(111) surface after irradiation with IR light pulses inducing hydrogen desorption. White dots in the figure 1.2.1.1 (b) and (c) are the SFG photons. The

hydrogen desorption was expected to occur at the dark areas drawn in fig. 1.2.1.1(a), corresponding to non-resonant SFG area (NR) marked in fig. 1.2.1.1(b). The IR non-irradiated area corresponds to resonant SF area (R) marked in fig. 1.2.1.1(b). From an optical second harmonic (SHG) images under the same condition [33], it was found that the hydrogen desorption truly occurred in the dark circular areas in Fig. 1.2.1.1(a). Fig. 1.2.1.1 (b) and (c) show the SFG intensity images obtained 10 min and 22 hours after desorption, respectively, with the probe infrared wavenumber of 2080 cm^{-1} (a resonant wavenumber with the monohydride Si-H vibration mode). The NR area should be dark because of no H-Si bonds, however it was as bright as the R area. The discussion about these irradiated areas was briefly reported by Y. Miyauchi *et.al* [33, 35]. The interesting point which I stress here is the appearance of the dark boundary between the areas with and without the irradiation (corresponding to the areas with non-resonant and resonant SFG signals), as indicated by a white arrow in fig. 1.2.1.1(b). It could not be explained by the negative interference of the resonant vibrational SFG and non-resonant SFG signals. It was suggested that the low density of the surface dangling bonds maybe the reason for the weak non-resonant SFG signals at the boundary area [33]. However, this unidentified bonding state of H-Si bonds is still mysterious and not understood well. The dynamics of the electrons and phonons on the edges of the light pulse spot become complicated because the IR light pulse not only raises the surface temperature but also simultaneously excites the electron-hole (e-h) plasma. From these problems I will concentrate on two main topic in this study. The first topic is the effect of surface temperature on hydrogen desorption. The second topic is construction of new instrument for directly observing the ultrafast phenomenon caused by the e-h plasma state.

In detail, Fig. 1.2.1.2 represents the temperature change and the reduction of

hydrogen coverage induced by an IR light pulse with wavelength 1064 nm, pulse duration ~6 μs, power 10 mJ/pulse, and spot size 35.3 μm. The temperature increases to 1300 K just after the IR light pulse irradiation at 0 μs. This temperature is higher than the hydrogen desorption temperature of over ~ 800K [12] . Then it is gradually reduced to room temperature at 160 μs. On the other hand, the hydrogen coverage is clearly reduced corresponding to the rise of temperature. That means the hydrogen desorption can be induced by IR light pulse irradiation. In order to clarify the effect of the surface temperature on the dynamics of H-Si species, H-Si(111) surfaces will be heated at a high temperature for each few of tens seconds, and SFG spectra will be observed after each time of heating. In addition, hydrogen desorption has shown the complicated process studied by R. S. Becker *et.al* [22]. They demonstrated that the atomic hydrogen terminating the Si surface may be selectively removed by low-energy electron bombardment (2 ~ 10 eV) from the STM tip, with the resultant surface spontaneously converting from 1x1 to the 2x1 π-bonded chains due to the free energy of the dangling bonds created at the vacancy site. Therefore, hydrogen desorption on Si surfaces still retains many problems.

The e-h pair is excited by the IR light pulse with photon energy of 1.17 eV via indirect electron transition beyond the bandgap of silicon ~ 1.1 eV [36]. If a high density of e-h pairs is excited, the medium is in a plasma state called e-h plasma. In order to clarify the dynamics at a particular part of this region, picoseconds-order snapshots of the hydride on a Si surface have to be taken after the pump light irradiation. Therefore, I will construct the pump-probe SFG microscopy by applying the pump-probe technique into the SFG microscope system.

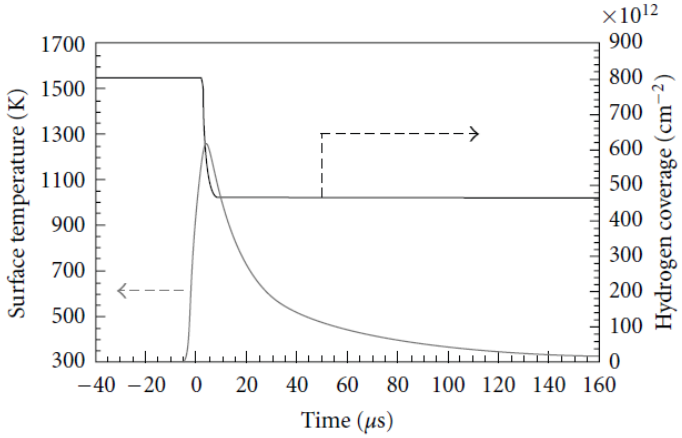

Fig. 1.2.1.2: The temperature change and the reduction of the hydrogen coverage after IR pulse irradiation with the pulse duration ~6 μs, wavelength 1064 nm.

1.2.2 Construction of pump-probe SFG microscopic system and its advantages

The ultrafast phenomenon occurs on picosecond, femtosecond and attosecond scales and gives information about transient changes within the electron, phonon and spin populations in materials. Ultrafast technology has been expected in applications such as biomedical imaging, chemical dynamics, frequency standards, and ultrahigh speed communications. However, monitoring these processes is not possible with any mechanical or electric equipment. Instead, pump and probe technique has been a powerful tool to do those for a long time in the past [37-40].

Pump and probe technique will be a much more powerful method if it can be combined with other equipments. In this work, I have constructed the pump-probe SFG microscopy and spectroscopy system. By this way, the vibrational mode and two dimensional distribution of vibration in hydride will be observed simultaneously on the same particular position on the surfaces. The SFG microscopy is the only method for nondestructive observation of hydrogen distribution on the silicon surfaces. Besides, the

snapshots of ultrafast phenomena of H-Si species can be detected. Especially, in my experiment, I used the pump light irradiation with a fluence which is larger than ~100 mJ/cm^2. The modulation caused by the stronger power is expected to be different from that excited by the weaker, since a laser with fluence higher than ~100 mJ/cm^2 may cause not only Auger recombination but also plasmon-phonon-assisted recombination of the excited carriers [41]. The diffusion also can be observed in micron scale. Therefore, my time-resolved SFG spectroscopy and microscopy are in themselves worthy of attention.

Recently, the optical microscopy setup has attracted many active scientists. K. Klass *et.al* [42] has introduced the advantage of SHG microscopy such as detection of diffusion, desorption on both vicinal and flat surfaces. They applied the SHG microscopy system into investigation of laser-induced diffusion of oxygen from the step edges onto the terrace site of a vicinal Pt(111) crystal. However, this system has a disadvantage that the relation between the SHG signal and surface coverage cannot be calibrated, except for hydrogen on silicon surface [43]. SHG microscope could not distinguish the different type of species on the surface. On the other hand, my SFG microscopic system can be applied for various adsorbate systems. For example, the monohydride H-Si, dihydride 2H-Si and trihydride 3H-Si will be clearly observed separately in SFG spectra when the IR energy is scanned near the vibrational resonance of these molecules. A scanning tunneling microscope (STM) and an electron-stimulated desorption (ESD) are also strong techniques to observe the spatial distribution of hydrogen molecules. However, it is difficult to distinguish between species. In this research, I will in investigate the dynamics of regular step H-Si surfaces by observing time dependence of SFG spectroscopy and microscopy at several high temperatures. The detail of optical setup of SFG microscope will be described in Chapter 4.

1.3 Summary of main purposes

As described in detail in the previous section, I would like to summarize the purposes of this research as follows:

(a) Construction of the pump-probe SFG microscopy system for the first time.

(b) By using the pump-probe SFG microscope, dynamics of H-Si species on the flat H-Si(111)1x1 surfaces affected by the visible light irradiation will be investigated by observing the time-resolved SFG spectroscopy and microscopy in UHV chamber. Also the diffusion will be seen in the SFG intensity images.

(c) The time dependence of SFG spectroscopy and microscopy of the H-Si(111)1x1 surface will be performed after heated at high temperatures. The reduction of hydrogen coverage due to heating surface at high temperatures will be observed for the first time. The dipole-dipole coupling among the H-Si bonds can be considered during the hydrogen desorption process.

(d) Investigation of hydrogen desorption from the regular step H-Si(111) surface with 9.5^{o} miscut toward $[\bar{1}\bar{1}2]$ direction. The H-Si surface will be prepared by dosing hydrogen molecules in UHV chamber. It will be heated at high temperatures, and time dependence of the SFG spectroscopy with different polarization combination will be taken. Dipole-dipole interaction between spices on the terrace and on the step is also considered. The hydrogen diffusion from terraces to steps will be visible in time dependence SFG intensity images.

1.4 Summary of thesis contents

The thesis is organized in six chapters. In chapter 1, I showed the historical study of hydrogenated Si(111) surfaces and retain problems. I explained why I choose the SFG to investigate H-Si surfaces among other surface analysis methods. Especially, the

pump-probe SFG microscopy is a very powerful tool to investigate the dynamics of H-Si species after the pump light irradiation. I also explained why I am interested in hydrogen desorption on Si surfaces.

In chapter 2, I explained briefly about SFG technique. I introduced a long distance microscope and how it was combined to SFG system. The pump-probe principle also was described.

In chapter 3, I briefly presented how were the H-Si(111) surfaces prepared by wet chemical treatment and dosing hydrogen molecules. The step bunches on H-Si(111) surfaces with 9.5^{o} miscut toward $[\bar{1}\bar{1}2]$ direction were created by using direct current (DC) heating.

In chapter 4, I briefly showed the schematic optical system of SFG generation, and then how it was developed into the pump-probe SFG spectroscopic and microscopic system. Then, the time-resolved SFG spectroscopy and microscopy were represented. The effect of electron-hole plasma and the surface temperature on vibrational dynamics of Si-H was considered.

In chapter 5, the effect of rising surface temperature on vibrational dynamics was presented. The H-Si surface was heated at several temperatures and SFG spectra and images were observed after cooling surface to room temperature. Dipole-dipole interaction among Si-H species on the Si(111)1x1 surface were discussed by using Coherent potential approximation (CPA) method.

In chapter 6, some interesting phenomena were shown in SFG spectra of the regular stepped Si(111) surface with 9.5^{o} miscut toward $[\bar{1}\bar{1}2]$ direction. For example, the difference between *ppp* and *ssp* polarization combination of SFG spectra was considered. The appearance and absence of step hydrogen vibration mode C_1, C_2, and C_3

were explained. From the time dependence of the SFG spectra observed when the surface was heated at high temperature, the main discussion of hydrogen desorption was presented.

In chapter 7, the general conclusion from this research was presented.

In chapter 8, I would like to show the work which I intend to do in the future.

References

1. Vilan, A., et al., *Molecules on Si: Electronics with Chemistry.* Advanced Materials, 2010. **22**(2): p. 140-159.
2. Hochberg, L.R., Serruya, Mijail D., Friehs, Gerhard M., Mukand, Jon A., Saleh, Maryam, Caplan, Abraham H., Branner, Almut, Chen, David, Penn, Richard D., Donoghue, John P., *Neuronal ensemble control of prosthetic devices by a human with tetraplegia.* Nature, 2006/07/13/print. **442**(7099): p. 164.
3. Jo, S. and K. Park, *Surface modification using silanated poly(ethylene glycol)s.* Biomaterials, 2000. **21**(6): p. 605-616.
4. Dekeyser, C.M., et al., *Oligo(ethylene glycol) monolayers by silanization of silicon wafers: Real nature and stability.* Journal of Colloid and Interface Science, 2008. **324**(1–2): p. 118-126.
5. Kilian, K.A., et al., *Si–C linked oligo(ethylene glycol) layers in silicon-based photonic crystals: Optimization for implantable optical materials.* Biomaterials, 2007. **28**(20): p. 3055-3062.
6. Buriak, J.M., *Organometallic Chemistry on Silicon and Germanium Surfaces.* Chemical Reviews, 2002. **102**(5): p. 1271-1308.
7. Cicero, R.L., M.R. Linford, and C.E.D. Chidsey, *Photoreactivity of Unsaturated Compounds with Hydrogen-Terminated Silicon(111).* Langmuir, 2000. **16**(13): p. 5688-5695.
8. Qin, G., et al., *Biofunctionalization on Alkylated Silicon Substrate Surfaces via "Click" Chemistry.* Journal of the American Chemical Society, 2010. **132**(46): p. 16432-16441.
9. Arai, T., et al., *DNA molecules sticking on a vicinal Si(111) surface observed by noncontact atomic force microscopy.* Applied Surface Science, 2002. **188**(3–4): p. 474-480.
10. Namiki, A., *Desorption related to adsorption of hydrogen via detailed balance on the Si(1 0 0) surfaces.* Progress in Surface Science, 2006. **81**(8–9): p. 337-366.
11. Flowers, M.C., et al., *Temperature programmed desorption of molecular hydrogen from a Si(111) surface: Theory and experiment.* The Journal of Chemical Physics, 1995. **102**(2): p. 1034-1043.
12. Koehler, B.G., et al., *Desorption kinetics of hydrogen and deuterium from Si(111) 7 x 7 studied using laser-induced thermal desorption.* The Journal of Chemical Physics, 1988. **89**(3): p. 1709-1718.
13. Sinniah, K., et al., *New Mechanism for Hydrogen Desorption from Covalent Surfaces: The Monohydride Phase on Si(100).* Physical Review Letters, 1989. **62**(5): p. 567-570.
14. Sinniah, K., et al., *Hydrogen desorption from the monohydride phase on Si(100).* The

Journal of Chemical Physics, 1990. **92**(9): p. 5700-5711.

15. Wise, M.L., et al., *Comparison of hydrogen desorption kinetics from Si(111)7 × 7 and Si(100)2 × 1.* Surface Science, 1991. **258**(1–3): p. 166-176.
16. Dürr, M., et al., *Probing High-Barrier Pathways of Surface Reactions by Scanning Tunneling Microscopy.* Science, 2002. **296**(5574): p. 1838-1841.
17. Morita, Y., K. Miki, and H. Tokumoto, *Kinetics of hydrogen desorption on a Si(111) surface.* Surface Science, 1995. **325**(1–2): p. 21-32.
18. Reider, G.A., U. Hofer, and T.F. Heinz, *Desorption kinetics of hydrogen from the Si(111)7 x 7 surface.* The Journal of Chemical Physics, 1991. **94**(5): p. 4080-4083.
19. Reider, G.A., U. Höfer, and T.F. Heinz, *Surface diffusion of hydrogen on Si(111)7×7.* Physical Review Letters, 1991. **66**(15): p. 1994-1997.
20. Gupta, P., V.L. Colvin, and S.M. George, *Hydrogen desorption kinetics from monohydride and dihydride species on silicon surfaces.* Physical Review B, 1988. **37**(14): p. 8234-8243.
21. Niwano, M., M. Terashi, and J. Kuge, *Hydrogen adsorption and desorption on Si(100) and Si(111) surfaces investigated by in situ surface infrared spectroscopy.* Surface Science, 1999. **420**(1): p. 6-16.
22. Becker, R.S., et al., *Atomic-scale conversion of clean Si(111):H-1×1 to Si(111)-2×1 by electron-stimulated desorption.* Physical Review Letters, 1990. **65**(15): p. 1917-1920.
23. Vinh, L.T., et al., *Low temperature formation of Si(111)7 x 7 surfaces from chemically prepared H/Si(111)-(1 x 1) surfaces.* Applied Physics Letters, 1994. **64**(24): p. 3308-3310.
24. Pusel, A., U. Wetterauer, and P. Hess, *Photochemical Hydrogen Desorption from H-Terminated Silicon(111) by VUV Photons.* Physical Review Letters, 1998. **81**(3): p. 645-648.
25. De Renzi, V., R. Biagi, and U. del Pennino, *Study of the transition from the ideal Si(1 1 1)–H(1×1) surface to the (7×7) reconstruction by HREELS, UPS and LEED.* Surface Science, 2002. **497**(1–3): p. 247-253.
26. Ye, S., et al., *Stability of the Si–H bond on the hydrogen-terminated Si(1 1 1) surface studied by sum frequency generation.* Surface Science, 2001. **476**(1–2): p. 121-128.
27. Luo, H. and C.E.D. Chidsey, *D--Si(111)(1 x 1) surface for the study of silicon etching in aqueous solutions.* Applied Physics Letters, 1998. **72**(4): p. 477-479.
28. Jakob, P., Y.L. Chabal, and K. Raghavachari, *Lineshape analysis of the Si ・ H stretching mode of the ideally H-terminated Si(111) surface: the role of dynamical dipole coupling.* Chemical Physics Letters, 1991. **187**(3): p. 325-333.
29. Hien, K.T.T., et al., *Hydrogen desorption from a Si(111)1×1 surface studied by sum frequency generation spectroscopy and microscopy.* Surface and Interface Analysis, 2012. **44**(6): p. 662-665.

30. Miyauchi, Y., H. Sano, and G. Mizutani, *Optical second harmonic intensity images of hydrogen deficiency on H-Si(111) surfaces.* e-Journal of Surface Science and Nanotechnology, 2006. **4**: p. 105-109.
31. Miyauchi, Y., H. Sano, and G. Mizutani, *Numerical analysis of second harmonic intensity images of a H–Si(1 1 1) surface after UV light pulse irradiation.* Applied Surface Science, 2008. **255**(5, Part 2): p. 3442-3446.
32. Ishikawa, K., K. Ueda, and M. Yoshimura, *New development of scanning-type microscope for two-dimensional hydrogen distribution using electron-stimulated desorption method.* Surface Science, 1999. **433–435**(0): p. 244-248.
33. Miyauchi, Y., et al., *Simultaneous optical second harmonic and sum frequency intensity image observation of hydrogen deficiency on a H–Si(1 1 1) 1 × 1 surface after IR light pulse irradiation.* Surface Science, 2009. **603**(19): p. 2972-2977.
34. Higashi, G.S., et al., *Ideal hydrogen termination of the Si (111) surface.* Applied Physics Letters, 1990. **56**(7): p. 656-658.
35. Mizutani, G. and Y. Miyauchi, *Development and application of optical sum frequency microscopy.* Surface and Interface Analysis, 2010. **42**(10-11): p. 1675-1679.
36. Guyot-Sionnest, P., *Effect of substrate photoexcitation on the dynamics of the Si-H stretch for Si(111)/H.* Journal of Electron Spectroscopy and Related Phenomena, 1993. **64–65**(0): p. 1-9.
37. Guyot-Sionnest, P., *Two-phonon bound state for the hydrogen vibration on the H/Si(111) surface.* Physical Review Letters, 1991. **67**(17): p. 2323-2326.
38. Harris, A.L., et al., *Molecular vibrational energy relaxation at a metal surface: Methyl thiolate on Ag(111).* Physical Review Letters, 1990. **64**(17): p. 2086-2089.
39. Sahrai, M., M. Mahmoudi, and R. Kheradmand, *Atom localization of a two-level pump-probe system via the absorption spectrum.* Laser Physics, 2007. **17**(1): p. 40-44.
40. Harris, A.L. and N.J. Levinos, *Vibrational energy relaxation in a molecular monolayer at a metal surface.* The Journal of Chemical Physics, 1989. **90**(7): p. 3878-3879.
41. Rasolt, M., A.M. Malvezzi, and H. Kurz, *Plasmon-phonon-assisted electron-hole recombination in silicon at high laser fluence.* Applied Physics Letters, 1987. **51**(26): p. 2208-2210.
42. Klass, K., et al., *Second-harmonic microscopy for fluence-dependent investigation of laser-induced surface reactions.* Physical Review B, 2011. **83**(12): p. 125116.
43. Dürr, M. and U. Höfer, *Dissociative adsorption of molecular hydrogen on silicon surfaces.* Surface Science Reports, 2006. **61**(12): p. 465-526.

Chapter 2: Methodology

2.1 Sum frequency generation (SFG) spectroscopy and its advantages

2.2 SFG microscopy in general

2.3 Pump-probe SFG microscopy and its advantages

References

2.1 Sum frequency generation (SFG) spectroscopy and its advantages:

SFG is one of three derived effects of lowest-order nonlinear optical processes. Before considering the SFG in much more detail, let's talk about the general nonlinear optics first.

The interaction of a weak light field with matter is dominated by linear processes, where it is assumed that properties such as the refractive index, absorption coefficient and reflectivity are independent of optical power. This approximation is only valid for low power light beams. However, with a highly intense light field such as that from pulsed lasers, non-linear processes can be observed. In the non-linear interaction between light and matter, the electric susceptibility and all the related properties vary with the strength of the electric field of the light beam.

In order to describe deeply the optical nonlinearity, we should consider how the dipole moment per unit volume, or polarization P of a material system depends on the strength E of an applied optical field: [1-3]

$$\vec{P} = \vec{P}^{(0)} + \varepsilon_0 \overleftrightarrow{\chi}^{(1)}.\vec{E} + \varepsilon_0 \overleftrightarrow{\chi}^{(2)}:\vec{E}\vec{E} + \varepsilon_0 \overleftrightarrow{\chi}^{(3)} \vdots \vec{E}\vec{E}\vec{E} + \cdots \quad (2.1.1)$$

Here, $\vec{P}^{(0)}$ is the static polarization, and $\overleftrightarrow{\chi}^{(i)}$ is the i^{th} order susceptibility tensor. In linear optics, field strengths are moderate and the higher order terms in Eq. (2.1.1) can be neglected. In this case, the polarization becomes proportional to the incoming field. The material specific constant of proportionality, $\chi^{(1)}$, is the first order susceptibility. The light generated has the same frequency and wavelength as the incident light. In non-linear optics, stronger field strengths are considered and the higher order terms can no longer be neglected. The tensor $\chi^{(2)}$ is known as the second order nonlinear optical susceptibility. It is very important to know that the second order susceptibility (susceptibilities with even power in general) is active only in the asymmetric media or on surfaces and interfaces where the

symmetry is broken. In contrast, third-order nonlinear optical interactions, $\chi^{(3)}$ (susceptibilities with odd power in general) can occur in both centro-symmetric and asymmetric media. Let's prove this rule by using the inversion symmetry operator I_{op}:

$$IopP = Iop(P^{(0)} + \varepsilon_0\chi^{(1)}.E + \varepsilon_0\chi^{(2)}:EE + \varepsilon_0\chi^{(3)} \vdots EEE \dots) \tag{2.1.2}$$

In the centro-symmetric medium:

$$I_{op}E = -E \tag{2.1.3}$$

Thus, eq. 2.1.2 becomes:

$$I_{op}P = -P = -P^{(0)} - \varepsilon_0\chi^{(1)}.E + \varepsilon_0\chi^{(2)}:EE - \varepsilon_0\chi^{(3)} \vdots EEE + \cdots \tag{2.1.4}$$

From eq. 2.1.2 and 2.1.4, we find the important relation: $\chi^{(2i)}$=0 and $\chi^{(2i+1)} \neq 0$.

When two intense light fields at frequencies ω_1 and ω_2 interact with the non-linear medium as:

$$E = E_1 + E_2 = E_1(r)\cos(\omega_1 t) + E_2(r)\cos(\omega_2 t) \tag{2.1.5}$$

The second order polarization becomes a radiating source of light at frequency ω_1+ω_2 which gives rise to SFG. The second order polarization:

$$P^{(2)}(\omega_1 + \omega_2) = 2\varepsilon_0\chi^{(2)}E_1E_2 \tag{2.1.6}$$

From equation (2.1.6), since $P^{(2)}$, E_1 and E_2 are vectors, $\chi^{(2)}$ is a 3x3x3 tensor, it contains the information of molecular organization at the surface such as orientation, conformational order and packing. Depending on the experimental geometry and beam polarization, $\chi^{(2)}$ can be represented as follows:

$$\chi^{(2)} = \sum_{ijk} L_i(\omega_{SFG})L_j(\omega_{vis})L_k(\omega_{IR})\,(\vec{\imath}.\overrightarrow{p_{SFG}})(\vec{\jmath}.\overrightarrow{p_{vis}})(\vec{k}.\overrightarrow{p_{IR}})\chi^{(2)}_{ijk}(\theta,\varphi,\psi) \tag{2.1.7}$$

Here $\vec{\imath}$, $\vec{\jmath}$, $\vec{k}$ are unit vectors along the axes x, y, z and $\vec{p}$ are unit vectors along the selected polarization of the fields (Fig. 2.1.1); the scalar products represent projections of the fields onto the surface frame. $L_j(\omega)$ $(j = x, y, z)$ are the Fresnel factors representing

local fields at the surface for the SFG, visible, and IR beams [4, 5].

$\chi^{(2)}_{ijk}(\theta, \varphi, \psi)$ is called the molecular surface susceptibility tensor

$$\chi^{(2)}_{ijk}(\theta, \varphi, \psi) = \sum_{lmn} U_{ijk,lmn}(\theta, \psi, \varphi)\beta^{(2)}_{lmn} \quad (2.1.8)$$

the susceptibility of a single molecular group whose orientation is given by the Euler angles (θ, ψ, φ) (Fig. 2.1.1). The 6th rank transformation tensor $U_{ijk,lmn}(\theta, \psi, \varphi)$ is a product of thress Euler matrices [6]. In the case of an azimuthally isotropic interface, there are only four independent non vanishing components of $\chi^{(2)}_{ijk}(\theta, \varphi, \psi)$. With the lab coordinates chosen such that z is along the interface normal and x in the incidence plane and with $C_{\infty v}$ symmetry, they are $\chi^{(2)}_{xxz} = \chi^{(2)}_{yyz}, \chi^{(2)}_{xzx} = \chi^{(2)}_{yzy}, \chi^{(2)}_{zxx} = \chi^{(2)}_{zyy}, \chi^{(2)}_{zzz}$ [4]. These four conponents can be deduced by measuring SFG signals from four different input and output polarization combinations signed *ssp*, *sps*, *pss* and *ppp* (with the order is SFG, visible and IR, respectively).

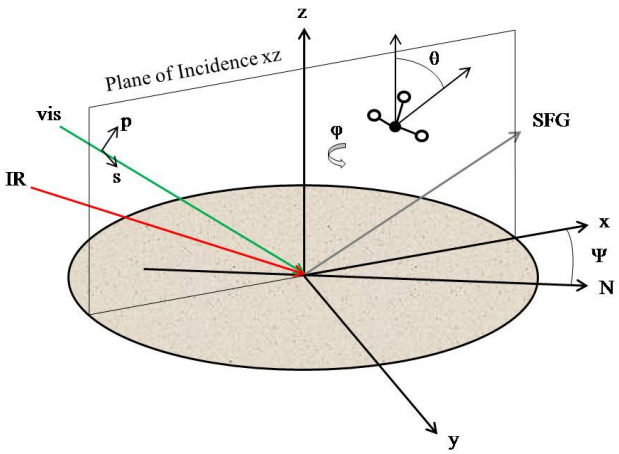

Fig. 2.1.1: Incident plane and Euler angles in xyz cordinates.

The second order nonlinear hyperpolarizability tensor, $\beta^{(2)}_{lmn}$, is dependent on the Raman and IR transition moments:

$$\beta^{(2)}_{lmn} \propto \frac{\partial \alpha_{lm}}{\partial q}\frac{\partial \mu_n}{\partial q} \tag{2.1.9}$$

where l, m, n represent the molecular frame, α_{lm} and μ_n are the polarizability and dipole moment, respectively. q is the normal mode coordinate. By estimating the magnitudes of the polarizability and dipole moment derivatives we can ascertain the relative values of the components of $\beta^{(2)}_{lmn}$. In our experiment, frequency of SFG is expressed as the sum of frequencies of visible and IR laser $\omega_{SFG} = \omega_{IR} + \omega_{vis}$. Overall intensity of SFG signal at a given polarization i, is proportional to the absolute value squared of the induced second order polarization.

$$I_{SFG} \propto \left|P_i^{(2)}\right|^2 \tag{2.1.10}$$

Visible and tunable IR light are often used in measuring SFG spectra which can be obtained by scanning IR frequencies. Fig. 2.1.2 illustrated the SFG energy diagram of resonant and non-resonant processes. Here, |g> is the ground state and |v> is the vibrational excited state. If the IR light energy is the same as the energy of vibrational excited level |v> as in Fig. 2.1.2, the resonance occurs and SFG intensity reaches maximum value. This process is called the vibrationally resonant SFG. In contrast, the non-resonant SFG process occurs when the IR energy is different from that of the vibrational excited level |v>. Therefore, SFG peak occurs when the IR light frequency is equal to the molecular vibrational frequency. This is the reason why SFG spectra have been viewed as a vibrational spectroscopy used in investigation of chemical bonds, molecular adsorption and desorption on substrates. The advantages of SFG spectroscopy are a higher sensitivity, occuring under any pressure and temperature and interacting with buried interfaces.

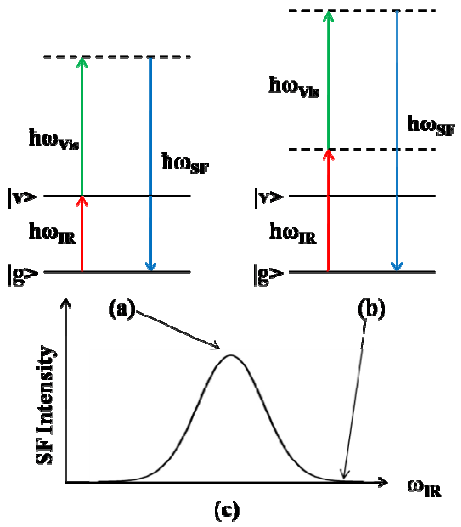

Fig. 2.1.2. SFG energy diagram of (a) the resonant, (b) non-resonant process. (c)The resonant and non-resonant SF as a function of IR wave number.

The reason why I choose the SFG phenomenon for studying the dynamics of H-Si species on the Si surface in this research is that this method has much advantage compared with other surface probe signals. We assume visible light at ω_{vis} and IR light at ω as the incident beams. The total SFG intensity can be calculated as this equation:

$$I_{\mathrm{SFG}} \sim |\chi^{(2)}|^2 = |\chi^{(2)}_{\mathrm{NR}} + \frac{A_0}{\omega - \omega_0 + i\Gamma_0}|^2. \tag{2.1.11}$$

Here, χ_{NR}, is the non-resonant nonlinear susceptibility, and A_0, ω_0 and Γ_0 are the strength, resonant frequency and damping constant of the resonant mode, respectively [7, 8]. Following this equation, the non-resonant components can be considered while the IR and Raman signal could not do it. This non-resonant component makes the SFG spectrum no longer symmetric. From the asymmetric SFG peak, many phenomena can be investigated such as interference with background, dipole-dipole coupling and inhomogeneous distribution of absorbates. On the other hand, if SFG is equipped with microscope, it will become very strong tool for observing the morphology of hydrogen

species as presented in next section below. IR and Raman conventional vibrational microscopy lack surface sensitivity.

2.2. SFG microscopy in general

The reason why the SFG microscope system is required was presented in chapter 1. The SFG observation with a Questar QM-1 long distance microscope is a powerful tool for observing the resonant and nonresonant SFG intensity images of a sample surface. First, I introduce the Questar QM-1 long distance microscope briefly and its operation as below.

The Questar QM-1 Long Distance Microscope is the first generation of three basic models of long distance microscopes such as QM-1, QM-100 and QM-200 designed by Questar Co. Ltd.. This was the first time allowed observing images of microscopic subjects. Good spatial resolution can be achieved from a longer distance without cluttering the work area with instrumentation. The QM-1 Long Distance Microscope are lightweight and offer superb performance and at reasonable cost for general industrial or research applications or for teaching. With a working range of 56cm (22 inches) to 152cm (66 inches), a 30 to 1 variability in field of view, and remarkable depth of field, linearity and chromatic correction, it is an indispensable tool for a wide variety of laboratory and industrial applications. The original version of the Questar QM-1 Long Distance Microscope was an arrangement that resembled a conventional telescope, but the QM-1 differs in that it has a longer barrel length. These Long Distance Microscopes can be employed for the long distance inspection of fine detail with an eyepiece, however, these are most commonly used for imaging with an optional CCD integrating or real time video camera, or with 35mm format film cameras. In my optical system, QM-1 was

combined with a charge couple device (CCD) camera in order to observe SFG images. SFG photon numbers were counted by the CCD camera (as black dots shown in SFG images in Fig. 4.4.2 of chapter 4). The optical setup of SFG – long distance microscope will be shown in Fig. 4.2.1 of chapter 4.

Similar to chapter 1, the advantages of the SFG microscopy were represented. This SFG microscopic system can be applied to various adsorbate systems. In this research, the monohydride H-Si, dihydride 2H-Si and trihydride 3H-Si will be clearly observed separately in SFG spectra when the IR energy is scanned near the vibrational resonance of these molecules. A scanning tunneling microscope (STM) and an electron-stimulated desorption (ESD) are also strong techniques to observe the spatial distribution of hydrogen molecules. However, it is difficult to distinguish between species. On the other hand, SFG microscopy is forbidden for centrosymmetric bulk. Thus, it is considered as a sensitive method for monolayer of adsorbate on the surface. Furthermore, if SFG microscopy is combined with a pump-probe technique, it becomes a more powerful tool to investigate the dynamics of surfaces.

2.3 Pump-probe SFG microscopy and its advantages

As already mentioned in chapter 1, creation the pump-probe SFG microscopy is one of my motivation in this research due to its much useful advantages. The optical setup of this system will be shown in section 4.2 for convenient logical of my result section. In this section, I have just explained about the pump-probe principle from laser light.

At first, the pump light excites the electronic state to a higher energy level. Then the probe light comes to the sample after ultrashort time (called the delay time) to detect the phenomena occurring immediately after the pump pulse irradiation. The experimental

set up for the pump-probe measurements requires two conditions as:

- The duration of the laser pulses must be shorter than a time scale of the dynamics of the phenomena.
- Intensity of the probe light must be much weaker than those of the pump light to ensure that no effect of the probe light occurs on the sample.

The principle of the pump-probe measurements can be shown in a schematic diagram below (Fig. 2.3.1).

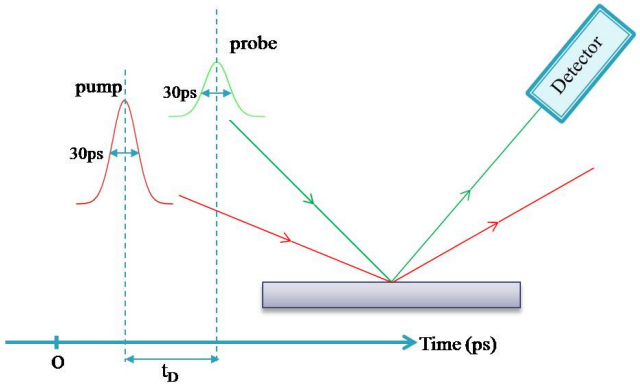

Fig. 2.3.1: Schematic diagram of pump-probe measurements.

Here, t_D is the delay time between the probe and pump light. t_D is defined as positive when the pump light come to sample before the probe light:

$$t_D = t_{probe} - t_{pump}$$

This definition of probe delay time will be used in the result section of chapter 4. For example, probe delay time of -53 ps means the probe light comes at 53 ps after the pump light irradiation. By using this pump-probe SFG microscope, I will in investigate the dynamics of regular step H-Si surfaces by observing time dependence of SFG spectroscopy and microscopy at several high temperatures. The detail of optical setup of SFG microscope will be described in chapter 4.

References

1. Bloembergen, N., *Nonlinear optics*, 1977.
2. Shen, Y.R., *The principles of nonlinear optics*, 1984, New York, Wiley.
3. Boyd, R.W., *Nonlinear Optics (third edition)*, 2008.
4. Zhuang, X., et al., *Mapping molecular orientation and conformation at interfaces by surface nonlinear optics.* Physical Review B, 1999. **59**(19): p. 12632-12640.
5. Shen, Y.R., *Optical Second Harmonic Generation at Interfaces.* Annual Review of Physical Chemistry, 1989. **40**: p. 327.
6. Hirose, C., N. Akamatsu, and K. Domen, *Formulas for the Analysis of the Surface SFG Spectrum and Transformation Coefficients of Cartesian SFG Tensor Components.* Appl. Spectrosc., 1992. **46**(6): p. 1051-1072.
7. Ye, S., et al., *Stability of the Si–H bond on the hydrogen-terminated Si(1 1 1) surface studied by sum frequency generation.* Surface Science, 2001. **476**(1–2): p. 121-128.
8. Shen, Y.R. and V. Ostroverkhov, *Sum-Frequency Vibrational Spectroscopy on Water Interfaces: Polar Orientation of Water Molecules at Interfaces.* Chemical Reviews, 2006. **106**(4): p. 1140-1154.

Chapter 3: Sample preparation

3.1. Chemical treatment of the Si(111) surface

The hydrogen terminated Si surface can be easily produced by etching in a HF solution only [1-5]. However, the Si surface can be rough due to strong interaction with HF solution. Large defects can be formed on the surface [6]. On the other hand, Higashi *et al* [7] and Jakob and Chabal [8] developed a novel preparation technique to obtain an atomically flat Si(111) surface using a buffered HF or NH_4F aqueous solution. However, HF solution is very strong acid and it makes the surface rough. NH_4F aqueous solution is believed that it can make the hydrogenated Si surface atomically flat.

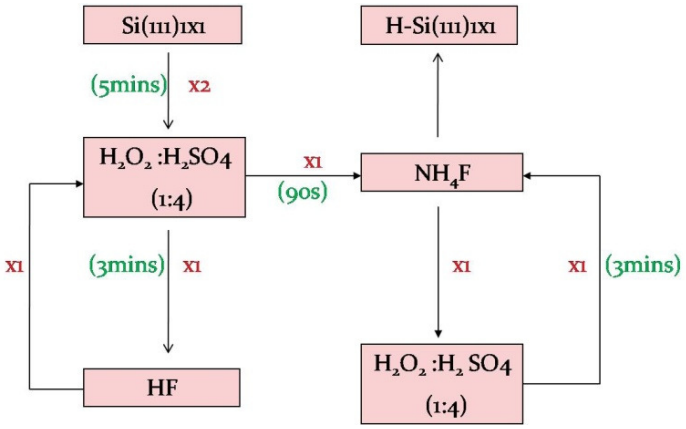

Fig. 3.1.1. H-Si (111)1x1 surface treatment produce.

Figure 3.1.1 roughly shows the steps of the wet chemical etching method of the H-Si (111)1×1 surface by using NH_4F solution. An n-type Si(111) wafer with resistivity ρ = 200 ~ 240 Ω.cm was dipped in solutions as described in detail as follows.

Step 1: An aqueous solution of sulfuric acid H_2SO_4 97% and H_2O_2 30% was mixed at a ratio of 4:1. The Si substrate was dipped in this solution for 5 min in order to remove the oxide surface, and then was rinsed with pured water for 1 minute. This process was repeated twice.

Step 2: The Si substrate was washed with a 1% HF solution in 3 min, then was

washed with pure water for 1 minute.

Step 3: Similar to the step 1, but this cleaning was taken one time.

Step 4: After the etching in 40% NH_4F solution for 90 seconds, it was washed with pure water for 1 minute.

Step 5: Completely the same as step 3.

Step 6: Etching for 3 minutes in 40% NH_4F solution. It was washed with pure water for 30 seconds.

After etching by this process, an automatically flat H-Si(111)1×1 surface was formed. The sample then was introduced into UHV chamber at room temperature. A 1×1 structure of the H-Si(111) surface was confirmed through a low energy electron diffraction (LEED) measurement.

The figure 3.1.2 describes the mechanism of hydrogen passivation on the Si surface by using HF and NH_4F solution.

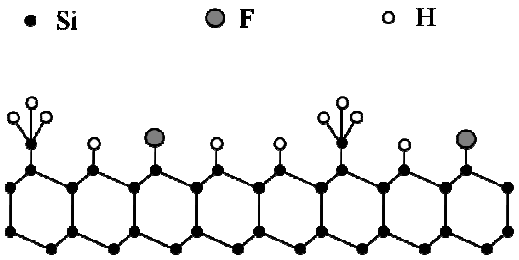

Fig.3.1.2a: The H-Si(111)1x1 surface with HF etching

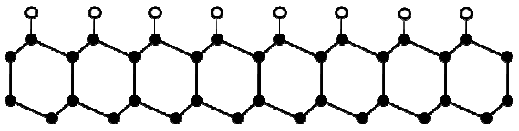

Fig. 3.1.2b: The H-Si(111)1x1 surface with NH_4F etching

3.2. Dosing of hydrogen molecules on the Si(111) surface

One of the hydrogenated Si(111) surface was exposed to hydrogen in a UHV chamber. For decades, atomic H dosing was employed for making the H-terminated Si surfaces [9-18]. However, the atomic H dosing usually make the surface rough and the structural defects appear. More recently, another method of H-covered Si surfaces using molecular-hydrogen dosing has been proposed and investigated [19-22]. Hydrogen adsorption on Si by molecular hydrogen dosing is a dissociative adsorption process. It is known that the sticking coefficient of H in such a process is extremely low at room temperature, and therefore the process was not considered useful for preparing H-terminated Si surfaces in practice. The low sticking coefficient for H_2 dissociative adsorption at room temperature suggested that there should exist a significant adsorption-energy barrier, which was found by Bratu *et. al* [19, 20] to be 0.9 eV. However, Hofer and co-workers [19, 20, 23] discovered that the sticking coefficient increases rapidly with temperature. Dosing of H_2 at a sufficiently high substrate temperature can yield a fully covered H-terminated Si(111) surface with a quality as good as the one prepared by the wet-chemical-etching method [21]. From the results of temperature dependent sticking coefficient, Hofer and co-workers [23] showed that H_2 dissociative adsorption must be a phonon-assisted process, with H_2 desorption appearing naturally as a reverse process. Theoretical models by Vittadini and Selloni [24] and Cho *et. al* [25] suggested that on adsorption, thermal backbond breaking would allow the adatom to move toward the incoming H_2 molecule and facilitate the formation of two surface Si-H bonds. On desorption, two neighboring adsorbed H atoms would recombine and desorb, leaving the Si atom dangling in an excited vibrational state.

Si wafer was dipped in acetone in a teflon cup. In order to clean the Si substrate, the teflon cup was kept in an ultrasound bath in 10 min. Then the substrate was released from acetone gradually for drying and then kept by the special holder (described in Chapter 4) in the UHV chamber. The chamber was baked at temperature of ~140 °C in few days for desorbing impurities. The best achieved pressure is at ~10^{-8} Pa.

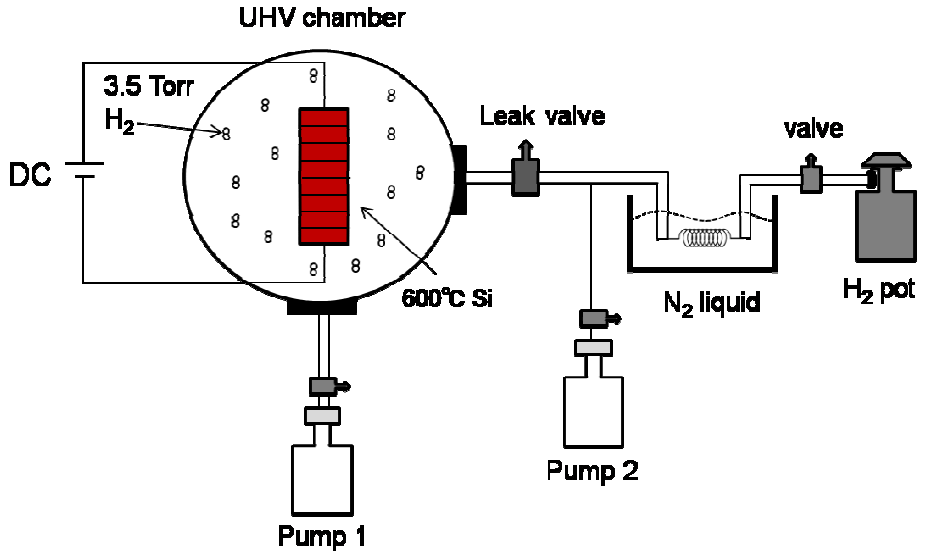

Fig. 3.2.1: The diagram of the hydrogen dosing process.

Figure 3.2.1 shows roughly the process of hydrogen dosing. The Si wafer was made clean by degassing at 600 °C in at least 6 hours. In order to make the well ordered 7x7 reconstruction, the Si wafer was heated at 1200 °C in 1 to 2 min. This step was done to diffuse residual surface carbon into the bulk. After that, it was cooled fast to the transition temperature from 7x7 to 1x1 structure. And then it was reduced to room temperature gradually in 5 min. This cooling process makes the 7x7 reconstruction in well order [19, 21, 23, 26]. This structure was confirmed by observing LEED pattern as shown briefly in Chapter 4. There are some different reports about the transition temperature from 7x7 to 1x1 structure. For example, one reported that it is about 830°C

was directly observed by reflection electron microscopy [27, 28]. The other said that is was 867 °C [29]. In my case, I checked this transition temperature by observing LEED patterns and I found that it was 856 °C. Therefore, in my research, I will treat the transition temperature between 7x7 and 1x1 as 856 °C.

The Si substrate was heated at ~ 600 °C. Ultrapure hydrogen molecules were introduced into the UHV chamber through a leak valve. Before going into the UHV chamber, it was further purified by passing through a 20 m length of a steel tube coil which was kept in liquid nitrogen to filter out the residual impurities. The pressure of hydrogen molecules was ~3.5 Torr. To avoid contamination of the sample, the hot filament in the UHV chamber was turned off during H_2 dosing. After 10 min of hydrogen dosing, one mono layer of hydrogen coverage was expected to be formed. The surface was reconstructed into the 1x1 structure which was observed by LEED patterns.

In this research, the hydrogen was terminated on two types Si surface. One is the flat Si wafer and the other is the regular steps Si(111) wafer with 9.45^o off miscut toward $\langle\bar{1}\bar{1}2\rangle$ direction. Both of them have the resistivity of ρ = 5 ~ 10 Ω.cm.

3.3. DC current heating for the step bunched Si(111) surface

I used a tilted Si surface with 9.5^o off miscut toward $\langle\bar{1}\bar{1}2\rangle$ direction and the resistivity of ρ = 5 ~ 10 Ω.cm. This sample has the flat terraces and steps. Jakob and Chabal [8] showed that the top atom on each step of this miscut surface had two dangling bonds and each Si atom on the (111) terrace had one dangling bond (fig.3.3.1).

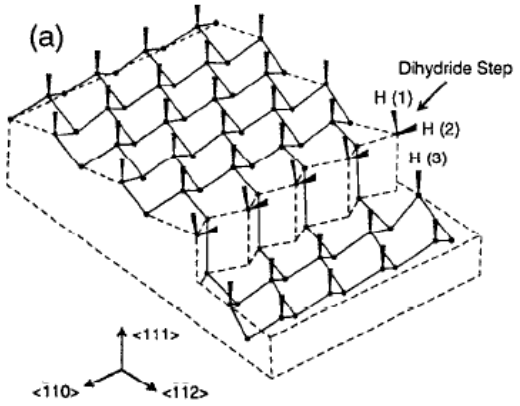

Fig. 3.3.1: Structure of the step Si(111) surface 9.5° off miscut toward $\langle \bar{1}\bar{1}2 \rangle$ *direction*

Similarly to the description in section 3.2, the tilted Si wafer was dipped in an acetone cup and cleaned in the ultrasonic bath for 10 min. Then it was introduced into the UHV chamber at the pressure of ~10^{-8} Pa. The Si wafer was made clean by degassing at 600 °C in at least 6 hours. The interesting point of making step bunches is that the DC current can be applied to heat the regular step Si substrate with either a step-up or step-down current direction. M. Degawa *et.al* [30] reported briefly on the DC current effect on the induction of step bunching as summarized in fig. 3.3.2. The step bunches will be induced by both the step-up and step-down DC current, but the relevant temperature is different. Figure 3.3.3 shows a schematic diagram of the regular step surface and step bunching (SB) surface. The terrace length becomes much larger than that of regular step surface. The number of step density is reduced.

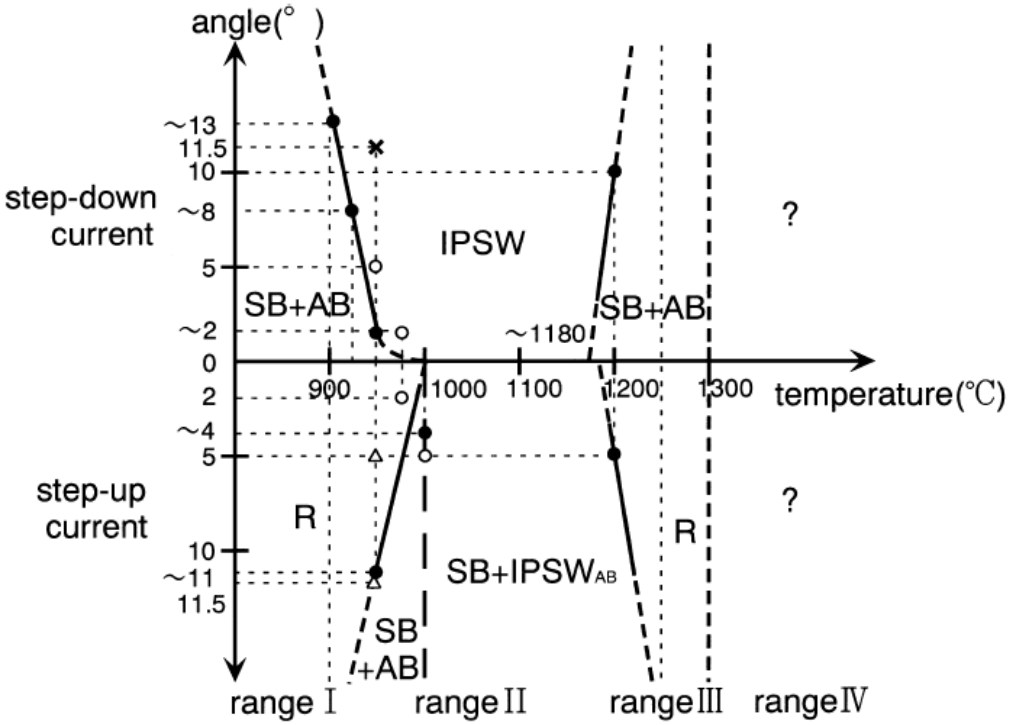

Fig. 3.3.2: A proposed phase diagram of surface morphology in the temperature-of-angle (including current direction) space. X-axis for temperature and y-axis for the off-angle of the vicinal surface. SB for SB surfaces, AB for ABS, R for R surfaces and IPSW for IPSW surfaces ($IPSW_{AB}$ for IPSW of Abs).

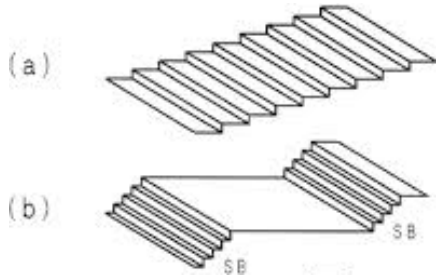

Fig. 3.3.3: (a) the regular Si surface and (b) the step bunching (SB) Si surface after heated at high temperature.

In this research, the step bunches on the Si surface were made by heating at 1100 °C within 18 hrs with the step-up current direction (range II in fig. 3.3.2). The step

bunches was roughly confirmed by C-MOS camera via a long distance microscope. The figure 3.3.4 shows the AFM image of the step bunched Si(111) surface with terrace width of ~ 5μm.

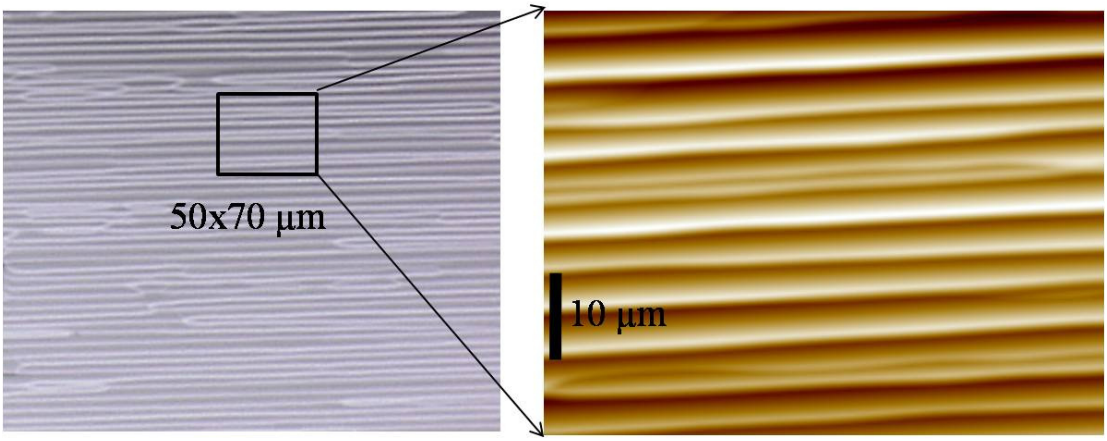

Fig. 3.3.4: The AFM image of the step bunched Si(111) surface heated at 1100 °C within 18 hrs with the step-up current direction.

References

1. Grundner, M. and H. Jacob, *Investigations on hydrophilic and hydrophobic silicon (100) wafer surfaces by X-ray photoelectron and high-resolution electron energy loss-spectroscopy.* Applied Physics A, 1986. **39**(2): p. 73-82.
2. Fenner, D.B., D.K. Biegelsen, and R.D. Bringans, *Silicon surface passivation by hydrogen termination: A comparative study of preparation methods.* Journal of Applied Physics, 1989. **66**(1): p. 419-424.
3. Takahagi, T., et al., *The formation of hydrogen passivated silicon single-crystal surfaces using ultraviolet cleaning and HF etching.* Journal of Applied Physics, 1988. **64**(7): p. 3516-3521.
4. Weinberger, B.R., et al., *Surface chemistry of HF passivated silicon: X-ray photoelectron and ion scattering spectroscopy results.* Journal of Applied Physics, 1986. **60**(9): p. 3232-3234.
5. Grunthaner, P.J., et al., *Hydrogen-terminated silicon substrates for low-temperature molecular beam epitaxy.* Thin Solid Films, 1989. **183**(1–2): p. 197-212.
6. Dumas, P., Y.J. Chabal, and P. Jakob, *Morphology of hydrogen-terminated Si(111) and Si(100) surfaces upon etching in HF and buffered-HF solutions.* Surface Science, 1992. **269–270**(0): p. 867-878.
7. Higashi, G.S., et al., *Ideal hydrogen termination of the Si (111) surface.* Applied Physics Letters, 1990. **56**(7): p. 656-658.
8. Jakob, P. and Y.J. Chabal, *Chemical etching of vicinal Si(111): Dependence of the surface structure and the hydrogen termination on the pH of the etching solutions.* The Journal of Chemical Physics, 1991. **95**(4): p. 2897-2909.
9. Ibach, H. and J.E. Rowe, *Hydrogen adsorption and surface structures of silicon.* Surface Science, 1974. **43**(2): p. 481-492.
10. Schulze, G. and M. Henzler, *Adsorption of atomic hydrogen on clean cleaved silicon (111).* Surface Science, 1983. **124**(2–3): p. 336-350.
11. Koehler, B.G., et al., *Desorption kinetics of hydrogen and deuterium from Si(111) 7 x 7 studied using laser-induced thermal desorption.* The Journal of Chemical Physics, 1988. **89**(3): p. 1709-1718.
12. Owman, F. and P. Mårtensson, *STM study of structural defects on in situ prepared Si(111) 1 × 1-H surfaces.* Surface Science, 1995. **324**(2–3): p. 211-225.
13. Mortensen, K., et al., *Two reaction channels directly observed for atomic hydrogen on the Si(111)-7×7 surface.* Physical Review B, 1991. **43**(2): p. 1816-1819.
14. Sakurai, T. and H.D. Hagstrum, *Chemisorption of atomic hydrogen on the silicon (111) 7 × 7 surface.* Physical Review B, 1975. **12**(12): p. 5349-5354.

15. McRae, E.G. and C.W. Caldwell, *Structure of Si(111)-(7×7)H.* Physical Review Letters, 1981. **46**(25): p. 1632-1635.
16. Chabal, Y.J., G.S. Higashi, and S.B. Christman, *Hydrogen chemisorption on Si(111)-(7×7) and -(1×1) surfaces. A comparative infrared study.* Physical Review B, 1983. **28**(8): p. 4472-4479.
17. Karlsson, C.J., et al., *Hydrogen chemisorption on Si(111)7×7 studied with surface-sensitive core-level spectroscopy and angle-resolved photoemission.* Physical Review B, 1990. **41**(3): p. 1521-1528.
18. Kolasinski, K.W., et al., *Hydrogen adsorption on and desorption from Si: Considerations on the applicability of detailed balance.* Physical Review Letters, 1994. **72**(9): p. 1356-1359.
19. Bratu, P. and U. Höfer, *Phonon-Assisted Sticking of Molecular Hydrogen on Si(111)-(7×7).* Physical Review Letters, 1995. **74**(9): p. 1625-1628.
20. Bratu, P., K.L. Kompa, and U. Höfer, *Optical second-harmonic investigations of H2 and D2 adsorption on Si (100) 2 × 1: the surface temperature dependence of the sticking coefficient.* Chemical Physics Letters, 1996. **251**(1–2): p. 1-7.
21. Mao, M.Y., et al., *Characterization of hydrogen-terminated Si(111) surfaces by sum-frequency surface vibrational spectroscopy.* Applied Physics Letters, 1999. **75**(21): p. 3357-3359.
22. Kolasinski, K.W., et al., *Beam investigations of D[sub 2] adsorption on Si(100): On the importance of lattice excitations in the reaction dynamics.* The Journal of Chemical Physics, 1994. **101**(8): p. 7082-7094.
23. Bratu, P., et al., *Reaction dynamics of molecular hydrogen on silicon surfaces.* Physical Review B, 1996. **54**(8): p. 5978-5991.
24. Vittadini, A. and A. Selloni, *H2 adsorption/desorption at Si(111)-(7 × 7): a density functional study.* Surface Science, 1997. **383**(2–3): p. L779-L784.
25. Cho, K., E. Kaxiras, and J.D. Joannopoulos, *Theory of Adsorption and Desorption of H_{2} Molecules on the Si(111)- (7×7) surface.* Physical Review Letters, 1997. **79**(25): p. 5078-5081.
26. Flowers, M.C., et al., *The desorption of molecular hydrogen from Si(100)-2 x 1 and Si(111)-7 x 7 surfaces at low coverages.* The Journal of Chemical Physics, 1998. **108**(8): p. 3342-3352.
27. Osakabe, N., K. Yagi, and G. Honjo, *Reflection Electron Microscope Observations of Dislocations and Surface Structure Phase Transition on Clean (111) Silicon Surfaces.* Jpn. J. Appl. Phys., 1980. **19**: p. L309.
28. Feltz, A., U. Memmert, and R.J. Behm, *STM study of the Cl induced high temperature Si(111) (7 × 7) ↔ (1 × 1) phase transitions.* Surface Science, 1994. **307–309, Part A**(0): p.

216-222.

29. Bennett, P.A. and M.W. Webb, *The Si(111) 7 × 7 TO "1 × 1" transition.* Surface Science, 1981. **104**(1): p. 74-104.

30. Degawa, M., et al., *New Phase Diagram of Step Instabilities on Si(111) Vicinal Surfaces Induced by DC Annealing.* J. Phys. Soc. Jpn. **70**(4): p. 1034.

Chapter 4: Pump-probe SFG spectroscopy and microscopy on the flat Si(111) surface

In this chapter 4, I briefly show the schematic optical system of SFG generation, and then how it was developed into the pump-probe SFG spectroscopic and microscopic system. Then, the time-resolved SFG spectroscopy and microscopy were presented. The SFG microscopy is the only method for nondestructive observation of hydrogen distribution on the silicon surfaces. Besides, the snapshots of ultrafast phenomena of H-Si species have to be detected after pump light irradiation. Therefore, the pump-probe technique must be applied to the SFG microscope. Furthermore, by this way of optical setup, the vibrational mode and two dimensional distribution of vibration in hydride will be observed simultaneously on the same particular position on the surfaces. The dynamics of H-Si species will be analyzed effectively. The time resolved SFG spectroscopy and microscopy of the H-Si(111) 1x1 surface was taken at several delay time of pump light irradiation.

4.1 Optical system of sum frequency generation

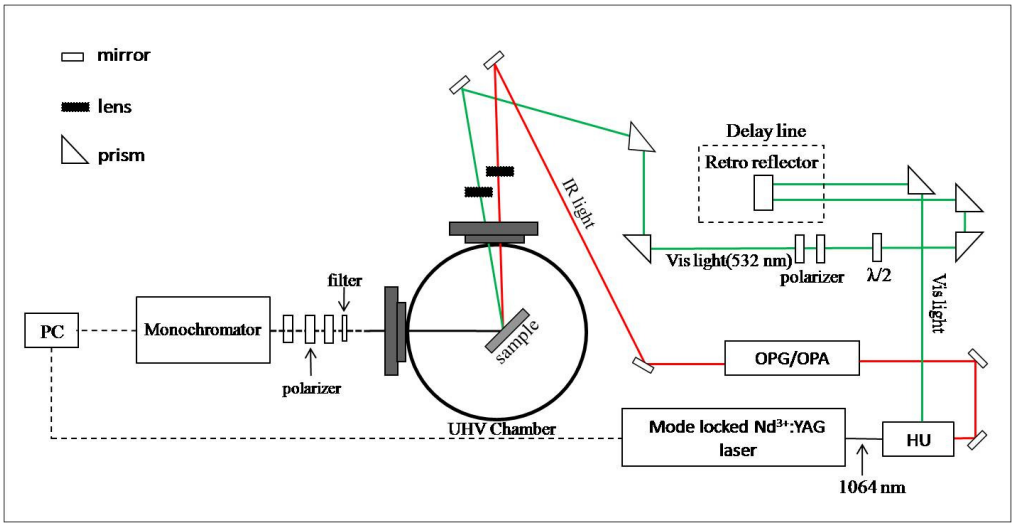

Fig.4.1.1 A schematic diagram of a SFG spectroscopic system. HU, OPG/OPA, M and PC are Harmonic Unit, Optical Parametric Generation/Optical Parametric Amplifier, Mirror and Personal Computer, respectively.

Following the theory presented in chapter 2, in order to get SFG signals, the visible and IR lights are guided to come to a surface at the same time. Fig.4.1.1 shows a schematic diagram of a SFG typical spectroscopic system before the improvement shown in section 4.2. As the incident visible light, we used a doubled frequency output with photon energy of 2.33 eV from a mode-locked Nd^{3+}: YAG laser operating at the repetition rate of 10 Hz and pulse width of 30 ps. The wavelength-tunable incident IR light is an output with photon energy ~ 0.26 eV from an optical parametric generator and amplifier system (OPG/OPA).

The incident visible and IR lights are guided to reach the surface at the same position, by adjusting the delay line between these optical lines. The SFG light generated from the sample in the reflective direction was passed through a glass/quarzt

window of the chamber, and was passed through high pass filters. It was then detected by a monochromator, and the SFG spectra were obtained as a function of the infrared light wavenumber. Fig. 4.1.2 shows a SFG spectrum of the H-Si(111) surface with a sharp peak at 2083.7 cm^{-1} attributed to the H-Si stretching vibration on the H-Si(111) 1x1 surface treated by ammonium fluoride NH_4F solution. There was no contribution from vibration of dihydride at ~2130 cm^{-1}. This is consistent with several reports that treatment with 40% NH_4F solution (pH ~ 7) provided the ideally monohydride terminated Si(111) 1x1 surface [1, 2], as explained in section 3.1 of chapter 3. This (all,p,p) SFG spectrum was obtained by tunning a IR input frequency (from 2060 to 2110 cm^{-1}) around the H-Si stretching vibrational mode. The pulse energies of IR light and probe visible light were 120 and 20 μJ/pulse.

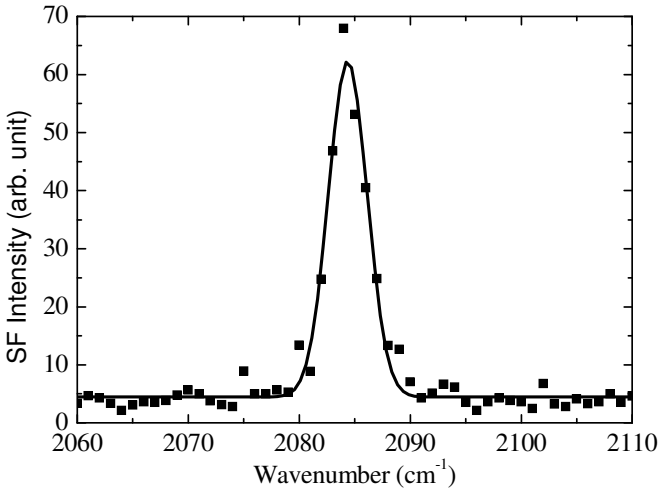

Fig. 4.1.2. SFG intensity spectrum of the H-Si(111) surface. The black dots are experimental data. The solid line is fitting curve. The sharp peak appeared at 2083.7 cm^{-1}.

I note here about our fluctuation limit of our system. The line width of our IR probe light was ~3 cm^{-1}, but the energy fluctuation limit in practice has been reported as

$\pm 0.15 cm^{-1}$ [3]. In order to find the fluctuation of the probe light tuning in our system, I took SFG spectra of eight different samples, and determined the center peak positions and the widths of the Si-H vibrational peaks. The standard deviations of the peak positions and widths were 0.15 and 0.23 cm^{-1}, respectively. Thus, I suggest that in practice, the fluctuation limit of our system was at least better than 0.3 cm^{-1}.

4.2 Construction of the pump-probe SF spectroscopic and microscopic system

Figure 4.2.1 shows the block diagram of the whole measurement setup after the improvement compared to fig. 4.1.1. The pump-probe SFG microscopy was equipped beside the SFG spectrometer. The SFG microscopy is the only method for nondestructive observation of hydrogen distribution on the silicon surfaces. Besides, the snapshots of ultrafast phenomena of H-Si species have to be detected after pump light irradiation. Therefore, the pump-probe technique must be applied to the SFG microscope. Furthermore, by this way of optical setup, the vibrational mode and two dimensional distribution of vibration in hydride will be observed simultaneously on the same particular position on the surfaces. The dynamics of H-Si species will be analyzed effectively. The polarization of the SFG spectroscopy, visible and IR light beams could be changed between *s* and *p*.

In order to get pump-probe SFG spectra in section 4.3, I inserted the mirror M in front of a glass window of the UHV chamber. The pump visible light and probe visible light were divided from the double frequency visible light beam (532 nm) by a beam splitter (BS). The probe visible light was passed through a $\lambda/2$ plate, a Glan polarizer, a bandpass filter with the center photon energy 2.33 eV, a lens with focal length f=250 mm. The IR probe light was focused by a CaF_2 lens with a focal length

of 300 mm. Both the visible light and the IR light were guided into an UHV chamber through a CaF_2 window. The probe visible and IR light reached the Si surface at the same position with incident angles of 38^o and 52^o and the pulse energies of 20 and 120 μJ/pulse, respectively. The SFG light from the sample generated in the reflective direction was passed through the glass window of the chamber, then reflected on mirror M to change direction, then passed dichroic filters to block the reflected visible light. It was then introduced into a monochromator. I measured the SFG spectra of the H-Si(111) surface as a function of the probe delay times.

In order to get SFG intensity images in section 4.4, the mirror M was flipped out, the SFG light was introduced into a long-distance Cassegrain-type microscope (Quester QM-1) and detected by a time-gated image intensified charge-coupled device camera (Hamamatsu PMA-100-H). Irradiated position on the sample with probe light beams was changed in raster scan by moving the focusing lenses with automatic X-Y stages. I accumulated the SFG photons by the CCD camera for 500 seconds, while I moved the position of the probe beam spots. The total number of laser pulse shots for one SFG intensity image was 5000. I measured the SFG intensity images of the H-Si(111) surface as a function of the probe delay times.

The H-Si(111) sample was heated at high temperature in a few tens of seconds and then cooled down to the room temperature (RT). Then SFG intensity spectra and images of the H-Si(111)1×1 surface were observed. The accumulation time for one image was 30 minutes.

The power of the pump visible light was 120 μJ/pulse and the power density on the sample surface was 0.12 J/cm^2.pulse. The pump light was nearly *p*-polarized and had the incident angle of 68.5^o. The optical delay of the probe visible and infrared pulses

was controlled by an automatic linear stage with the positioning accuracy of ~5 μm. The timing of the pump and probe light was adjusted by monitoring the SFG of the pump visible and probe IR light from the sample with its surface tilted differently from the final SFG measurement. In the final SFG measurement, this SFG light did not hit the detector because it traveled off the optical path by the angle of ~30°. No damage was observed in the linear microphotograph of the sample surface after the pump light irradiation. The invariance of the Si-H vibrational peak in the SFG spectra before and after the pump-probe measurement indicated the absence of the change of hydrogen coverage and disorder of the Si-H bonds during the strong pump light irradiation. The advantages of the optical SFG spectroscopic system as shown in Fig.4.2.1 were shown in chapter 2.

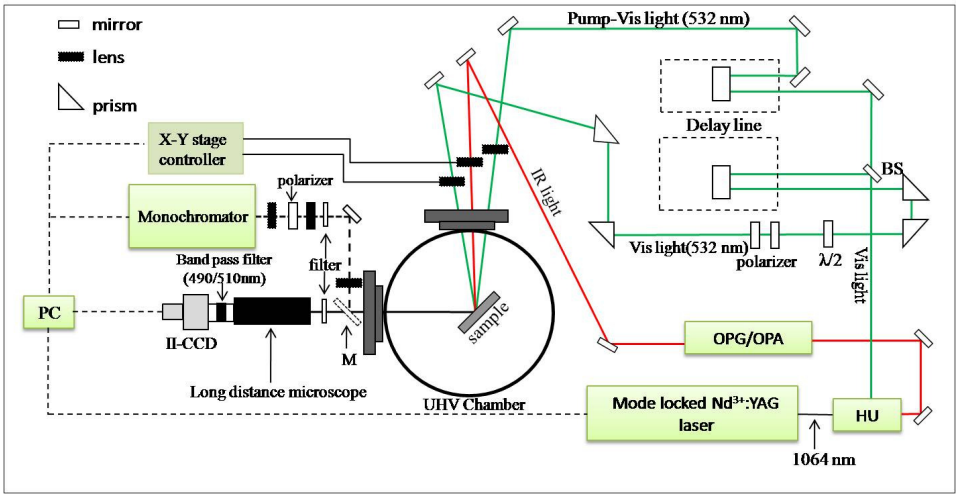

Fig.4.2.1: The schematic diagram of a pump-probe SF intensity microscopic and spectroscopic system. HU, OPA/OPG, M, BS and PC are Harmonic Unit, Optical Parametric Generation/ Optical Parametric Amplifier, Mirror, Beam splitter and Personal Computer, respectively.

4.3 Time-resolved SFG spectroscopy

As presented in the section 1.2.1 of chapter 1, the dynamics of Si-H bonds on the Si surface were affected by not only rise the surface temperature but also by the e-h plasma simultaneously created by the pump light irradiation. In chapter 5, I will discuss the effect of surface temperature. In this chapter, I will discuss the effect of excited e-h pairs on vibrational dynamics of Si-H species. The visible pump light irradiated the Si surface, after that the SFG spectroscopy was performed at several probe delay times. The optical setup in Fig. 4.2.1 was used.

In this experiment, a flat H-Si(111)1x1 surface was prepared by the wet chemical treatment as written in section 3.1 of chapter 3. After that, it was introduced immediately into the UHV chamber at a pressure of ~10^{-8} Pa. The energy of the pump visible light 532 nm was 120 μJ/pulse and the power density at the silicon surface was 0.12 J/cm^2. The C-MOS camera roughly confirmed that this power did not damage the surface. The SFG spectra of the surface were observed at several delay times after the pump light irradiation.

Before the pump light irradiation, I confirmed that there was a sharp peak at 2083.7 cm^{-1} attributed to the stretching vibration of the monohydride species in the SFG spectrum of the sample as shown in Fig. 4.1.2. Then I studied the change of non-resonant and resonant SFG signals as a function of the probe delay time. The monitoring of the non-resonant SFG component is as important as the resonant one for an accurate analysis, since the SFG intensity I_{SFG} is proportional to the square of the absolute value of the nonlinear susceptibility $\left|\chi^{(2)}\right|^2$ as:

$$I_{SFG} \sim \left|\chi^{(2)}\right|^2 = \left|\chi_{NR}^{(2)} + \frac{A_0}{\omega-\omega_0+i\gamma}\right|^2 \qquad (4.3.1)$$

Here, χ_{NR}, is the non-resonant nonlinear susceptibility, and A_0, ω_0 and γ are the strength, resonant frequency and damping constant of the resonant mode, respectively [4].

Figure 4.3.1 shows the SFG spectra at several delay times. The delay time is indicated on the right hand side of each SFG spectrum. Before the pump light irradiation (-53 ps), a symmetric peak is seen at 2083.7 cm^{-1} attributed to the Si-H stretching vibration. After the pump light irradiation, three significant modifications are observed in the SFG spectra. First, the non-resonant signals jump up at ~0 ps, and then decreases gradually with the life time of ~1ns. Second, from 0 ps to 66 ps, the peak rapidly decreases along with the increase of the non-resonant SFG signal background. From 66 ps to 930 ps, the peak recovers gradually. Third, at 930 ps, the peak has a remarkably asymmetric lineshape. All these features except the rapid decrease of the resonant peak from 0 to 66 ps were not observed by Guyot-Sionnest [3]. I discuss the origins of these three modifications below.

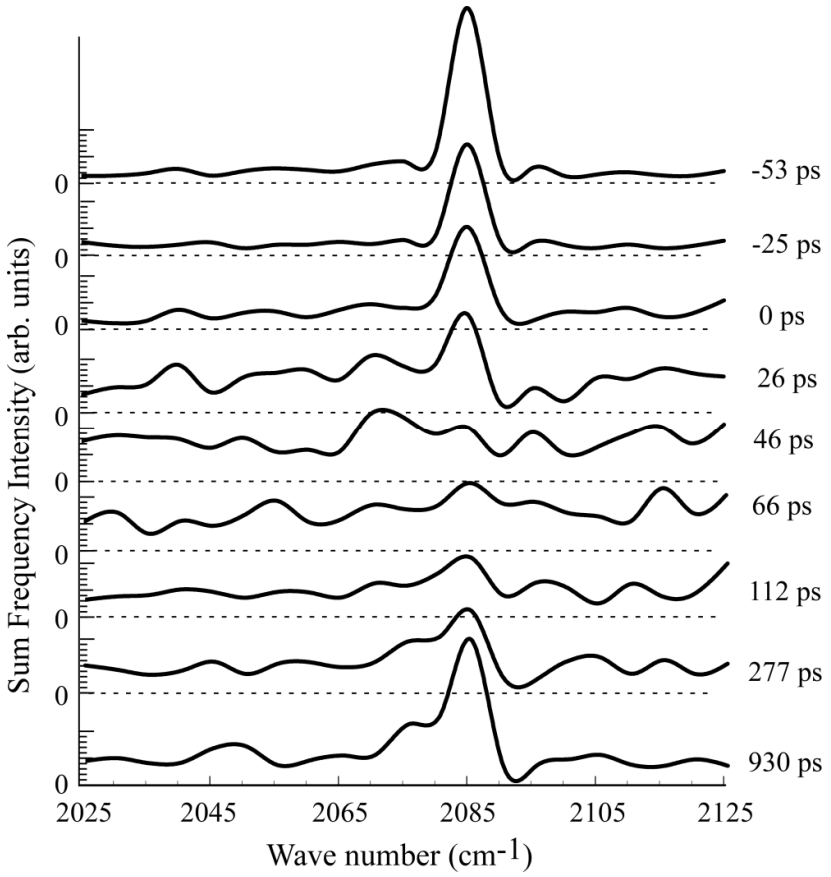

Fig. 4.3.1. SFG intensity spectra with (ppp) polarization combination of a H-Si(111) surface at several probe delay times. The delay times are written on the right hand side of each SFG intensity spectrum.

In order to analyze the change of the non-resonant SFG signal, we measured the SFG intensity as a function of the probe delay time with the IR wavenumber of 2020 cm^{-1} as shown in Fig. 4.3.2(a). The solid curve represents a guide to the eye. This IR probe wavenumber is in off-resonance of the surface Si-H vibrational frequency. In Fig. 4.3.2(a) the signal jumps up at ~0 ps and then decreases gradually with the life time of ~1ns.

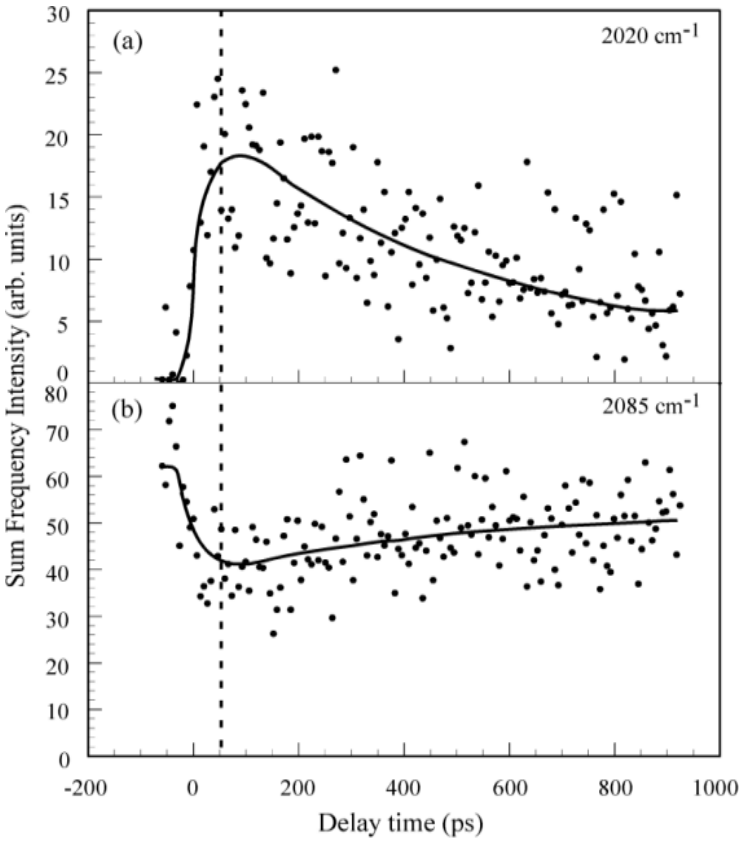

Fig. 4.3.2. SFG intensity as a function of the delay time of the probe visible and IR pulses with respect to the pump visible pulses. The IR light wavenumbers are (a) 2020 cm^{-1} and (b) 2085 cm^{-1}. Solid lines represent guide to the eyes.

The visible pump light energy was E ~120 μJ/pulse and the pump spot area was estimated as a ~ 0.1 mm^2. The density of coming photon *n* can be calculated as:

$$n = \frac{E}{E_p.a.\sigma} \tag{4.3.2}$$

Here, σ ~ 960 nm is a penetration depth of the visible light 532 nm on the silicon surface. I get n ~ 3×10^{21} $cm^{-3}\cdot pulse^{-1}$ and it is high enough to make a plasma state. Thus, as one candidate origin of the enhancement of the non-resonant SFG signal at ~0 ps, the e-h plasma may modify the dielectric constant of the Si substrate at the probe IR light frequency [3]. It has been reported that the modulation of the Fresnel factor for

IR light enhances the SFG signal [3]. However, the life time of the plasma should be smaller than ~100 ps due to the Auger recombination or faster processes like plasmon-phon-assisted recombination [5]. This life time is not compatible with the observed life time of the signal. On the other hand, the modulation of the dielectric constant for visible and SFG light by the plasma is negligible [3, 6].

As another candidate, the nonlinear susceptibility $\chi_{\mathrm{NR}}^{(2)}$ in Eq. (4.3.1) may have been enhanced by the electric field accompanying the e-h pairs excited at ~0 ps, due to the electric field induced sum frequency generation [7]. After that the susceptibility $\chi_{\mathrm{NR}}^{(2)}$ may have decreased due to the relaxation of the e-h pairs. As we mentioned above, the number of the excited carriers reduces via Auger recombination or plasmon-phonon-assisted recombination process in ~100ps, but a small amount of carriers should remain after the recombination. The remaining carriers diffuse slowly with the life time of ~900 ps according to my calculation. This is typical calculation, thus I don't show in detail here. The life time is consistent with the observed life time of the signal in Fig. 4.3.2 (a). I also note that no background SFG signal was observed for the *ssp* polarization (s- *polarized* SFG, s-*polarized* visible, and *p-polarized* IR) combination in a separate experiment. This result suggests that the non-resonant background signal observed for the *ppp* polarization combination in Fig. 4.3.2(a) does not originate from any trivial optical process such as scattering due to surface damages.

As the third candidate origin, I do not deny the effect of the temperature rise on the Si surface. Guyot-Sionnest pointed out that the surface temperature rises immediately after the visible excitation and is kept constant within the timescale of 500ps. The high density phonons excited in the quasi-thermal equilibrium may induce

some broad second-order nonlinearity. However, the non-resonant signal was not reported with the laser power used by Guyot-Sionnest [3]. Thus the non-resonant signal observed in this work may be a high fluence effect by the visible excitation light.

Figure 4.3.2(b) shows the SFG signal as a function of the delay time with the IR wavenumber of 2085cm^{-1}. The SFG signal contains both the resonant and non-resonant contribution. Contrary to the change of the non-resonant SFG signal, the signal drops down to a half of its initial value at ~0ps and slowly recovers after that. This result indicates that the Si-H stretching vibration is modulated strongly after the pump light irradiation.

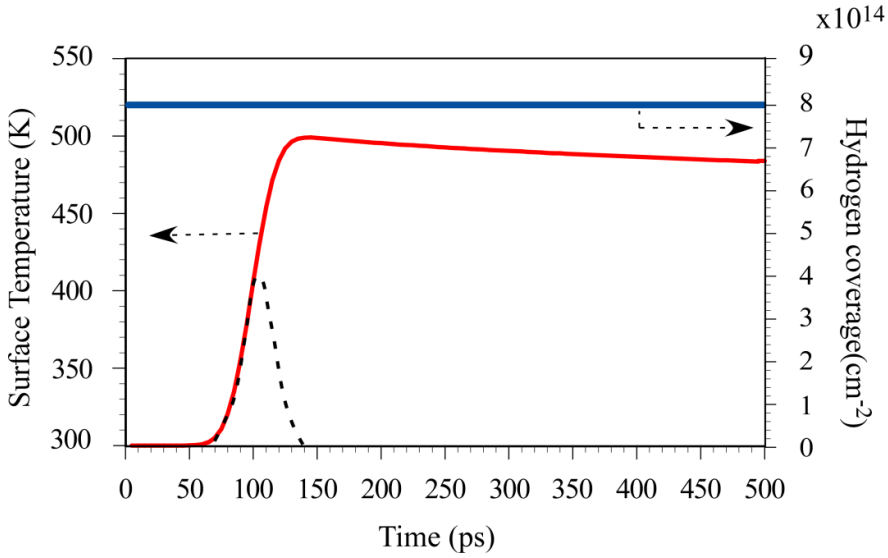

Fig.4.3.4. Temperature and coverage change after pump light irradiation. Incident power: 120μJ/pulse, Radius of the spot: 180μm

Figure 4.3.4 show the calculated change of the surface temperature and hydrogen coverage after the pump light irradiation. The surface temperature could be calculated based on the laser induced thermal desorption (LITD) model suggested by Koehler and George [8]:

$$\frac{\partial T}{\partial t} = D\nabla^2 T + Q \tag{4.3.3}$$

Here, T is the surface temperature [K], t is the time [s], D is the thermal diffusivity [cm^2/s], and Q is the source term [k/s]. The source term is defined as:

$$Q^n_{i,j,k} = \frac{E^n_{i,j,k}}{\rho C_P} \tag{4.3.4}$$

Here, E is the laser power absorbed per unit volume of Si [GW/cm^2], ρ is the density of the material [g/cm^3], and C_p is the heat capacity [J/gK]. The subscripts i, j and k are the step number in z, x, and y directions, respectively, and n is the number of steps. The z direction is defined to be perpendicular to the surface and z is defined to increase in the direction from the surface into the bulk.

The coverage change on the Si surface is given by [8]:

$$\frac{d\theta}{dt} = -\nu_d \theta^n exp\left(-\frac{E_d}{kT}\right) \tag{4.3.5}$$

Here, θ is the coverage, E_d is the activation energy, ν_d is the pre-exponential factor, n is the desorption order, k is the Boltzmann constant, and T is the surface temperature. In my calculation, the surface temperature reaches ~500K at 20ps after the pump light irradiation (Fig. 4.3.4). With the temperature increase, the damping constant γ of the resonant term in Eq. (4.3.1) may increase due to the weak unharmonic coupling between the Si-H vibration and the optical phonon of ~$200cm^{-1}$ [3]. I suggest that the peak of the Si-H stretching vibration is considered to drop due to the broadening. In addition, since the surface temperature is over 300K, the strong unharmonic coupling with the bending mode may also modify the Si-H stretching vibration [9]. The peak of the Si-H vibration disappears at 46 ps in Fig. 4.3.1, while in the work of Guyot-Sionnest [3] the signal was more than a half of the initial intensity at every delay time after the light

pulse irradiation. Indeed the stronger excitation gives rise to more severe modification of the Si-H vibration. Unfortunately, however, I could not estimate the change of the damping constant γ and the peak shift after the pump light irradiation due to the insufficient signal to noise ratio in my results.

The asymmetric lineshape at 930 ps in Fig. 4.3.1 could originate from a non-uniform temperature drop on the surface. However, as pointed out by Guyot-Sionnest [3] and in our previous theoretical work [10], the temperature drop should be very slow after the temperature jump to 500K at 20 ps. For instance, the temperature is calculated to be still at 483K at 500 ps (Fig.4.3.4). The Si surface is rather in quasi-thermal equilibrium up to 1ns, and the peak recovery and the change of the lineshape due to the temperature change is not expected. In order to understand the recovery of the peak and the origin of the asymmetric lineshape, further theoretical study is necessary.

4.4 Time-resolved SFG microscopy

As shown is previous section about the time-resolved SFG spectroscopy, some interesting phenomena occurred after the pump light irradiation. In the excited state of Si surface, the Si-H vibration was modulated. In order to observe directly the dynamics of Si-H on the surface, we also observed the time-resolved SFG intensity images.

Before observing the time-resolved SFG intensity images of the H-Si(111)1x1 surface by using a long distance microscope, I estimated the pump spot size by observing a SFG intensity image of the Si surface with the incident IR light and pump visible light. Fig. 4.4.1(a) shows the SFG intensity image reflecting spatial

distribution of the pump spot. Fig. 4.4.1(b) depicts the profile of the image at dashed line shown in Fig. 4.4.1(a). With Gaussian fitting of the profile, I estimated the FWHM of the pump spot as 304±2 μm.

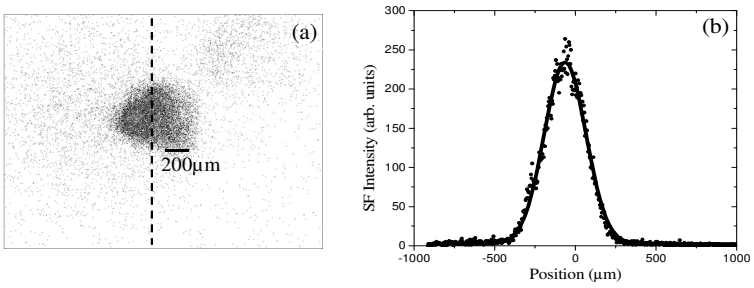

Fig. 4.4.1: The pump pulse spot size image (a) and the profile of the pump pulse spot size image (b).

At several delay times from -53 to 930 ps after the pump light irradiation, I observed non-resonant and resonant SFG intensity images of the Si surface. The results of pump-probe SFG microscopy are shown in Fig. 4.4.2. Figs. 4.4.2(a) to (e) show non-resonant SFG intensity images of the area irradiated by the pump light on the Si surface with the IR light of 2020 cm^{-1} and the delay time from -53 to 930 ps. The dark dots in Fig. 4.4.2 represent SFG photons and the dashed rectangles roughly show the pump-irradiated areas. In Figs. 4.4.2(a) to (e), the number of non-resonant SFG photons at the pump-irradiated area increased from 0 to 26 ps, and then decreased gradually with the life time of ~1 ns. On the other hands, the change of the resonant SFG intensity images with the IR light of 2085 cm^{-1} and the delay time -53 to 930 ps are shown in Figs. 4.4.2(a') to (e'), respectively. From Figs. 4.4.2(a') to (c') the number of the resonant SFG photons decreases due to the pump light irradiation, and then

recovers from Figs. 4.4.2(c') to (e'). These results are consistent with the time-resolved SFG spectroscopy shown in Fig. 4.3.1.

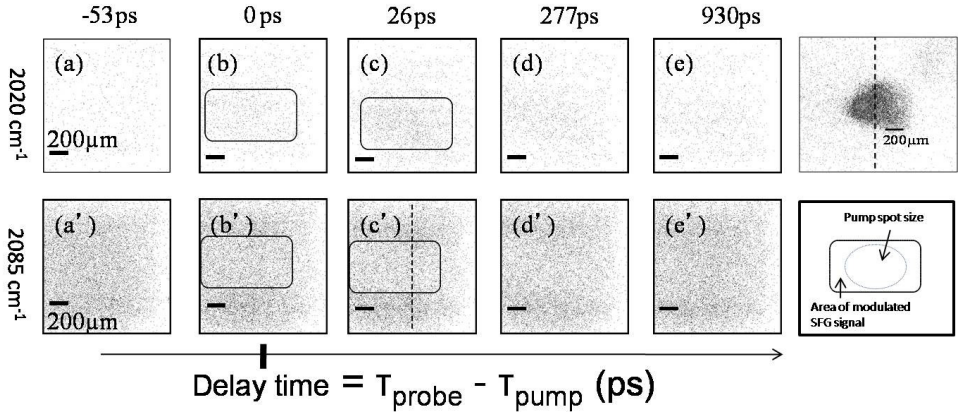

Fig. 4.4.2. Non-resonant SF (a) and resonant SF (b) images as a function of the delay time with the IR light wavenumber of 2020 and 2085 cm^{-1}, respectively.

It is interesting if I compare the pump spot size (Fig. 4.4.1) and the areas of modulated SFG signals in Fig. 4.4.2. The areas of modulated SFG signals are ~ two times larger than the pump spot size. This is not due to the carrier diffusion, since the diffusion constant is ~ 20 cm^2/s [9], and thus the carriers diffuse in only 2 μm at 1 ns after pump light irradiation. Moreover, in my calculation, in-plane propagation of heat is also negligible. The phenomenon may be related to phonon-phonon and/or phonon-vibration coupling at the surface with temperature gradient; the analysis of these images is the topic of future studies.

I show the profiles of the SFG intensity in Figs. 4.4.3(a) and (b) obtained from the non-resonant and resonant SFG intensity images in Fig. 4.4.2, respectively. In Fig. 4.4.3, the vertical axis represents the SFG intensity, and the horizontal axis represents the position corresponding the dashed line in Fig. 4.4.2(c'). The solid curves in Fig. 4.4.3(a) represent Gaussian fitting and those in (b) are a guide to the eye. The

significant change of the SFG signals was observed in the area between vertical dashed lines at the positions of ±350 μm in Fig. 4.4.2. From the delay time 0 ps to 26 ps in Fig. 4.4.3(b), the profile around the center becomes hollow, and then gradually recovers with the life time of ~1 ns.

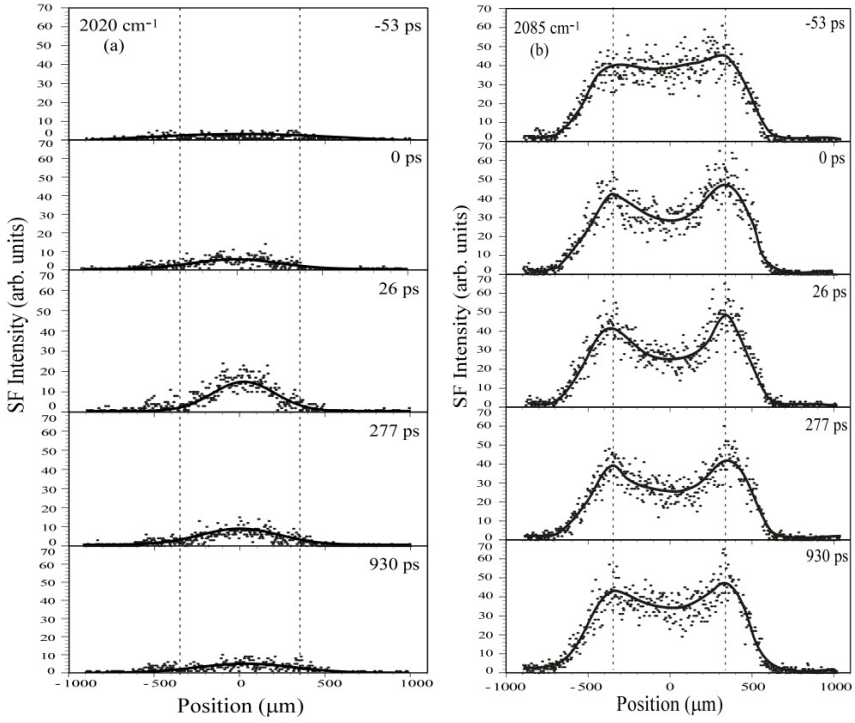

Fig. 4.4.3: The profiles of the time-resolved SFG intensity images with the pump photon energy 2.33 eV; (a) the non resonant signal with IR wavenumber of 2020 cm^{-1}; (b) the resonant signal with IR wavenumber of 2085 cm^{-1}.

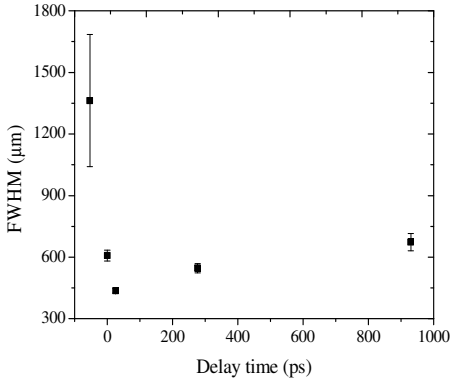

Fig. 4.4.4: The width of the profiles of the non-resonant SFG signals as a function of the probe delay time.

The FWHM of the profiles of the non-resonant SFG signals of Fig. 4.4.3(a) are shown in Fig. 4.4.4 as a function of the delay time from -53 ps to 930 ps. The FWHM of the non-resonant SF signal at -53 ps is ~1363 μm, and then became narrower to ~436 μm at 26 ps. After 26 ps, the FWHM increased gradually, and then became ~673 μm at 930 ps. The FWHM broadens as a function of the delay time after 0 ps. Carrier diffusion along the surface could not be a possible origin of the broadening due to the low diffusivity [9]. As another possibility, the broadening may represent a different decay time for each position, corresponding the spatial distribution of pump light intensity. At the center area irradiated by pump pulses with high fluence, a number of e-h pairs were generated, and thus the pairs quickly decayed due to Auger recombination or PPAR processes. On the other hand, a handful of e-h pairs were generated by pump pulse irradiation with low fluence at the outer area. The decay time of the outer area should be slower than that in the center, and thus FWHM could broaden as a function of time due to the difference in decay times.

4.5 Conclusion

The pump-probe SFG microscopy was successfully constructed for the first time. This technique is very powerful tool for directly observing Si-H species on the surface in two dimensions.

In order to consider the effect of excited e-h pairs on vibrational dynamics of Si-H species, the time resolved SFG spectroscopy of the H-Si(111) 1x1 surface was performed at several delay time of pump light irradiation. The visible pump light irradiated the Si surface, after that the SFG spectra was taken at several probe delay

times. The power of the pump visible light at 532 nm was 120 μJ/pulse. The power of the probe visible and IR light were 20 and 120 μJ/pulse, respectively. The polarization combination of SFG signal, visible and IR light were *p*, *p*, and *p*, respectively. Before the pump light irradiation, the symmetric peak attributed to the Si-H stretching mode appeared. After visible pump light irradiation non-resonant SFG signal increased at probe delay time ~0 ps, and then decreased with the life time of ~1 ns. From 0 to 66 ps, the Si-H peak rapidly decreased and after that gradually recovered. At 930 ps after pump light irradiation, the Si-H peak had a remarkably asymmetric lineshape.

In order to clarify the modulation of Si–H bonds induced by light pulses, I observed time-resolved SFG intensity images of a H–Si(111)1 × 1 surface. After visible pump light irradiation, non-resonant SFG signal increased at probe delay time 0 ps, and then decreased over a life time of ~1 ns. The resonant SFG signal with 2085 cm^{-1} reduced dramatically at 0 ps and then gradually recovered. This result is consistent with the time resolved SFG spectroscopy. The spatial width of the non-resonant signal was larger than that of the pump laser beam and was a function of the delay time.

References

1. Mao, M.Y., et al., *Kinetics of molecular hydrogen dissociative adsorption on Si(111) studied by sum-frequency vibrational spectroscopy and second harmonic generation.* Physical Review B, 2001. **64**(3): p. 035415.
2. Higashi, G.S., et al., *Ideal hydrogen termination of the Si (111) surface.* Applied Physics Letters, 1990. **56**(7): p. 656-658.
3. Guyot-Sionnest, P., *Effect of substrate photoexcitation on the dynamics of the Si-H stretch for Si(111)/H.* Journal of Electron Spectroscopy and Related Phenomena, 1993. **64–65**(0): p. 1-9.
4. Ye, S., et al., *Stability of the Si–H bond on the hydrogen-terminated Si(1 1 1) surface studied by sum frequency generation.* Surface Science, 2001. **476**(1–2): p. 121-128.
5. Rasolt, M., A.M. Malvezzi, and H. Kurz, *Plasmon-phonon-assisted electron-hole recombination in silicon at high laser fluence.* Applied Physics Letters, 1987. **51**(26): p. 2208-2210.
6. Mao, M.Y., et al., *Characterization of hydrogen-terminated Si(111) surfaces by sum-frequency surface vibrational spectroscopy.* Applied Physics Letters, 1999. **75**(21): p. 3357-3359.
7. Glinka, Y.D., et al., *Hot-phonon-assisted absorption at semiconductor heterointerfaces monitored by pump-probe second-harmonic generation.* Physical Review B, 2008. **77**(11): p. 113310.
8. Koehler, B.G. and S.M. George, *Laser-induced desorption of H2 from Si(111)7 × 7.* Surface Science, 1991. **248**(1–2): p. 158-172.
9. Rowe, M.W., et al., *Picosecond photoelectron spectroscopy of excited states at Si(111) √3 × √3 R30° -B, Si(111)7×7, Si(100)2×1, and laser-annealed Si(111)1×1 surfaces.* Physical Review B, 1993. **47**(4): p. 2048-2064.
10. Miyauchi, Y., H. Sano, and G. Mizutani, *Numerical analysis of second harmonic intensity images of a H–Si(1 1 1) surface after UV light pulse irradiation.* Applied Surface Science, 2008. **255**(5, Part 2): p. 3442-3446.

Chapter 5: SFG spectra of the flat H-Si(111) surface heated at high temperature

As mentioned in chapter 1, isothermal desorption of hydrogen on the Si(111) surface is one of the targets in order to understand the desorption mechanism at the boundary of IR irradiated area. Furthermore, knowing how the thermal desorption proceeds on the H-Si(111) 1x1 surface is critical for understanding the elementary steps in the CVD growth of absorbates on Si substrates. In this experiment, I obtained isothermal desorption spectra of the H-Si(111)1x1 surface at temperatures of ~711, 732, 752 and 771 K by probing the vibrational resonant optical SFG. These temperatures were calibrated from the I-V curve measured in the Si(111) sample [1]. Hydrogen desorption requires the breaking of the bonds. Thus, the change of the bonding states during the desorption process must be investigated. Si-H bonds on the Si(111)1×1 surface have big dipole moments and interact with each other via dipole coupling [2, 3]. Thus, the bonds are influenced not only by the electronic states in the Si-H structures, but also by the coverage and the domain structures [3]. I used coherent potential approximation (CPA) method in order to calculate the dipole-dipole interaction among Si-H bonds.

5.1 SFG spectra of the H-Si(111)1x1 surface heated at high temperatures

After treated with NH_4F as shown in Section 3.1, the H-Si(111)1x1 surface was introduced immediately into an UHV chamber with pressure of ~10^{-5} Pa. At each temperature of heating, the sample was heated for ~10 s several times and then heated for a few tens of seconds. After each heating, the SFG spectrum was taken at room temperature. The polarization of the SFG, visible and IR light beams were *s*, *s* and *p*, respectively. Figure 5.1.1 shows the SFG spectra of the H-Si(111)1x1 surface after each time of heating at 711 K. The sharp peak at 2085 cm^{-1} is attributed to the stretching vibration of monohydride on the Si surface. The red dots are experimental results and the solid lines are Gaussian fitting. At room temperature, the hydrogen coverage is considered as 1 monolayer (ML).

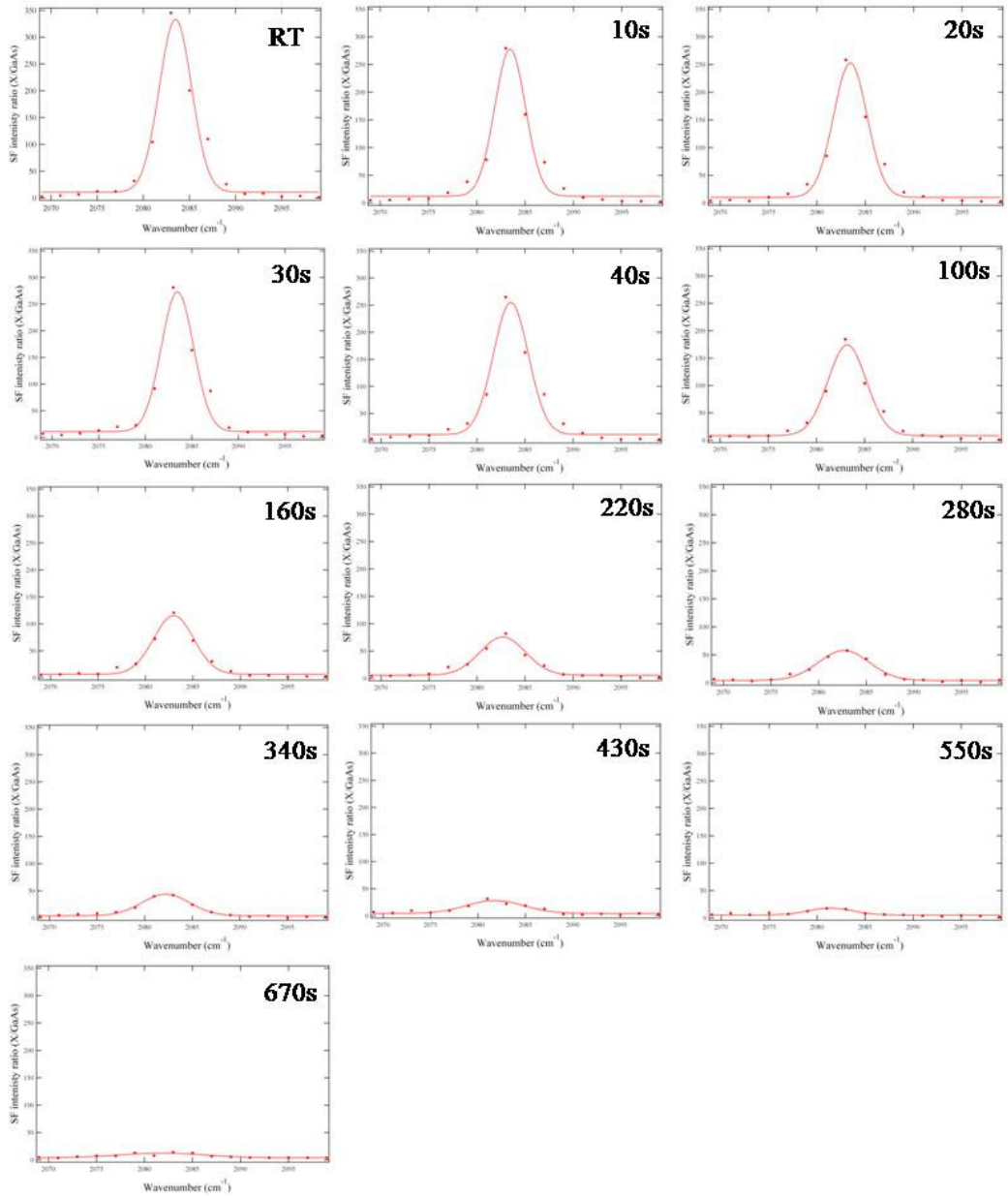

Fig. 5.1.1. SFG spectra during the hydrogen desorption from the H-Si(111)1x1 surface at ~711 K. The points are experimental results. The solid lines are Gaussian fitting curves.

Hydrogen desorption requires the breaking of the bonds. Thus, the change of the bonding state during desorption process must be investigated. Si-H bonds on the Si(111)1x1 surface have big dipole moments and interact with each other via dipole coupling [2, 3]. Thus, the bonds are influenced not only by the electronic states in the Si-H structures, but also by the coverage and the domain structures [3]. I used a theory of dipole coupling to analyze the modulation of Si-H vibrations [4]. A simulation of the dipole-dipole interaction using coherent potential approzimation (CPA) was developed by Persson and Ryberg [5]. The calculation of the nonlinear susceptibility based on the CPA method has been reported by Backus [6], Backus and Bonn [7], and Cho, Hess, and Bonn [8]. The calculated susceptibility well described an experimental SFG spectrum. In this part, I calculated the non-linear susceptibility of the H-Si(111)1x1 surface using their method. I will explain in detail my surface model and how I choose the parameters for simulating the H-Si(111)1x1 surface.

5.2. Coherent potential approximation (CPA) method

The derivation of nonlinear susceptibility χ by a simulation of dipole-dipole interaction has already been reported by several researchers [6-8]. Here I only summarize the theory and explain how I apply this method and chose parameters for the calculation of the H-Si(111)1×1 surface.

When an outer field E_i irradiates the sample, the dipole moment of an oscillator at $\vec{x}_i$ on a surface is written as

$$p_i = \alpha(E_i - \sum_{j \neq i} U_{ij} p_j), \tag{5.2.1}$$

where $U_{ij}p_j$ is the electric field at $\vec{x}_i$ from a dipole p_j at $\vec{x}_j$. U_{ij} is written as

$$U_{ij} = \frac{1}{|\vec{x}_i - \vec{x}_j|^3} + \ldots. \tag{5.2.2}$$

If the system has translational invariance, the Fourier transformed dipole moment p_q and the total polarizability α_0 is

$$p_q = \frac{\alpha}{1+\alpha\widetilde{U}(\vec{q})} E_q \equiv \alpha_0(\vec{q},\omega)E_q. \tag{5.2.3}$$

The $\widetilde{U}(\vec{q})$ is written as

$$\widetilde{U}(\vec{q}) = \sum_j U_{ij} \exp(-\mathrm{i}\vec{q}\cdot(\vec{x}_i - \vec{x}_j)). \tag{5.2.4}$$

Here $\vec{q}$ is a vector in the momentum space [4].

If the translational invariance of the system is broken due to the coexistence of isotopes or the existence of vacancy sites, it is difficult to obtain the polarizability analytically. Thus, Persson and Ryberg proposed a simplified method using coherent potential approximation (CPA) [5]. In CPA, the ensemble of all possible configurations is represented by a system based on an average molecule at each site.

According to the CPA theory, the ensemble average polarizability α on a surface can be calculated by the self-consistent equation [5-8]:

$$\sum_\mu \frac{c_\mu \alpha_\mu}{1+(\alpha_\mu - \alpha)Q} = \alpha. \tag{5.2.5}$$

Here α_μ is the polarizability of an oscillator μ, and c_μ represents the coverage of the oscillator μ on a solid surface. When I calculated the average polarizability α, I assumed that oscillators with only one singular Si-H vibrational mode are on the H-Si(111) surface. The Q value [5-8] is an integral over the Brillouin zone of the adsorbate lattice cell:

$$Q = \frac{1}{A^*}\int_{BZ} d^2q \frac{\widetilde{U}(\vec{q})}{1+\alpha\widetilde{U}(\vec{q})} \tag{5.2.6}$$

where, A^* is the area of the 1st Brillouin zone. In order to calculate the Q value, I approximated $\widetilde{U}(\vec{q})$ as the quadratic function

$$\widetilde{U}(\vec{q}) = U_0[1 + A\frac{q}{q_0} + B(\frac{q}{q_0})^2] \quad (5.2.7)$$

with the direction q[10]=q[11] in case of the Si surface. The q_0 is the radius of a circular area πq_0^2, and the latter is the same as the area $A^* = \left[\frac{2\pi}{a}\right]^2$. Here a is the distance among the Si-H oscillators, and it is 3.84 Å [3]. I used eq. (5.2.4) to calculate the values of $\widetilde{U}(\vec{q})$ from the distance.

I use a model of Si atoms on the 1x1 surface as shown in Fig. 5.2.1. I consider the H-Si dipole labeled A is effected by neighbors labeled 1, 2, 3, 4, 5, 6. q(01) is chosen as a symmetric axis. Therefore, the dipoles on the perpendicular h axis do not interact with the A dipole. The dipoles on the *k* and *l* axes are considered as the same interaction with A. The dipoles on the q(10) and q(11) axes are considered as the same interaction with A. Similarly, the dipoles marked with 2, 4, 5 and 6 have the same interaction with A, respectively.

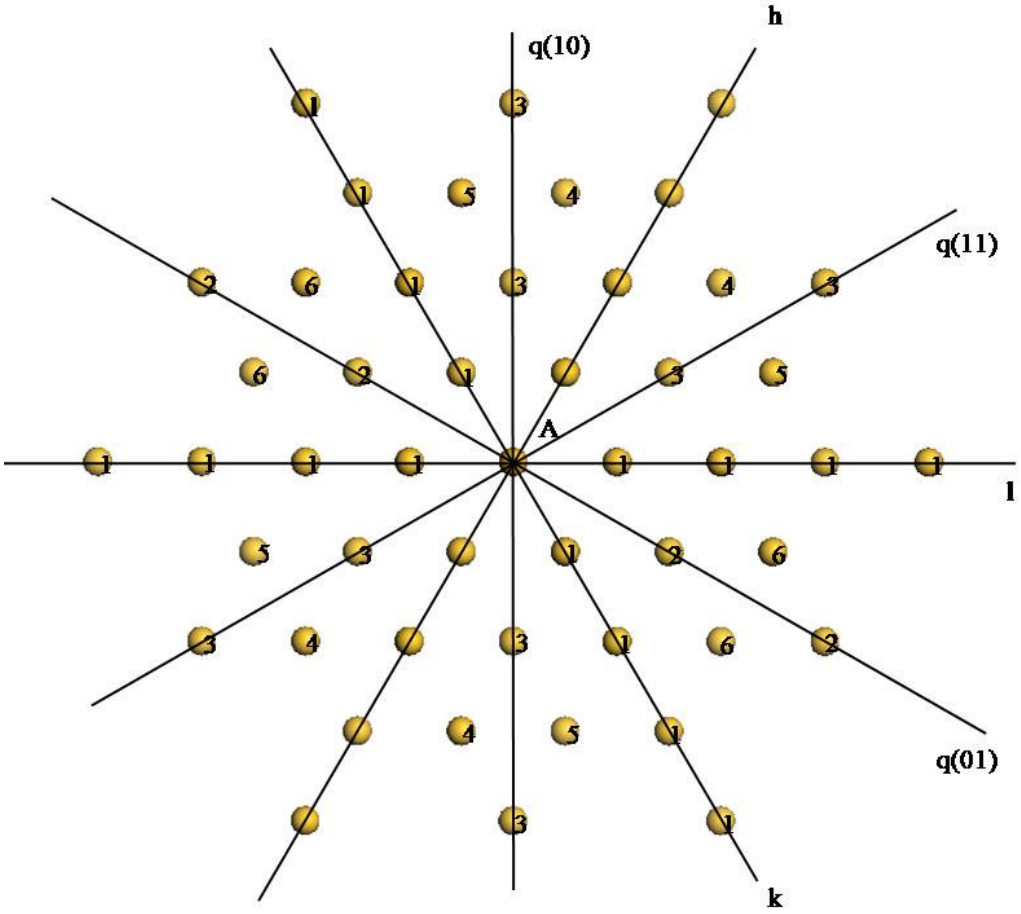

Fig. 5.2.1. Model for calculation of the dipole interaction on the Si(111)1x1 surface. A dipole is affected by neighbors labeled 1, 2, 3, 4, 5 and 6.

Interaction potential between the dipole i and j can be expressed by an equation:

$$U_{ij}(q) = \frac{1}{|x_i - x_j|^3} e^{i\vec{q}(\vec{x}_{ij})} = \frac{1}{|x_i - x_j|^3} \times \left(e^{iqx_{ij}} + e^{-iqx_{ij}}\right) = \frac{1}{|x_i - x_j|^3} \times 2 \times \cos\left(qx_{ij}\right) \tag{5.2.8}$$

If I consider the image plane of dipole, the dipole A is affected by not only the dipole 1 but also the dipole 1' as described in fig. 5.2.2 below. The distance between 1 and 1' is *d* which was defined as the height above the image plane of the center of mass of the

Si-H bond. In this calculation, I suggest that *d* varies from 0 to infinity. *m* is the image plane.

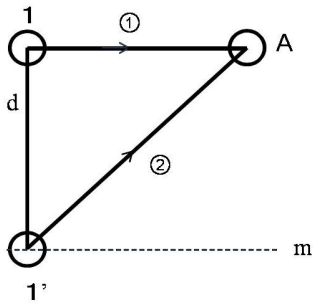

Fig. 5.2.2: The description of dipole interaction between 1 and 1' with A dipole. d is the height above the image plane of the center of mass of the Si-H bond. m is image plane.

In this case, the interaction potential of neighbor dipoles (from 1 to 6) on A dipole can be written as:

$$U_{1A} = \sum_{n=1}^{\infty}\sum_{i=1}^{\infty}\left(\frac{1}{(na)^3}+\frac{1}{((na)^3+d^2)^{\frac{3}{2}}}\right)\times 2\times cos\left(q\times(na)\times\frac{\sqrt{3}}{2}\right) \quad (5.2.9)$$

$$U_{2A} = \sum_{n=1}\sum_{i=1}\left(\frac{1}{(n\sqrt{3}a)^3}+\frac{1}{\left((n\sqrt{3}a)^2+d^2\right)^{\frac{3}{2}}}\right)\times 2\times cos\left(q\times n\sqrt{3}a\right) \quad (5.2.10)$$

$$U_{3A} = \sum_{n=1}\sum_{i=1}\left(\frac{1}{(n\sqrt{3}a)^3}+\frac{1}{\left((n\sqrt{3}a)^2+d^2\right)^{\frac{3}{2}}}\right)\times 2\times cos\left(q\times n\frac{3}{2}a\right) \quad (5.2.11)$$

$$U_{4A} = \sum_{n=1}\sum_{i=1}\left(\frac{1}{(n\sqrt{7}a)^3}+\frac{1}{\left((n\sqrt{7}a)^2+d^2\right)^{\frac{3}{2}}}\right)\times 2\times cos\left(q\times n\frac{\sqrt{3}}{2}a\right) \quad (5.2.12)$$

$$U_{5A} = \sum_{n=1}\sum_{i=1}\left(\frac{1}{(n\sqrt{7}a)^3}+\frac{1}{\left((n\sqrt{7}a)^2+d^2\right)^{\frac{3}{2}}}\right)\times 2\times cos\left(q\times\sqrt{3}na\right) \quad (5.2.13)$$

$$U_{6A} = \sum_{n=1}\sum_{i=1}\left(\frac{1}{(n\sqrt{7}a)^3}+\frac{1}{\left((n\sqrt{7}a)^2+d^2\right)^{\frac{3}{2}}}\right)\times 2\times cos\left(q\times\frac{3\sqrt{3}}{2}na\right) \quad (5.2.14)$$

The results of $\tilde{U}(\vec{q})$ are shown as solid dots in Fig. 5.2.3. The vertical axis is the strength of $\tilde{U}(\vec{q})$, and the horizontal axis represents the wavenumber q along [11] direction. By fitting $\tilde{U}(\vec{q})$ with eq. (5.2.7), I obtained U_0=0.17 Å^{-3}, A=-3.04, and B=1.56. I note that I calculated the $\tilde{U}(\vec{q})$ while changing the height of the image plane, but there were few differences in $\tilde{U}(\vec{q})$. Thus, I neglected dipoles on the image plane in this calculation.

Then, I calculated the integral Q after having $\tilde{U}(\vec{q})$ [5-8].

The polarizability α_μ in Eq. (5.2.5) is written as

$$\alpha_\mu = \alpha_e + \frac{\alpha_v}{1-(\omega/\omega_\mu)(\omega/\omega_\mu+i\gamma)}. \qquad (5.2.15)$$

Here α_e is the electronic polarizability, α_v is the vibrational polarizability, ω_μ is the resonance frequency and γ is the damping constant. Chabal *et al.* estimated the value of α_e as 5.7 Å^3 [3]. The dynamic dipole moment was also measured as 0.1D [9], and thus α_v should be 0.043 Å^3 [10].

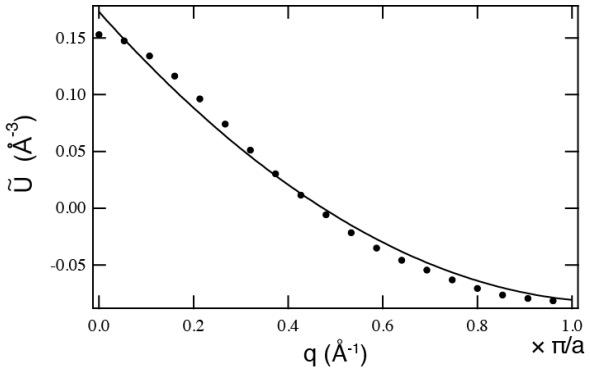

Fig.5.2.3. $\tilde{U}(\vec{q})$ of the dipole field for [11] direction in the two-dimensional Brillouin-zone on a Si(111) surface. The horizontal axis represents the wavenumber q along [11] direction and the vertical axis shows the strength of Fourier transformed $\tilde{U}(\vec{q})$. We obtained $\tilde{U}(\vec{q})$ by calculating eq. (5.2.4) from the distance between 3.84 Å of the Si-H oscillators. The results are shown as solid dots. By fitting them with eq. (5.2.7), we obtained the parameters U_0=0.17 Å^{-3}, A=-3.04, and B=1.56.

I chose a theoretical peak width of 0.1 cm^{-1}. The experimental peak width was observed as 3.2 cm^{-1} at 1ML, but this is an extrinsic width due to my optical system, especially my OPG/DFG source. The intrinsic width of the Si-H bond was 0.9 cm^{-1} at room temperature [11]. The width was broadened due to the coupling of the Si-H stretching vibration with a bending mode and an optical phonon [12]. In this calculation, I treat only one Si-H oscillator, and thus I should consider only lifetime broadening. The observed lifetime broadening of the Si-H vibrational peak width is less than 0.005cm^{-1} [3]. However, this width was much smaller than the limitation of wavenumber step size in my calculation. I therefore set the width as 0.1cm^{-1} in this calculation. I set another adjustable parameter ω_μ as 2079.8 cm^{-1}. After obtaining the average polarizability α by calculating Eqs. (5.2.5) and (5.2.6), I got the total polarizability α_0 by inserting α into Eq. (5.2.3).

Based on this theory and the model of dipole system, I calculated the dipole-dipole interaction. The results will be presented in the next section.

5.3. Calculation of dipole-dipole interaction among Si-H species on the H-Si(111) surface

The coverage θ of the hydrogen atoms on the H-Si(111) surface could be approximately expressed as [13]:

$$\theta \propto \sqrt{I_{SFG}} \propto \chi_v \qquad (5.3.1)$$

However, in the case of strong dipole coupling between oscillators [6-8, 14], the relation in Eq. (5.3.1) is not correct any more. Based on my model of calculation, I calculated the θ-χ_v relation of the hydrogenated Si surface and the result is shown as the solid curve in Fig. 5.3.1. The value of χ_v is not proportional to the coverage θ in a precise

sense. I use this relation in Fig. 5.3.1 for determining the coverage in this study.

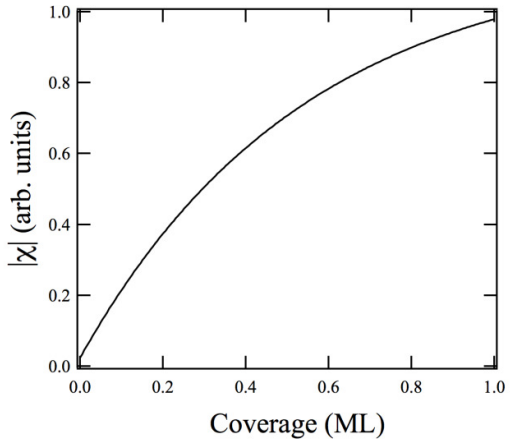

Fig. 5.3.1: Nonlinear susceptibility as a function of coverage on a Si(111)1×1 surface calculated by coherent potential approximation (CPA) method. The horizontal axis represents coverage, and the vertical one shows the absolute value of the nonlinear susceptibility χ. In this calculation, we set the wavenumber of an isolated Si-H oscillator as 2079.8 cm^{-1}, and the peak width as 0.1 cm^{-1}. As mentioned previously, we also set the distance between Si-H oscillators as 3.84 Å, and the permanent and dynamic dipoles as 5.7 and 0.043 $Å^3$, respectively. We simulated the nonlinear susceptibility using the calculation method reported by Backus and Bonn [7].

As shown in fig. 5.1.1, the hydrogen coverage on the H-Si(111) 1x1 surface was reduced respect to time when it was heated at 711 K. Figure 5.3.2 presents the hydrogen coverage when the SFG signals were fitted with eq. (5.3.2). Error bars are standard deviations.

$$\chi^{SFG} = \chi^{NR} e^{i\varphi} + \frac{\chi_v}{\omega - \omega_v + i\gamma} \tag{5.3.2}$$

Here, χ^{NR}, χ_v, φ, ω_v, and γ are nonlinear susceptibility, total hyperpolarizability of the Si-H molecules, phase difference between the resonant and non-resonant terms, the resonant frequency, and the damping constant of the resonant mode, respectively [13]. The solid curve represents the result of fitting by second-order hydrogen desorption as

$\frac{d\theta}{dt} = -k\theta^2$. Here, *t* is the heating time and *k* reprents the desorption rate.

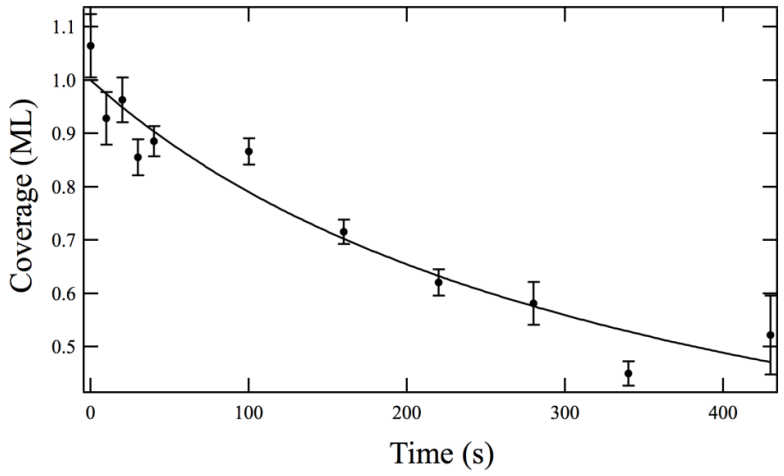

Fig. 5.3.2. An isothermal desorption spectrum from a Si(111)1×1 surface at 711 K. The horizontal axis shows time and the vertical represents hydrogen coverage on the Si surface. We fitted the SFG spectra at each time by eq. (5.3.2), obtained the nonlinear susceptibility χ, and then calculated the coverage using the χ-coverage relation shown in Fig. 5.3.1. The solid dots are experimental results, and the error bars represent the standard deviation. The solid curve was fitted to the experiment by $\frac{d\theta}{dt} = -k\theta^2$.

The reduction of the coverage is well-described as second order desorption, and thus at least the desorption process is consistent with that on the Si(111)7x7 surface [15-17]. In the second-order process, one hydrogen atom leaves a Si atom and diffuses toward another Si-H site where they combine to form a dihydride ($Si-H_2$). For a while, the dihydride state sustains. Finally the hydrogen atoms go beyond the highest potential barrier in the reaction coordinate, associate themselves with each other and desorb from the Si atom [18]. In this way, the hydrogen recombinative desorption occurs at a single Si atom. The vacancy sites are thus created randomly on the Si surface in a microscopic scale. The remaining Si-H bonds on the surface do not have translational invariance due to the random vacancy sites, and theoretically their vibration should be

reproducible by the CPA method.

The modulation of the polarizability was investigated by calculating the change of the Si-H vibrational peak shapes in the SFG spectra. Figures 5.3.3 (a) and (b) show experimental and theoretical SFG spectra as a function of the coverage. While the SFG spectra in Fig. 5.3.3(a) are in the region from 2070 to 2100 cm^{-1}, those in Fig. 5.3.3(b) were drawn in the region from 2080 to 2085 cm^{-1}. In both panels, peaks are seen at 2083.7 cm^{-1} at 1ML, and then the peak intensities weaken at lower hydrogen coverages. The solid curves in Fig. 5.3.3(a) are the fitting curves following the eq. (5.3.2). The peak positions of the spectra are shifted toward the lower frequency side. The experimental peaks broadened significantly at coverage below 0.85 ML, while the theoretical peaks maintained their sharpness. A peak shift and inhomogeneous broadening were observed in the SFG spectra at temperatures from 711 to 771 K. I note that the SFG measurements were performed at room temperature with sufficient cooling down after the heating, and thus these modulations are not due to coupling with phonons [12].

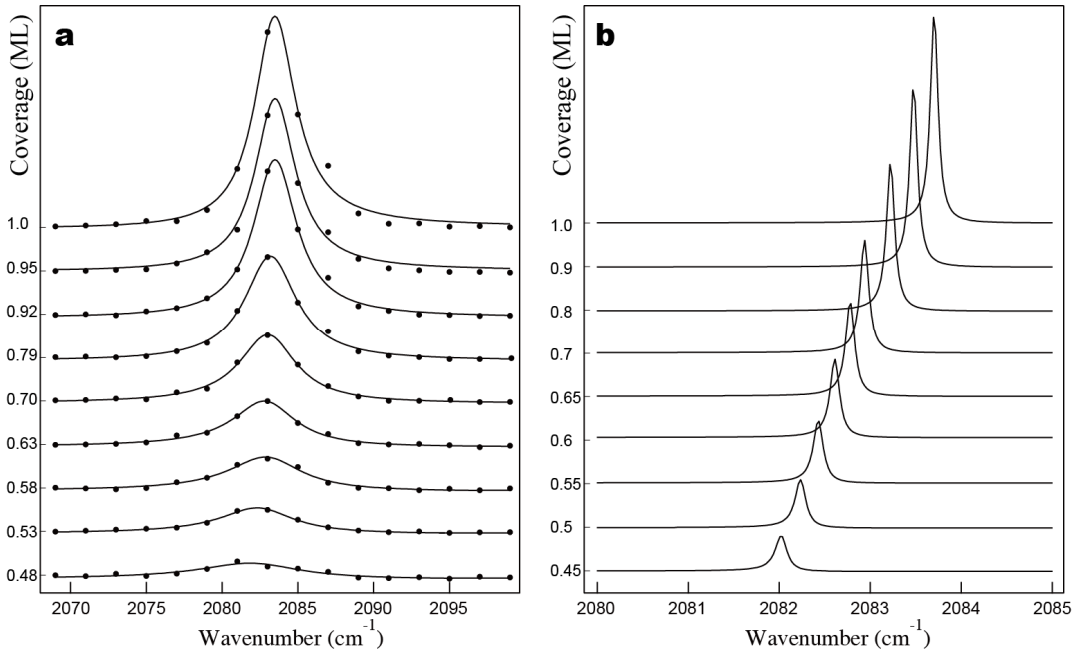

Fig.5.3.3: (a) Experimental and (b) calculated SFG spectra as a function of the coverage. The horizontal axis represents the wavenumber of the IR probe light and the vertical axis shows the SFG intensity. Hydrogen coverage is denoted on the left side of each SFG spectrum. The solid dots represent the observed SFG intensity and the curve represents the fitting by eq. (5.3.2). The SFG spectra were observed at room temperature after heating the sample to 711 K. The polarizations of SFG, visible, and IR light were s, s, and p, respectively. The wavelength of the visible light was 532.1nm. The solid curves shown in (b) represent the SFG intensity calculated by the CPA method.

Figures 5.3.4 (a) and (b) show the peak positions and the widths of the SFG spectra in Fig. 5.3.3 as a function of coverage. The points represent experimental results, while solid curves show theoretical ones. The full width of half maximum (FWHM) of the experimental peak width is 3.2 cm^{-1} at 1 ML, as shown in Fig. 5.3.4(b). The incident line width was incorporated in the theoretical width in Fig. 5.3.4(b) using the Voigt function as:

$$I^{SFG} \propto \left|\int_{-\infty}^{\infty} G(\omega_{IR}-\tau)\chi^{(2)}(\tau)d\tau\right|^2. \qquad (5.3.3)$$

Here $G(\omega)$ is a Gaussian function with the full width at half maximum of 3 cm^{-1}. The inset in Fig. 5.3.4(b) shows the calculated peak width with a magnified vertical scale.

In Fig. 5.3.4(a), the red-shifting theoretical curve is quantitatively consistent with the experimental peak positions. This indicates that the peak shift is attributed to the modulation of the polarizability of the singular Si-H oscillators via dipole coupling with the increase of vacancy sites.

On the other hand, in Fig. 5.3.4(b), the experimental peak widths are far wider than the theoretical ones. In the inset of Fig. 5.3.4(b), the calculated width is seen to increase only by 0.001 cm^{-1} order as a function of the hydrogen deficiency via dipole coupling. The calculated width is ~3.25 cm^{-1} at 0.45 ML. However, the experimental width broadenings at coverages below 0.79 ML are far wider than the calculated ones. As an example, the experimental width was ~8 cm^{-1} at 0.48 ML.

I note that the width broadening of ~1 cm^{-1} in the IR spectra of the H and D terminated Si(111) surface was mainly due to the dipole couplings of Si-H and Si-D molecules [2]. The experimental broadening of ~8cm^{-1} observed in this study is much larger than ~1 cm^{-1}, and thus, the observed broadening at low coverages in Fig. 5.3.3(a) cannot be explained by the dipole coupling effect.

As the first step toward understanding the origin of the width broadening, I needed to ascertain whether the broadening should be classified as homogeneous or inhomogeneous one. I fitted the experimental vibrational peaks by Gaussian and Lorentzian functions, and then evaluated the Pearson's correlation coefficient *r* among the experimental and fitted curves [19]. At 1 ML, the coefficient *r* for the case of a Gaussian curve was 0.980, while the *r* for the case of a Lorentzian curve was 0.993. Thus, the experimental peak at 1 ML was judged to have pure homogeneous broadening.

With reduction of coverage, the coefficient *r* for the case of Gaussian curves gradually increased, becoming ~0.99 at 0.58 ML, while the *r* for the case of Lorentzian curves does not change. This indicates that the spectra contained inhomogeneous broadenings at coverages lower than 0.58 ML.

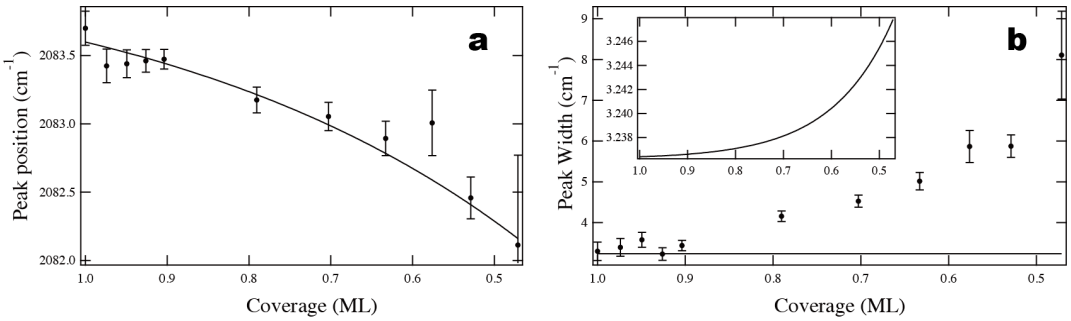

Fig. 5.3.4. (a) Peak position and (b) peak width of Si-H stretching vibration as a function of coverage. The horizontal axis shows the coverage obtained by fitting with eq. (5.3.2). Solid dots shown in (a) and (b) are the observed peak positions and widths. The error bars are standard deviations. Solid curves shown in (a) and (b) represent theoretical peak width and position, respectively. In (b), we show the width of a Voigt function convoluting intrinsic theoretical width and extrinsic width ~3cm^{-1} corresponding to the optical system. The inset shows theoretical peak width with the magnified vertical scale of (b).

According to Chabal *et al.*, there are three candidate origins of the inhomogeneous broadening of hydrogen vibration on a Si surface [3].

(a) Point defects such as foreign atoms and local structural defects in the microscopic scale.

(b) Mesoscopic defects due to finite size domains and the boundary

(c) Extrinsic macroscopic inhomogeneities such as spatial and/or temporal variations of temperature, coverage, distribution, domain size, and density of point defects.

Considering the candidate (c), the inhomogeneous broadening observed in this study is not due to macroscopic inhomogeneities. With ~5 μm resolution, I observed

SFG microscopic images of an area 200×200 μm^2 on the Si(111) surface at several surface temperatures as shown in Fig. 5.3.5. The SFG intensity decreased at higher temperatures but showed isotropic spatial distribution at and below 728 K. This result indicates that candidate (c) is not feasible as the origin of the broadening.

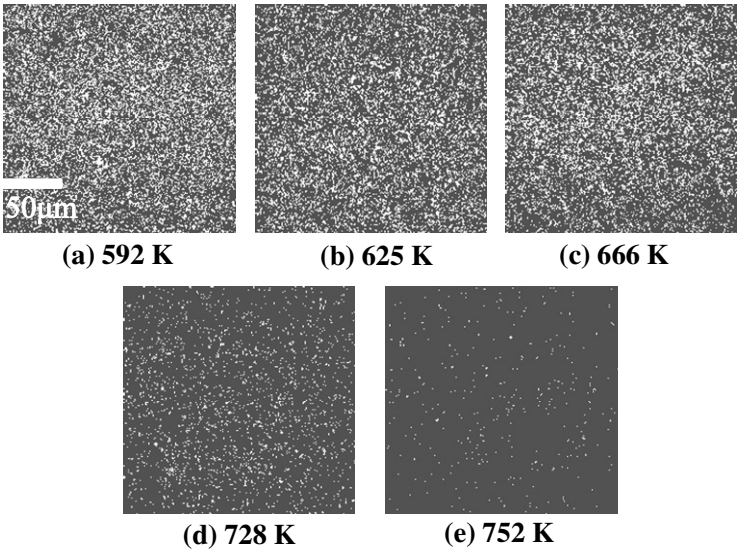

Fig.5.3.5: SFG intensity images of the H/Si(111) surface after heating in 10s with several temperatures.

Next, I discuss candidate (b). According to the simulation by Chabal et al., the vibrational peak of Si-H moves with dipole coupling between domains toward the red side with decrease of the domain size [3]. Due to the coupling between the domains, a Si-H peak on the H-Si(111) surface can have asymmetric inhomogeneous broadening. However, this inhomogeneous width was 0.07 cm^{-1} at 70 K on the surface observed by ATR-FTIR measurement with 0.04 cm^{-1} resolution [2], and it was far smaller than the width ~8 cm^{-1} at 0.48 ML in this study. In fact, no modulation of the Si-H vibrational mode caused by the change of domain size was observed by Luo *et al.* [2]. Thus, candidate (b) also can be excluded as the origin of the broadening.

The only remaining candidate for the origin of the inhomogeneous broadening is point defects, as categorized in (a). Since the 1×1 structure remains at least below 738 K, only local structural defects can influence the Si-H vibration. Point defects such as oxidization due to adsorption of impurities are not applicable here because the sample was kept in a high vacuum of 10^{-5} Pa. Ye and his colleagues used SFG to study laser-induced oxidization of the Si surface in ambient conditions [13]. With an increase of laser irradiation time, the nonlinear susceptibility χ_v of the SFG signal reduced, but neither peak shift nor width broadening was observed in the spectra. Thus, oxidization due to impurities adsorption does not modify the peak shape, and local structural defects at the vacancy sites remain as the origin of the broadening.

In their discussion of candidate origins, Chabal et al. [3] note that point defects could be the main origin of the experimental inhomogeneity. In addition, I point out that the dangling bonds created after hydrogen desorption may influence the electronic states and orientation of neighboring Si-H bonds. The frequency of a Si-H oscillator could be changed with an increase of neighboring dangling bonds. Hence, I suggest that while oxidization on the surface is not adaptable, the point defects and/or the dangling bonds are feasible candidates as origins of the inhomogeneity. In order to understand the inhomogeneity more clearly, I should use a quantum mechanical simulation to analyze the frequency change of a Si-H oscillator as a function of the number of neighboring dangling bonds. This will be the subject of a future study.

The experimental inhomogeneity indicates that many kinds of Si-H oscillators emerged on the surface at lower coverages. On the other hand, the peak position shift observed by the experiment is in good agreement with my calculations. Thus, I suggest that the many kinds of oscillators corresponding to the experimental

inhomogeneity could be approximately treated as a single oscillator modeled by my calculation, so far as their mean susceptibility is concerned.

5.4 Conclusion

In this experiment, I obtained isothermal desorption spectra of the H-Si(111) 1×1 surface at temperatures of ~711, 732, 752 and 771 K by probing directly the vibrationally resonant optical SFG spectra. This is the first time the reduction of hydrogen coverage on the H-Si(111) 1×1 surface was measured from one monolayer. I have calculated modulation of the Si-H vibrational mode on a Si(111) 1×1 surface by a partial absence of Si-H bonds using CPA method, and made a comparison between modulations in the experimental and theoretical SFG spectra of the surface. As the first time of discovery, a theoretical peak shift reproduced the experiment quantitatively, and thus the peak shift was due to the modulation of average polarizability of the Si-H oscillators via dipole coupling. On the other hand, inhomogeneous broadenings of the theoretical peaks in the SFG spectra at lower coverages were much larger than those of the calculated peaks.

References

1. Ichimiya, A., *RHEED and AES study of Si(111) √3 x√3- R30° structure induced by adsorption of impurity gases.* ISIJ International, 1989. **29**(7): p. 576.
2. Luo, H. and C.E.D. Chidsey, *D--Si(111)(1 x 1) surface for the study of silicon etching in aqueous solutions.* Applied Physics Letters, 1998. **72**(4): p. 477-479.
3. Jakob, P., Y.L. Chabal, and K. Raghavachari, *Lineshape analysis of the Si・H stretching mode of the ideally H-terminated Si(111) surface: the role of dynamical dipole coupling.* Chemical Physics Letters, 1991. **187**(3): p. 325-333.
4. Guyot-Sionnest, P., *Effect of substrate photoexcitation on the dynamics of the Si-H stretch for Si(111)/H.* Journal of Electron Spectroscopy and Related Phenomena, 1993. **64–65**(0): p. 1-9.
5. Persson, B.N.J. and R. Ryberg, *Vibrational interaction between molecules adsorbed on a metal surface: The dipole-dipole interaction.* Physical Review B, 1981. **24**(12): p. 6954-6970.
6. Backus, E.H.G., *Driving and probing surfaces with light.* Leiden University, 2005: p. 119.
7. Backus, E.H.G. and M. Bonn, *A quantitative comparison between reflection absorption infrared and sum-frequency generation spectroscopy.* Chemical Physics Letters, 2005. **412**(1–3): p. 152-157.
8. Cho, M., C. Hess, and M. Bonn, *Lateral interactions between adsorbed molecules: Investigations of CO on Ru(001) using nonlinear surface vibrational spectroscopies.* Physical Review B, 2002. **65**(20): p. 205423.
9. Gupta, P., V.L. Colvin, and S.M. George, *Hydrogen desorption kinetics from monohydride and dihydride species on silicon surfaces.* Physical Review B, 1988. **37**(14): p. 8234-8243.
10. Morin, M., et al., *Vibrational energy transfer on hydrogen-terminated vicinal Si(111) surfaces: Interadsorbate energy flow.* The Journal of Chemical Physics, 1992. **96**(8): p. 6203-6212.
11. Higashi, G.S., et al., *Ideal hydrogen termination of the Si (111) surface.* Applied Physics Letters, 1990. **56**(7): p. 656-658.
12. Dumas, P., Y.J. Chabal, and G.S. Higashi, *Coupling of an adsorbate vibration to a substrate surface phonon: H on Si(111).* Physical Review Letters, 1990. **65**(9): p. 1124-1127.
13. Ye, S., et al., *Stability of the Si–H bond on the hydrogen-terminated Si(1 1 1) surface studied by sum frequency generation.* Surface Science, 2001. **476**(1–2): p. 121-128.
14. Katano, S., et al., *Screening of SFG signals from bridged CO on Ni(111) by the*

coexistence of linear CO. Surface Science, 1999. **427–428**(0): p. 337-342.

15. Koehler, B.G., et al., *Desorption kinetics of hydrogen and deuterium from Si(111) 7 x 7 studied using laser-induced thermal desorption.* The Journal of Chemical Physics, 1988. **89**(3): p. 1709-1718.
16. Wise, M.L., et al., *Comparison of hydrogen desorption kinetics from Si(111)7 × 7 and Si(100)2 × 1.* Surface Science, 1991. **258**(1–3): p. 166-176.
17. Reider, G.A., U. Hofer, and T.F. Heinz, *Desorption kinetics of hydrogen from the Si(111)7 x 7 surface.* The Journal of Chemical Physics, 1991. **94**(5): p. 4080-4083.
18. Vittadini, A. and A. Selloni, *H2 adsorption/desorption at Si(111)-(7 × 7): a density functional study.* Surface Science, 1997. **383**(2–3): p. L779-L784.

Chapter 6: Hydrogen desorption from the regular step Si(111) surface with 9.5^{o} miscut toward $[\bar{1}\bar{1}2]$ direction

6.1 Development of a sample holder for heating the Si substrate

6.2 LEED patterns and the estimated terrace size

6.3 Polarization dependence of SFG spectroscopy

6.4 Assignment of 2094 cm^{-1} (C_1) peak

6.5 Observation of direction dependence of SFG spectroscopy

6.6 Time dependence of the SFG spectroscopy

6.7 Conclusion

References

In this chapter, I presented the investigation the hydrogen absorption and desorption on regular step H-Si(111) surfaces with 9.5^{o} miscut toward $[\bar{1}\bar{1}2]$ direction. The hydrogen was terminated on the regular stepped Si(111) surface by dosing hydrogen molecules in the UHV chamber. After hydrogen termination on the vicinal Si surface, the upstairs and downstairs SFG spectra with *ppp* and *ssp* polarization combination were taken. The number of step bunches on the Si surface after flashed at 1200 °C was calculated from LEED patterns. After considering about hydrogen adsorption on the stepped Si(111) surfaces, they were heated at several high temperatures, and time dependence of the upstairs SFG spectra with *ppp* and *ssp* polarization combination were taken.

6.1 Development of a sample holder for heating the Si substrate

In this research, hydrogen termination of the Si surface was performed by dosing hydrogen molecules into a UHV chamber with pressure of ~10^{-8} Pa. The thermal hydrogen desorption from H-Si surface was also investigated. Therefore, heating the Si surface required a special sample holder in UHV condition. The resistivity of Si wafer was ~10 Ω.cm and the size was 20x2x0.1mm. The sample was small so that it was difficult to install onto the sample holder. This sample holder is drawn in fig. 6.1.1. In order to make the uniformity of the electric field distribution on the Si wafer, four Ta plates were added at the end of the two electric rods (number 11 in fig. 6.1.1). More important part is the Ta cover drawn as number 7. The shape of this cover set around the sample holder was very complicatedly. It was separated to the electric rod by ceramic screw. This cover is very important for avoid the electric charge on the Si surface when observing LEED patterns. Electric charge on the Si sample makes the LEED pattern unobservable. However, it easily touches to the sample holder and the short circuit occurs. In that case, the Si sample could not be heated. This is the difficult point and is the advantage of this sample holder.

Si wafers can be mounted on this sample holder with step-up or step-down heating current direction. With each current direction, the observed SFG spectrum showed the different number of peaks and the different intensity of terrace and step mode (see section 6.3).

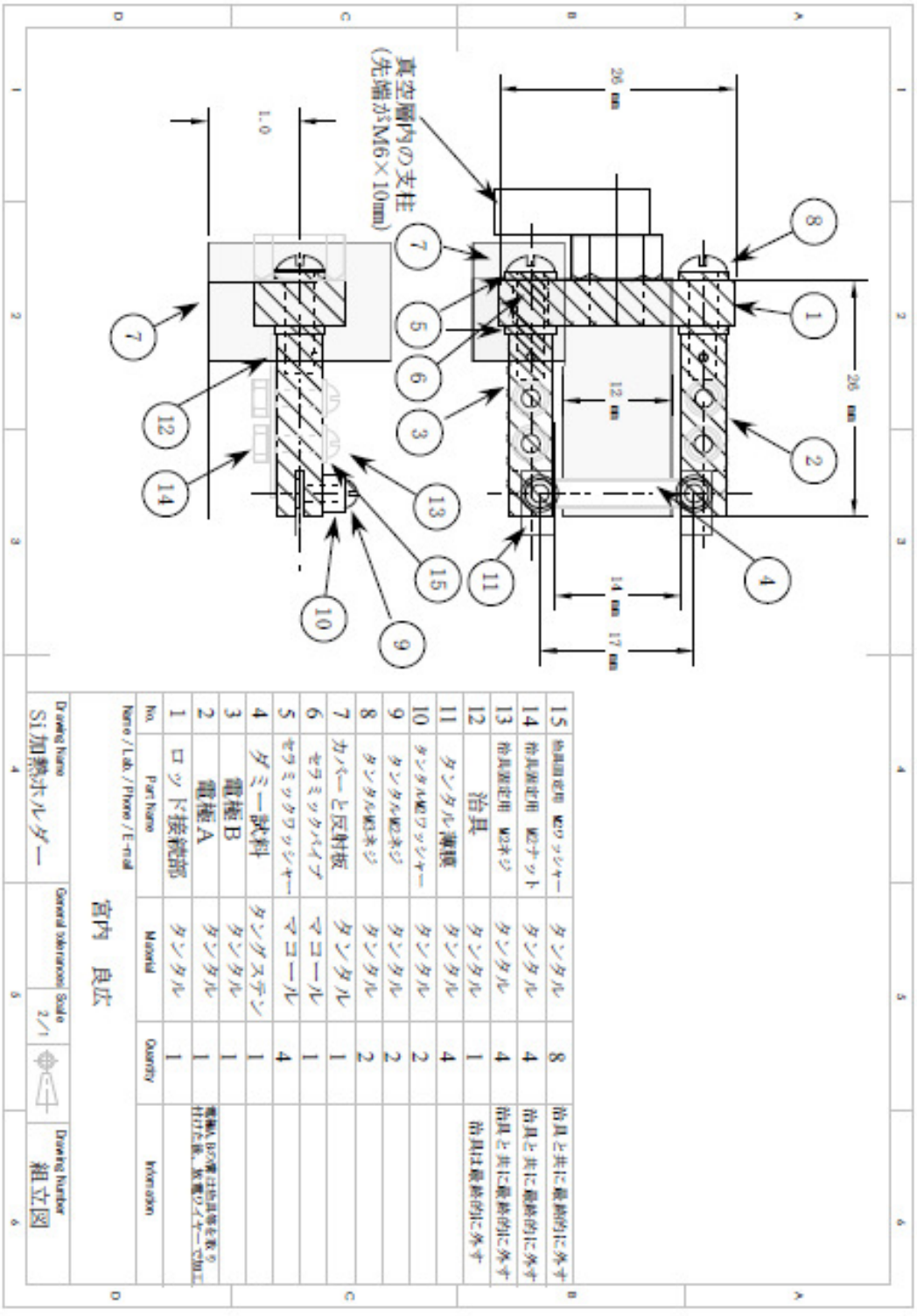

Fig. 6.1.1: The designation of the sample holder.

6.2 LEED patterns and the estimated terrace size

The structure of the regular step Si(111) surface with a miscut toward $[\bar{1}\bar{1}2]$ direction was described by some researchers several years ago as shown in fig. 6.2.1 [2-4]. Terraces are terminated in a (1x1) monohydride overlayer, with a bulk (111) termination and one hydrogen atom on each surface silicon atom. The distance between monohydrides on the terrace is 3.84 Å. In the absence of surface relaxation the step heigh is 3.14 Å and the average terrace length is 18.86 Å (fig. 6.2.1(b)). There are on average 5 monohydrides across each terrace and the step has a dihydride termination (fig. 6.2.1(a)). The dihydride Si-H bonds lie in a plane perpendicular to both the (111) surface and to the step edge.

A regular step Si(111) wafer with 9.5^{o} miscut toward $[\bar{1}\bar{1}2]$ direction was cleaned in an ultrasonic bath with acetone in 10 min. After that, it was mounted on the tungsten sample holder (as described above) in UHV chamber with pressure of ~10^{-8} Pa. The Si sample was degassed in 6 hours at 600 ℃ in order to remove contaminants. The method of hydrogen dosing on the vicinal Si(111) surface was briefly presented in chapter 3. In this section, I present the structure of the stepped Si(111) with 9.5^{o} miscut toward $[\bar{1}\bar{1}2]$ direction after flash heating at high temperature of 1200 ℃ based on its LEED patterns.

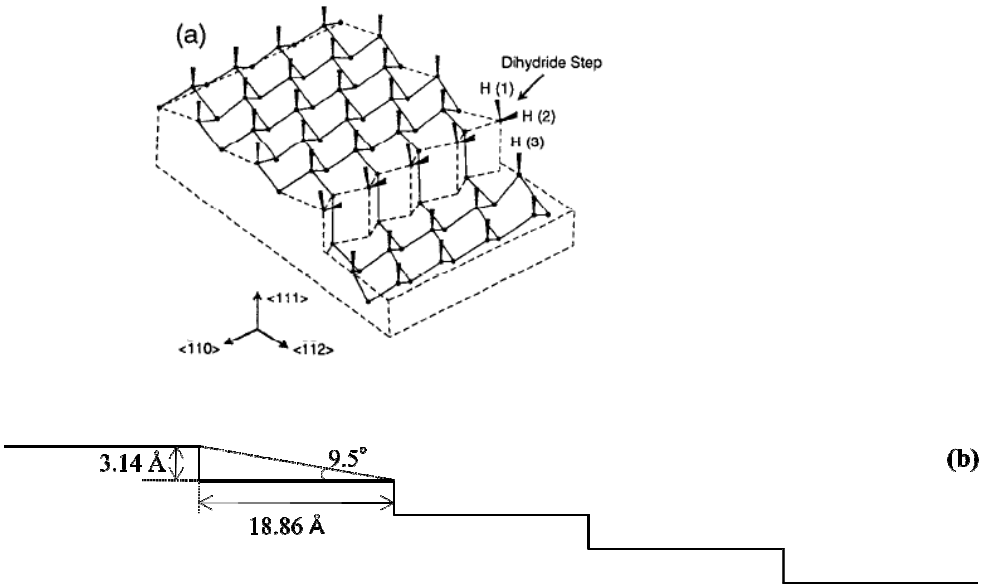

Fig. 6.2.1: The structure of H-Si(111) with 9.5° miscut toward $[1\bar{1}2]$ *direction*

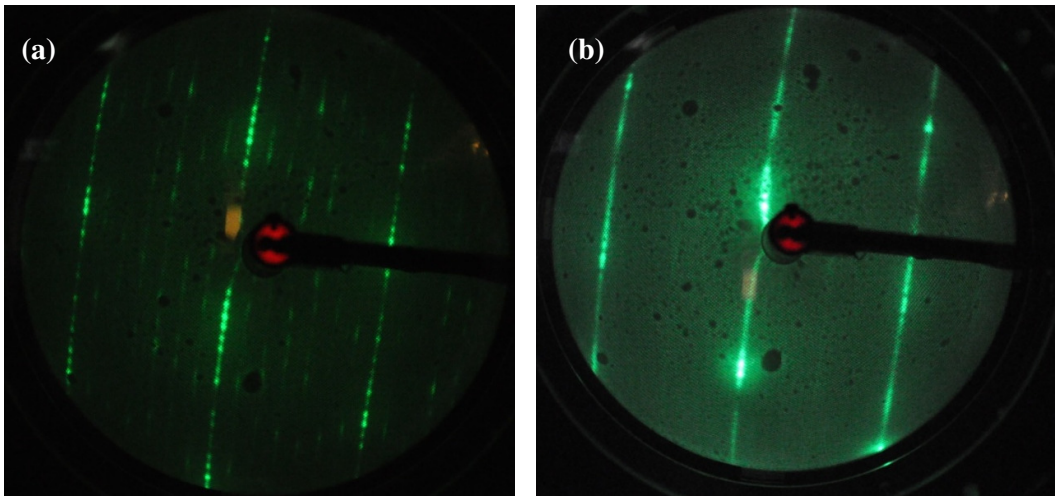

Fig. 6.2.2: LEED patterns of vicinal Si surface before and after hydrogen dosing. (a) 7x7 structure after flash heating, (b) 1x1 structure after hydrogen dosing.

Figure 6.2.2(a) show the LEED patterns of the Si surface after flash heating at 1200 ℃. The 7x7 reconstruction structure can be clearly observed. The separated bright spots correspond to steps on the vicinal Si surface. Fig. 6.2.2(b) shows the 1x1 structure after 10 min of hydrogen dosing.

I assume that the terrace length and atomic silicon distance on the real Si surface after flashed are l and a~3.84 Å, respectively. The terrace length L and the atomic distance in reciprocal lattice A (in LEED patterns) are shown in Figure 6.2.3 below.

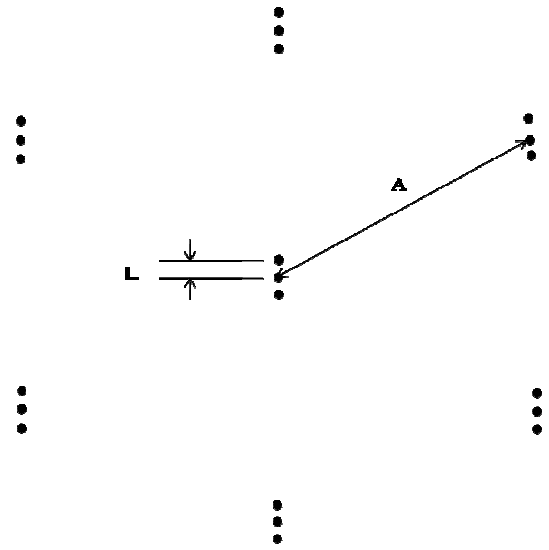

Fig. 6.2.3: The terrace length is calculated from LEED patterns.

The relation between the terrace length in real space and in reciprocal lattice is:

$$\frac{2\pi}{a} : A = \frac{2\pi}{l} : L \qquad (6.2.1)$$

From the LEED patterns in fig. 6.2.2, the values of L and A were measured as ~53 ± 3 mm and ~1.5 ± 0.5 mm. Putting these values into equation (6.2.1):

$$\frac{2\pi}{3.84} : 53 = \frac{2\pi}{l} : 1.5 \qquad (6.2.2)$$

From this equation, l is ~135.68 ± 35 Å. This value is 5~7 times larger than regular terrace length ~18.86 Å. Therefore, step bunching occurred after flash heating at 1200 ℃ with 5~7 steps. The reproducibility of this result was confirmed several times.

Compared to the Si surface studied by Chabal *et al.* [2] and Morin *et al.* [3], my sample is similar. However, they terminated hydrogen on the Si surface by chemical treatment. In my case, I use molecular hydrogen dosing method.

6.3 Polarization dependence of SFG spectroscopy

The vicinal H-Si(111) 1x1 with 9.5^{o} off $[\bar{1}\bar{1}2]$ direction was prepared by dosing hydrogen molecules in UHV condition. Vibration of the Si-H bonds on the terrace and Si-2H on the step is considered to have C_{3v} and C_s symmetry, respectively. In both cases, the SFG active combinations of polarization components are *ppp*, *spp*, *ssp*, *psp*, *sps*, *pps*, *pss* and *sss*. By varying the polarization and orientation of both the incident and detected light fields, I expected that quantitative information on the orientation and normal mode character of Si-H bonds can be obtained. SFG spectroscopy was observed with all the above polarization combinations and the IR range from 2060 to 2140 cm^{-1} (see appendix A). However, only the SFG spectra with *ppp* and *ssp* polarization combinations show clear two peaks at 2082 cm^{-1} and 2094 cm^{-1} (fig. 6.3.1). The dots are the experimental data and the solid curves are fitting curves. The peak 2082 cm^{-1} is attributed to terrace vibrational monohydride consistent to that in IR [2, 5, 6], Raman [7] and SFG spectroscopy [3, 8, 9]. The other peak at 2094 cm^{-1} has the same frequency with C_1 peak in IR and Raman spectra of Chabal's report [2, 7]. However, this C_1 mode vibration is still mysterious in previous litterature. Interesting point is that C_1 peak has been believed to be absent in the SFG spectrum but it really appeared in my circumstance as shown in fig. 6.3.1. On the other hand, C_2 and C_3 were not observed in my SFG spectra with all polarization combinations (see appendix A). The reason why there is this difference will be explained in the next sections.

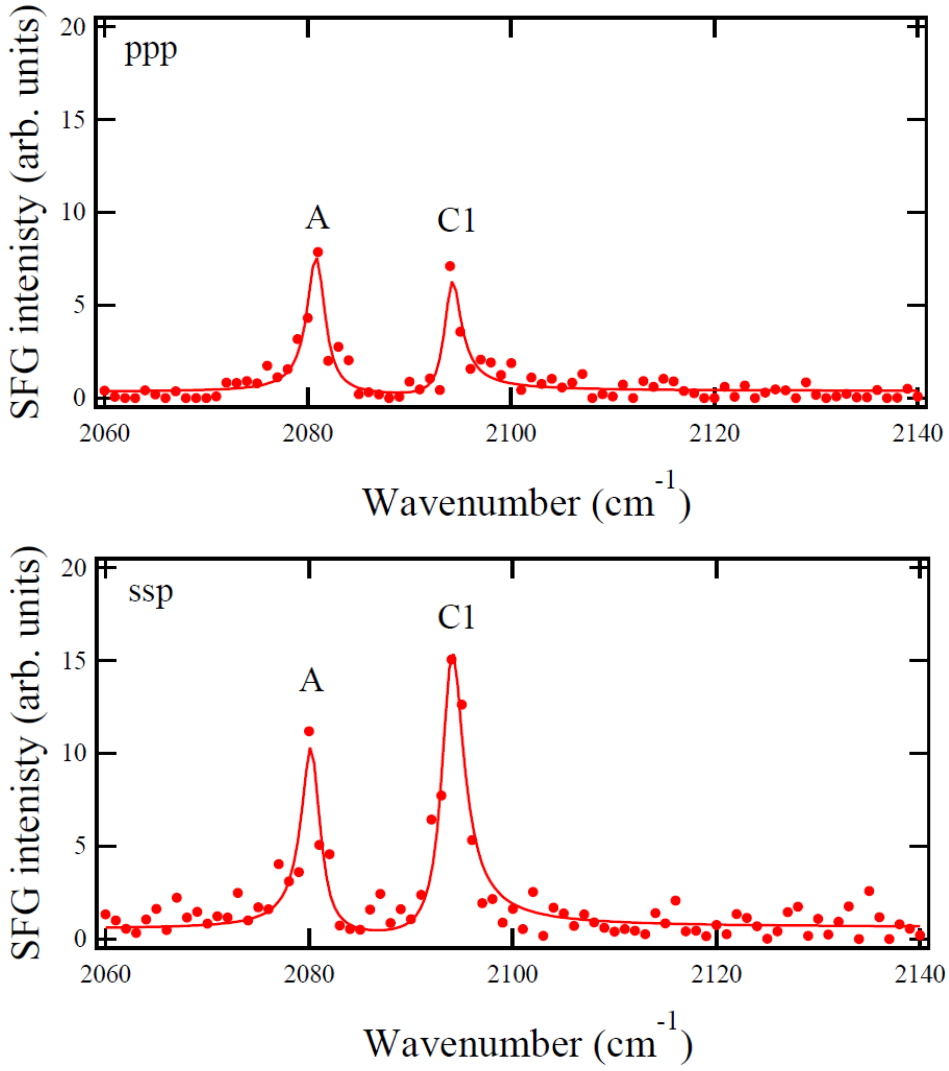

Fig. 6.3.1: SFG spectra of the vicinal H-Si(111)1x1 miscut 9.5° off $[\bar{1}\bar{1}2]$ *direction with ssp and ppp polarization combination.*

6.4 Observation of step direction dependence of SFG spectroscopy

In this research, the hydrogenated Si surface was prepared by dosing hydrogen molecules in UHV chamber. The Si sample could be mounted on the sample holder with step-up or step-down heating current corresponding to downstairs and upstairs directions, respectively. The incident visible and IR lights come to the H-Si surface with two geometries shown in Figure 6.4.1 [3]. Figure 6.4.2 presents the SFG

spectra of the H-Si surface corresponding to upstairs and downstairs configuration with the polarization combination *ppp*. In the upstairs SFG spectrum, there are two peaks at 2082 (A) and 2094 cm^{-1} (C_1), while there is only the terrace mode A in the downstairs SFG spectrum. This difference occurred for *ppp* polarization only. The number of peaks did not change for *ssp* polarization as shown in Fig. 6.4.3. However, the ratio of the peak intensity between A and C_1 modes depended on the configuration.

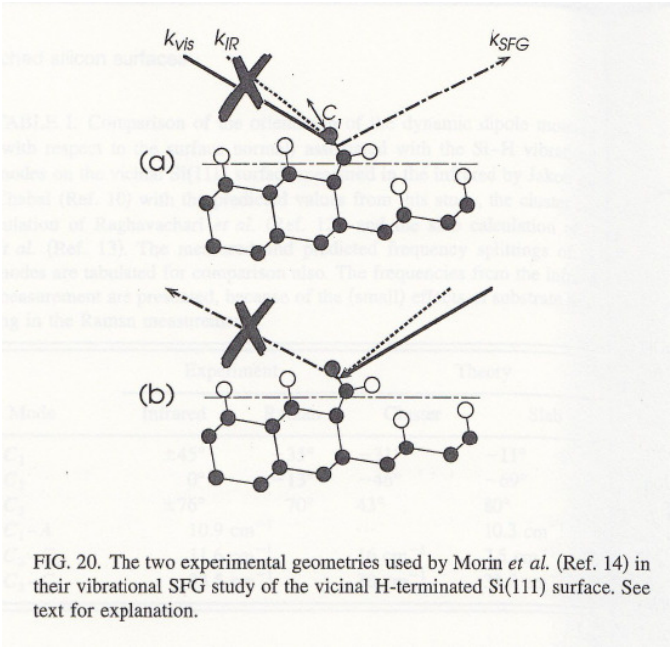

FIG. 20. The two experimental geometries used by Morin *et al.* (Ref. 14) in their vibrational SFG study of the vicinal H-terminated Si(111) surface. See text for explanation.

Fig. 6.4.1: The two experimental geometries used by Morin et al. [3] in their vibrational SFG study of the vicinal H-terminated Si(111) surface.

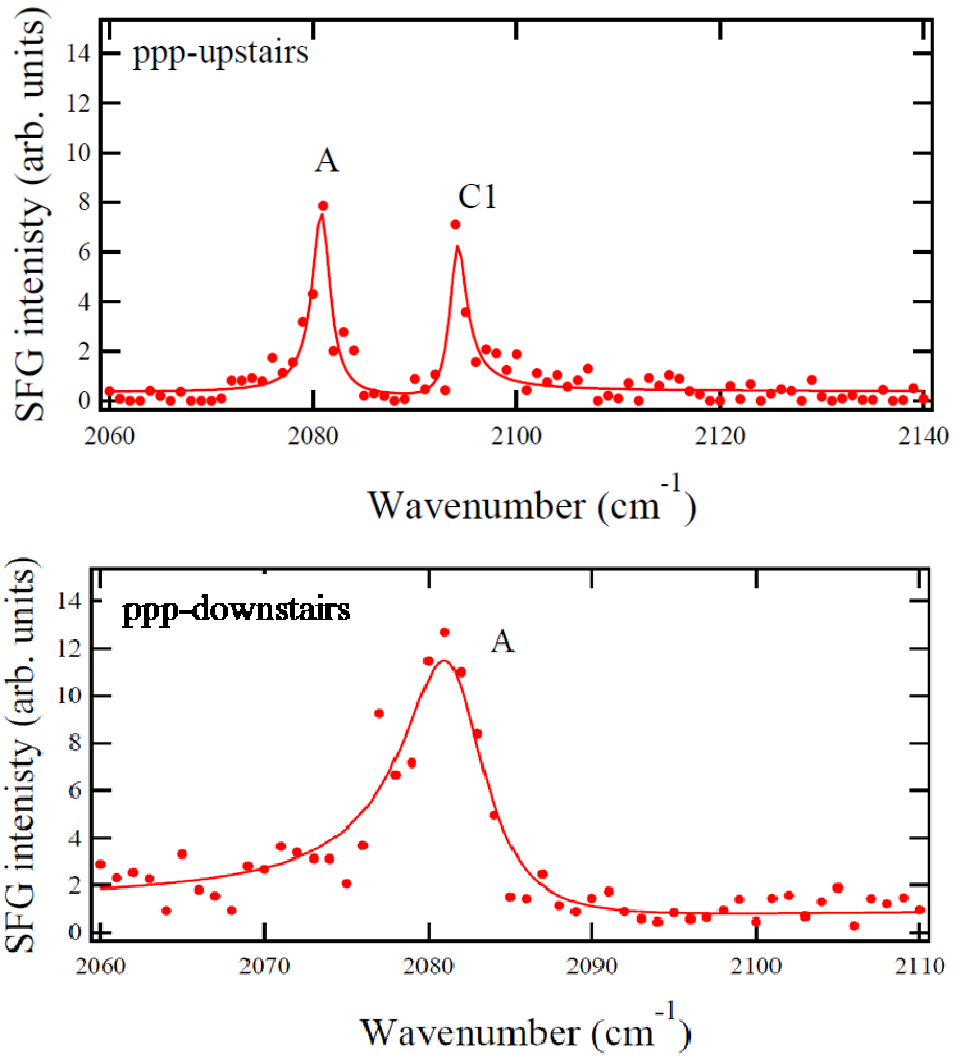

Fig. 6.4.2: SFG spectra of the H-Si(111) surface 9.5° miscut toward $[\bar{1}\bar{1}2]$ *direction in downstairs and upstairs directions. The polarization combination is ppp.*

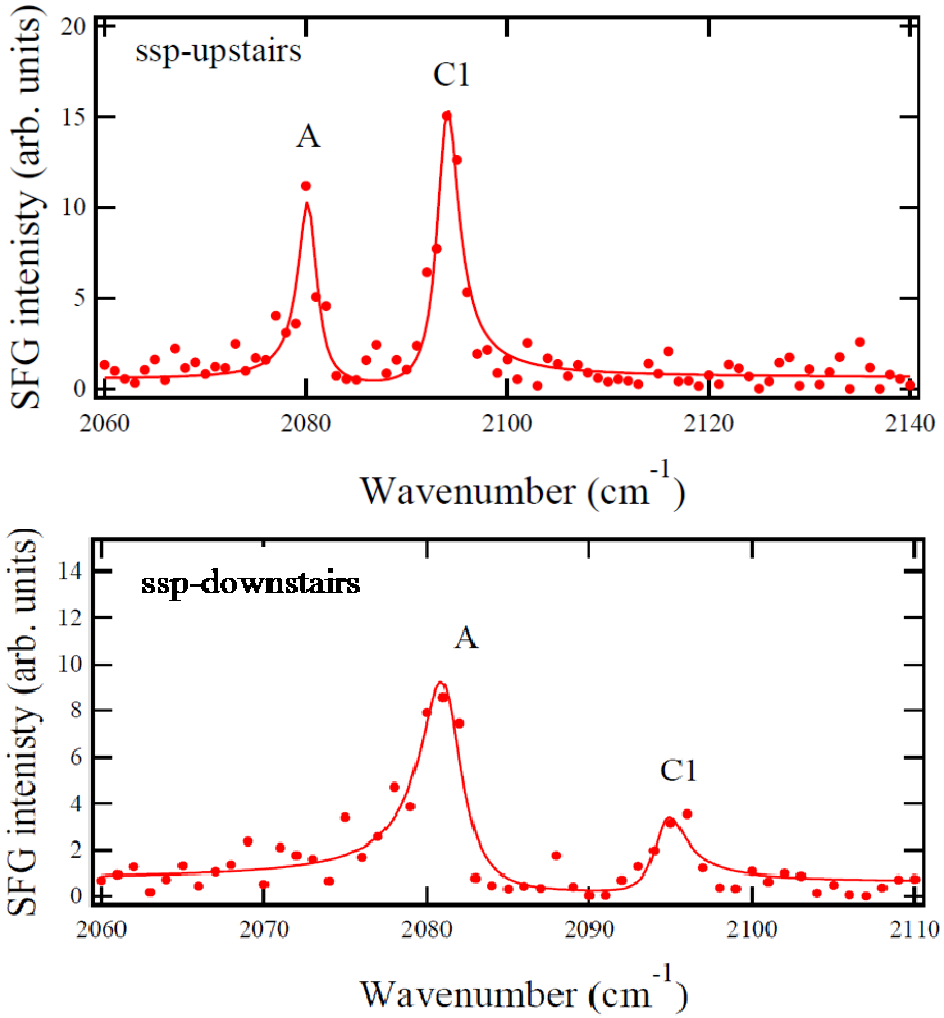

Fig. 6.4.3: SFG spectra of the H-Si(111) surface 9.5° miscut toward $[\bar{1}\bar{1}2]$ *direction with and downstair and upstair. The polarization combination is ssp.*

In the experimental process, I confirmed that the ratio of peaks intensity was sensitive to the angle of incident light. I have not yet quantitatively controlled this angle, however, the ratio of peak intensity is related to the angle between the sample and the incident lights. Therefore, one contribution for C_1 mode is the orientation of the step Si-H(1) bond. In my opinion, the different intensity of C_1 mode is not related to sensitivity of *s* or *p* polarization of SFG signal because the intensity of the terrace

mode A is similar in all the spectra. Understanding of C_1 mode may be clearer in next section.

6.5. Assignment of 2094 cm^{-1} (C_1) peak

Here, I summarize the work of Chabal and co-authors [2, 4] investigating the vibrational modes on a vicinal H-Si(111) in 9° off $[\bar{1}\bar{1}2]$ direction which is similar to my sample. This surface has a structure similar to my sample as shown in fig. 6.2.1 above. The hydrogenated Si surface was prepared by chemical etching by hydrofluoric acid with pH of 6.6. In the IR spectrum with p-polarization, there are four vibrational modes marked A, C_1, C_2, and C_3 corresponding to the peak frequencies 083.6, 2093.6, 2101.3 and 2134.7 cm^{-1}, respectively. These vibrational modes were also observed in Raman study [7] done by the same group. In the Raman spectra, A, C_1, C_2, and C_3 had the peak position at frequencies of 2082, 2093, 2101 and 2134 cm^{-1}, respectively. The A mode is readily attributed to the in-phase terrace vibration of the monohydride. About the other step vibrational modes (C_1, C_2, and C_3), the assignment are related to structure relaxation of the dihydride-terminated step. They were calculated by two theoretical methods: a cluster calculation and a slab calculation.

According to the cluster calculation [4], the dihydride Si-2H at step is predicted to rotate away from the lower terrace by 22°. In spite of this large relaxation, steric interactions dominate the vibrational spectrum. As the result, steric effects lead to concerted motion of H(2) and H(3) (shown in Fig. 6.2.1(a)) producing an out-of-phase (C_2) and in-phase (C_3) pair of vibration. Besides that, H(1) is not sterically constrained, and it is decoupled from H(2). Therefore, the C_1 mode appearing at 2093 cm^{-1} was assigned to the isolated stretching vibration of Si-H(1).

Although the cluster calculations qualitatively agree with C_1 mode in the infrared and Raman measurements, there are discrepancies in both the frequency splitting and the polarization ratios. This differences between theory and experiment is likely due to the finite size of the cluster and lack of bonding interaction [10].

On the other hand, Li *et. al* [11] attempted to address the limitations of the cluster calculation by performing a slab calculation using first principles pseudopotentials within the framework of density functional theory and the local density approximation. The surface of their slab consisted of 5 atom wide terraces separated by double layer steps. The slab itself contained 4 double layers of Si terminated with hydrogen on both sides; these slabs were separated by a 2-double-layer-thick vacuum. This is very large size of the supercell so that it is close to the real H-Si surface (Fig. 6.5.1). Therefore, "ultrasoft pseudopotentials" [12] were used to make the calculation feasible. In the fully relaxed structure, they predict a 3.5^o rotation of the dihydride away from the lower terrace and a 2^o compression of the H(1)-Si-H(2) bond angle. The high-energy modes C_1, C_2, and C_3 are mainly the Si-H stretching vibrations corresponding to H(1), H(3) and H(2), respectively. However, when they considered appearance of large coupling between the stretching vibrations, the agreement with experiment was better than expected. The C_1 mode has significant contributions from Si-H vibrations on the terreace: about 81% of its weight on H(1), 6% on H(3) and 12% on H(4).

In accordance with Raman measurement, the cluster calculation and the slab calculation show a difference of fitting C_1 mode as seen in figure 6.5.2. The black points are Raman measurement results, the line is cluster calculation and the dash-dot line is slab calculations. The assignment of C_1 mode should be considered more. In

addition, this mode was believed that to be absent in the SFG spectrum. Here I will explain why it is strongly observable in my SFG spectrum.

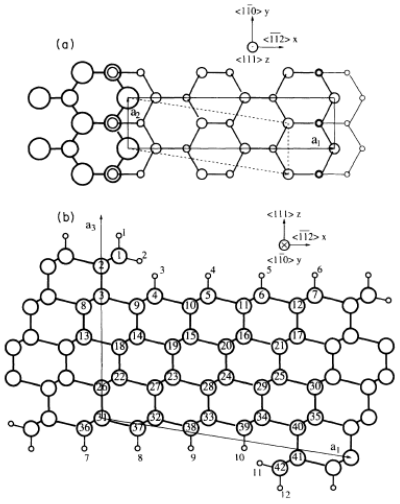

FIG. 1. Supercell used in the calculation. (a) Top view: H atoms are not shown, larger circles stand for higher positions (larger z coordinates). The dashed lines show the would-be supercell if n were 4. (b) Side view: larger circles are Si atoms and smaller circles are H atoms. All the numbered atoms are within the supercell.

Fig. 6.5.1: Supercell was used in the slab calculation. H1, H2 and H3 correspond to H(1), H(2) and H(3) in fig. 6.2.1 [11].

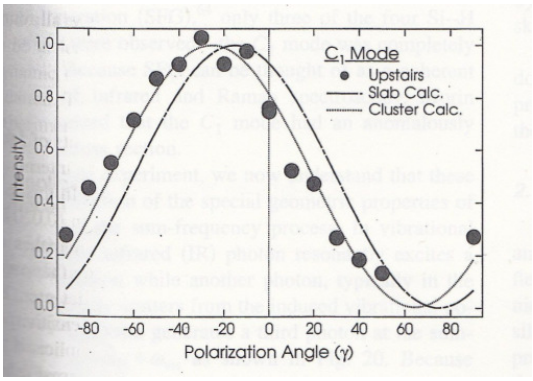

Fig. 6.5.2: Comparison of the observed polarization dependence of the C_1 mode observed in the upstairs direction with the predictions of both the cluster (dotted line) and slab (dash-dot line) calculations [10].

Figure 6.5.3 shows the SFG spectrum on the 9.5° surface miscut toward $[\bar{1}\bar{1}2]$ direction with IR range from 2060 to 2140 cm^{-1}. Comparing to SFG spectrum

on similar surface of the 9° surface miscut toward $[\bar{1}\bar{1}2]$ direction done by Morin *et al.* [3] (inset figure), the C_1 mode is clearly observable while there is lack of C_2 and C_3 modes. Basically, Shen *et al.* [13] shows that the SFG intensity depends on both the IR and Raman cross sections. Chabal *et al.* [10] explained the disappearance of the C_1 mode in SFG spectrum as shown in fig. 6.4.1. Two different geometries were tried in this experiment. In one case, the IR and visible laser were incident in the downstairs direction shown in fig. 6.4.1(a). This orientation is unfavorable for SFG excitation because the polarizations of both lasers are nearly perpendicular to the bond axis. Thus, neither the IR nor the Raman transitions could be efficiently excited. The second geometry is more subtle. Here, both excitation lasers pointed up the stairs as in fig. 6.4.1(b). This orientation was excellent for excitation of SFG; however, because the signal beam is constrained to come out in the near-specular direction, this orientation is poor for signal generation. Raman scattering is not subject to this constraint because the very small calculated value of the relative respond of the Si-H bond to an electric field is δ ~0.263. Therefore, appearance of C_1 mode in my SFG spectrum is still mysterious. It is not caused by neither Raman scattering nor Fresnel factors. The candidates of origin of this C_1 mode are:

- Orientation of the step dihydride H_A-Si-H_B to the optical surface may be suitable for SFG excitation.
- Energy transfer between the terrace and step vibrational modes via dipole-dipole coupling makes the C_1 peak intensity stronger.

Let me discuss about the energy transfer between adsorbates. On the regular step Si with 9.5° degree off angle, the ratio of concentration between monohydride on terrace and dihydride on step mode C1 is 5 times. That means SFG intensity of A

mode should be 5 times larger than C1 mode. However, they are similar in my SFG spectra - even C_1 peak intensity is higher. As calculated by Persson [1], he assumed the coverage of absorbate A and B as 0.1 and 0.9 ML. If there is no dipole-dipole (d-d) interaction between molecules, the ratio of absorbates is shown in red color peaks in Fig. 6.5.4. However, if there is d-d interaction, large amount of intensity removed from low frequency peak to high frequency peak. It makes similar intensity. Therefore, high intensity of C1 mode in my SFG spectrum may be explained by transfer energy via d-d interaction among H-Si species. Further calculation using CPA methods will be carried out to make clear this point. In order to elucidate the step C_1 mode and its high intensity, the time dependence of thermal hydrogen desorption was investigated at several heating temperatures.

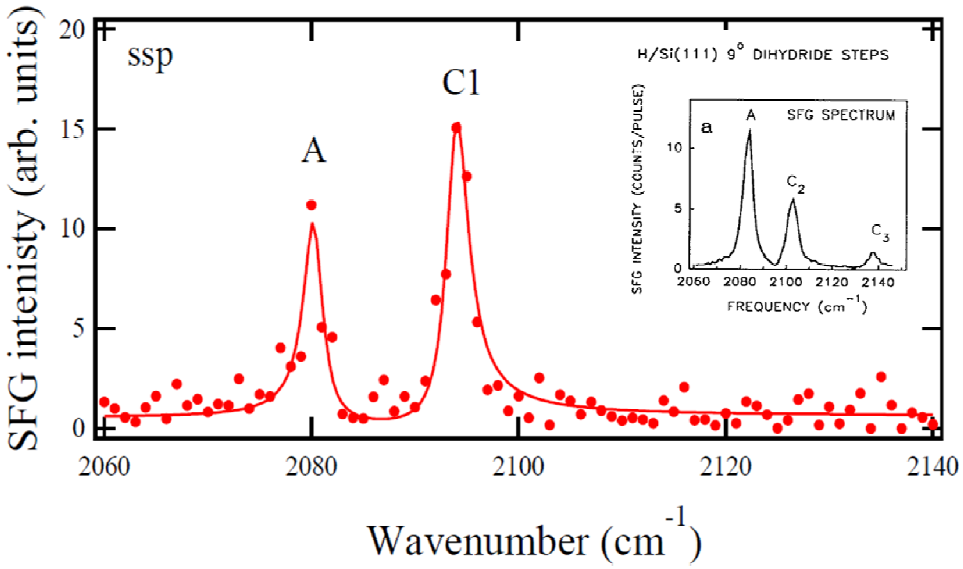

Fig. 6.5.3: SFG spectrum on the 9.5° surface miscut toward $[\bar{1}\bar{1}2]$ *direction. The inset figure is SFG spectrum on the 9° miscut toward* $[\bar{1}\bar{1}2]$ *direction* [3].

Next, I will discuss the reason for the absence of C_2 and C_3 modes in the SFG spectrum. Shen *et al.* [13] reported that the SFG intensity depended on square of the

density of the oscillators. One evidence was reported by Morin *et al.* [3]. The reduction of C_2 peak in SFG spectrum of the 5° mis-cut Si(111) surface with the lower step density compared to the 9° mis-cut surface could be reasonable [3]. With the 9° surface miscut toward $[\bar{1}\bar{1}2]$ direction, the number ratio of step dihydrides Si-2H to terrace monohydrides should be twice larger than that on the 5° surface. Therefore, the ratio of the intensity of the step C_2 mode to the terrace mode A on the 5° surface should decrease by a factor of ~4 compared to the 9° cut surface. Actually, this ratio decreases by a factor of ~10. The authors suggested that this might indicate that the terraces are longer than 9.3 monohydrides calculated from the 5° miscut angle, signifying that some step bunching is occurring. In my experiment, the 9.5° surface miscut toward $[\bar{1}\bar{1}2]$ direction was flash heated at high temperature of ~1200 °C, then the step bunching occurred. The terrace length ~135.68 ± 35 Å and number of steps 5~7 was calculated in section 6.2. Therefore, the C_2 peak may be unobservable in the SFG spectrum of the step bunched H-Si(111) surface 9.5° miscut toward $[\bar{1}\bar{1}2]$ direction. The step C_3 mode was already weak on the SFG spectrum of the 9° cut surface so that it cannot be detected on the step bunched 9.5° cut surface because of the decrease in the step mode intensities.

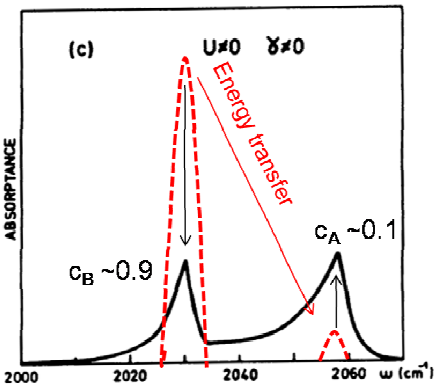

[1]Persson *et al.*, PRB 24(12), (1981) 6954.

Fig. 6.5.4: Energy transfer between the A and B adsorbates via dipole-dipole interaction [1].

6.6 Time dependence of the upstairs SFG spectroscopy

Recently, hydrogen passivated flat Si(111) surfaces have been used as effective substrates of silicon-based bioelectrical sensors and devices [14, 15]. Therefore, the adsorption and stability of hydrogen on the Si substrates are very important for securing the quality of ultrathin films. Although the hydrogen was terminated on Si surfaces by wet chemical etching [2, 5, 16] or hydrogen dosing [17-20], defects and kinks on the surface play a very important role in chemical reaction resulting in rearrangement of surface structure and adsorbate orientation [18, 21, 22]. In addition, the morphology of vicinal Si(111) surfaces could be evaluated near the edges of patterned structures such as craters and mesas during UHV annealing [23]. Therefore, defects or steps are critical effects on the surface interaction. In this research, step structure and orientation of dihydride on vicinal Si(111) surfaces with miscut angle of 9.5^{o} toward $[\bar{1}\bar{1}2]$ direction will be studied after hydrogen adsorption in an UHV chamber. Here I noted that nowadays stepped Si(111) surfaces have been considered as natural templates for ordered growth of quantum dots and nanowires due to their active sites

In the following experiments, the Si(111) wafer with 9.5^{o} miscut toward $[\bar{1}\bar{1}2]$ direction was used in the same way as before. The hydrogenated Si surface was prepared by dosing hydrogen molecules in UHV chamber (see chapter 3). The H-Si(111) 9.5^{o} surface was heated at several temperatures of 381, 423, 436, 449, 478 ^{o}C with upstairs observation. After each time of heating in 40 s, the SFG spectrum was measured with *ppp* and *ssp* polarization combination. Similarly, the downstairs-SFG spectra were also observed. Figure 6.6.1 below shows the SFG spectra of the vicinal H-Si(111) heated at 449 ^{o}C.

The peak intensity of both terrace and step mode was reduced when the heating time was increased. However, the reduction rate of step mode looks like faster than the terrace mode which is shown in Fig. 6.6.2. The reduction is the best fit with the 2nd order of hydrogen desorption.

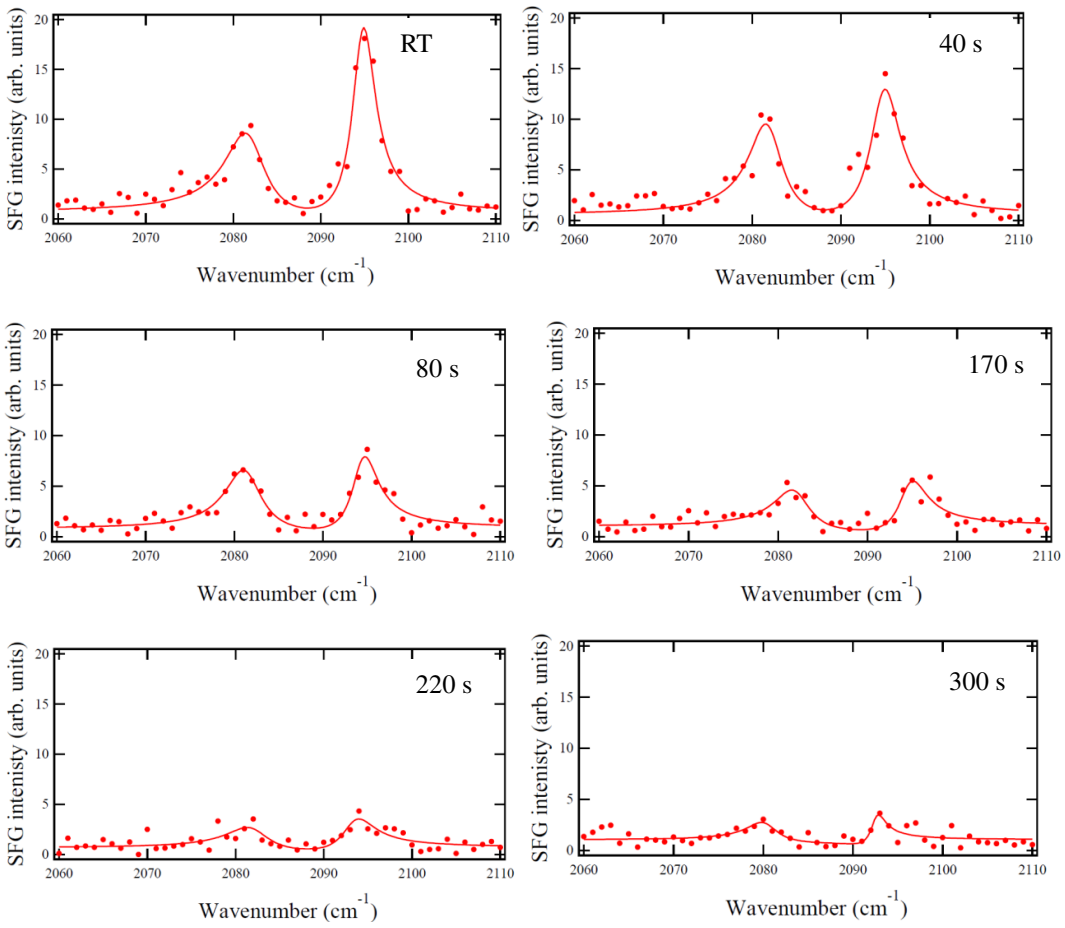

Fig. 6.6.1: The time dependence of SFG spectra of the vicinal 9.5° surface heated at 449 °C with upstair observation.

Figure 6.6.3 shows the peak intensities of the terrace and step modes as a function of time. The step mode peak was shifted ~2 cm^{-1}. It may be related to the dipole-dipole interaction among the H-Si species. The activation energy of the terrace

and step modes and calculation of dipole-dipole interaction should be calculated in the future.

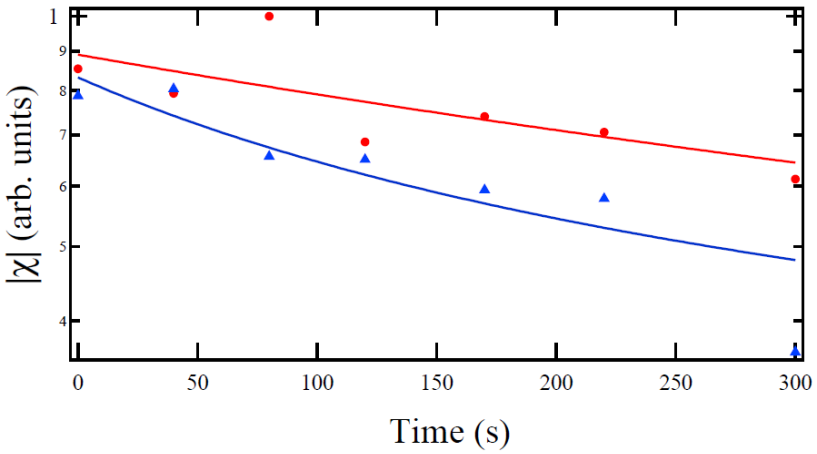

Fig. 6.6.2: The reduction of SFG respect to time. The dots are the experimental data. The solid lines are the 2nd order fitting.

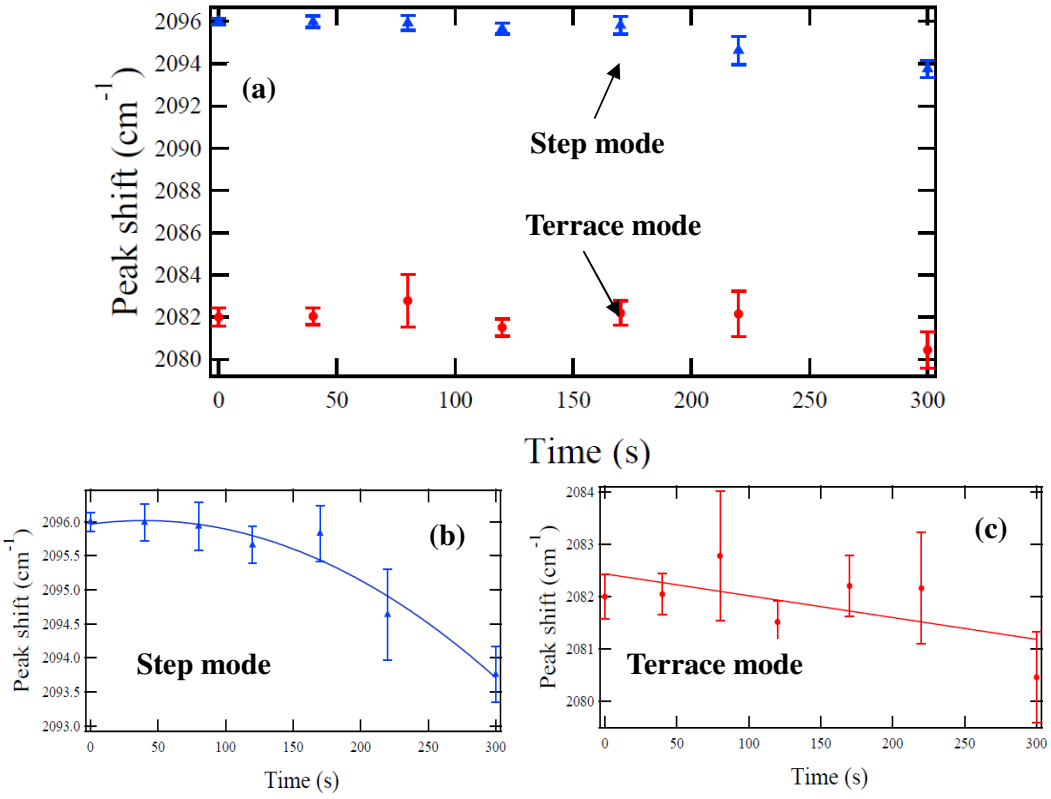

Fig. 6.6.3: The peak shift of the terrace and step mode respect to time. The lines in (b) and (c) are fitting curves.

6.7 Conclusion

I investigated the hydrogen absorption and desorption on regular step H-Si(111) surfaces with 9.5^{o} miscut toward $[\bar{1}\bar{1}2]$ direction. The hydrogen was terminated on the regular stepped Si(111) surface by dosing hydrogen molecules in the UHV chamber. When the visible and IR lights reach to the surface with step up direction, the SFG signal is called the upstairs SFG. Inversely, when they reach to the surface with step down direction, the SFG signal is called the downstairs SFG. After hydrogen termination on the vicinal Si surface, the upstairs SFG spectra with *ppp* and *ssp* polarization combination were taken. In both cases, the terrace mode A (2082cm^{-1}), and step modes C_1 (2094 cm^{-1}) peaks were clearly observed, while C_2 (2101 cm^{-1}) and C_3 (2134 cm^{-1}) were not. The A mode is readily attributed to the in-phase terrace vibration of the monohydride. The step C_2, C_3 modes cannot be detected on the step bunched 9.5^{o} surface because of the decrease in the step mode intensities (step bunches appeared when the Si surface was flashed at 1200 °C). On the other hand, the downstairs SFG spectra with *ppp* and *ssp* polarization combination were also observed. The terrace mode A appeared in all spectra while the step C_1 mode appeared in *ssp* only.

The regular stepped H-Si(111)1x1 surfaces miscut toward $[\bar{1}\bar{1}2]$ direction were heated at several high temperatures, and time dependence of the upstairs SFG spectra with *ppp* and *ssp* polarization combination were taken. The peak intensities of both terrace and step modes were reduced when the heating time was increased, but the step mode reduction was faster. The reduction is the best fit with the 2nd order of hydrogen desorption. The step mode C_1 was shifted ~2 cm^{-1}. I suggest that it may be related to the dipole-dipole interaction among the H-Si species. However, the theoretical calculation is required to clarify this point.

References

1. Persson, B.N.J. and R. Ryberg, *Vibrational interaction between molecules adsorbed on a metal surface: The dipole-dipole interaction.* Physical Review B, 1981. **24**(12): p. 6954-6970.
2. Jakob, P. and Y.J. Chabal, *Chemical etching of vicinal Si(111): Dependence of the surface structure and the hydrogen termination on the pH of the etching solutions.* The Journal of Chemical Physics, 1991. **95**(4): p. 2897-2909.
3. Morin, M., et al., *Vibrational energy transfer on hydrogen-terminated vicinal Si(111) surfaces: Interadsorbate energy flow.* The Journal of Chemical Physics, 1992. **96**(8): p. 6203-6212.
4. Raghavachari, K., P. Jakob, and Y.J. Chabal, *Step relaxation and surface stress at H-terminated vicinal Si(111).* Chemical Physics Letters, 1993. **206**(1–4): p. 156-160.
5. Higashi, G.S., et al., *Ideal hydrogen termination of the Si (111) surface.* Applied Physics Letters, 1990. **56**(7): p. 656-658.
6. Dumas, P., Y.J. Chabal, and G.S. Higashi, *Coupling of an adsorbate vibration to a substrate surface phonon: H on Si(111).* Physical Review Letters, 1990. **65**(9): p. 1124-1127.
7. Hines, M.A., et al., *Raman studies of steric hindrance and surface relaxation of stepped H-terminated silicon surfaces.* Physical Review Letters, 1993. **71**(14): p. 2280-2283.
8. Guyot-Sionnest, P., et al., *Lifetime of an adsorbate-substrate vibration: H on Si(111).* Physical Review Letters, 1990. **64**(18): p. 2156-2159.
9. Guyot-Sionnest, P., P. Dumas, and Y.J. Chabal, *Lifetime of an adsorbate-substrate vibration measured by sum frequency generation : H on Si(111).* Journal of Electron Spectroscopy and Related Phenomena, 1990. **54–55**(0): p. 27-38.
10. Hines, M.A., et al., *Measuring the structure of etched silicon surfaces with Raman spectroscopy.* The Journal of Chemical Physics, 1994. **101**(9): p. 8055-8072.
11. Li, X.P., D. Vanderbilt, and R.D. King-Smith, *First-principles study of steps on the Si(111):H surface.* Physical Review B, 1994. **50**(7): p. 4637-4641.
12. Vanderbilt, D., *Soft self-consistent pseudopotentials in a generalized eigenvalue formalism.* Physical Review B, 1990. **41**(11): p. 7892-7895.
13. Zhu, X.D., H. Suhr, and Y.R. Shen, *Surface vibrational spectroscopy by infrared-visible sum frequency generation.* Physical Review B, 1987. **35**(6): p. 3047-3050.
14. Hochberg, L.R., Serruya, Mijail D., Friehs, Gerhard M., Mukand, Jon A., Saleh,

Maryam, Caplan, Abraham H., Branner, Almut, Chen, David, Penn, Richard D., Donoghue, John P., *Neuronal ensemble control of prosthetic devices by a human with tetraplegia.* Nature, 2006/07/13/print. **442**(7099): p. 164.

15. Vilan, A., et al., *Molecules on Si: Electronics with Chemistry.* Advanced Materials, 2010. **22**(2): p. 140-159.
16. Fenner, D.B., D.K. Biegelsen, and R.D. Bringans, *Silicon surface passivation by hydrogen termination: A comparative study of preparation methods.* Journal of Applied Physics, 1989. **66**(1): p. 419-424.
17. Schulze, G. and M. Henzler, *Adsorption of atomic hydrogen on clean cleaved silicon (111).* Surface Science, 1983. **124**(2–3): p. 336-350.
18. Owman, F. and P. Mårtensson, *STM study of structural defects on in situ prepared Si(111) 1 × 1-H surfaces.* Surface Science, 1995. **324**(2–3): p. 211-225.
19. Bratu, P. and U. Höfer, *Phonon-Assisted Sticking of Molecular Hydrogen on Si(111)-(7×7).* Physical Review Letters, 1995. **74**(9): p. 1625-1628.
20. Bratu, P., K.L. Kompa, and U. Höfer, *Optical second-harmonic investigations of H2 and D2 adsorption on Si (100) 2 × 1: the surface temperature dependence of the sticking coefficient.* Chemical Physics Letters, 1996. **251**(1–2): p. 1-7.
21. M.B. Raschke, U.H., *influence of steps and defets on the dissociative adsorption of molecular hydrogen on silicon surfaces.* Appl. Phys. B, 1999. **68**: p. 649.
22. Dumas, P., Y.J. Chabal, and P. Jakob, *Morphology of hydrogen-terminated Si(111) and Si(100) surfaces upon etching in HF and buffered-HF solutions.* Surface Science, 1992. **269–270**(0): p. 867-878.
23. Ignatescu, V. and J.M. Blakely, *Early morphological changes on Si(111) surfaces during UHV processing.* Journal of Vacuum Science & Technology A: Vacuum, Surfaces, and Films, 2007. **25**(5): p. 1449-1455.

Chapter 7: General conclusion

In this study, a pump-probe SFG microscopy and spectroscopy system was constructed for the first time. The SFG microscopy is the only method for nondestructive observation of hydrogen distribution on the silicon surfaces. Besides, the snapshots of ultrafast phenomena of H-Si species were obtained. It contributes to surface science as a new analysis systems, and opens new opportunity for directly observing two dimensional images of particular adsorbate species

By using this system, dynamics of H-Si species on the flat H-Si(111)1x1 surfaces were investigated by observing the time-resolved *ppp*-SFG spectra and microscopic images in a UHV chamber. The SFG intensity images showed consistent results with the time resolved SFG spectroscopy. The power of the pump visible light at 532 nm was 120 μJ/pulse and the power density on the sample surface was 0.12 J/cm^2.pulse. Before the pump light irradiation, the symmetric peak attributed to the Si-H stretching mode appeared. After visible pump light irradiation non-resonant SFG signal increased, and then decreased with the life time of ~1 ns. This reduction was not due to the rise of the surface temperature or effect of e-h plasma. The candidate origin of this change of the non-resonant SFG signal is suggested to be the excitation and relaxation of e-h pairs after the pump light irradiation. From 0 to 66 ps, the Si-H peak rapidly decreased and after that gradually recovered. At 930 ps after pump light irradiation, the Si-H peak had a remarkably asymmetric lineshape. Through this demonstration, the pump-probe SFG microscope was judged to work properly.

Also the reduction of hydrogen coverage of the H-Si(111)1x1 surface due to high surface temperatures was observed for the first time. I obtained isothermal desorption spectra of the H-Si(111) 1×1 surface at temperatures of ~711, 732, 752 and

771 K by probing directly the vibrationally resonant optical SFG spectra. The desorption order of hydrogen was consistent with the second order scheme. I also discovered a shift of Si-H vibrational peak towards the low-frequency side experimentally as the desorption proceeds. This is considered to be a big finding. The dipole-dipole coupling among the H-Si bonds could be considered during the hydrogen desorption process. I have calculated modulation of the Si-H vibrational mode on a Si(111) 1×1 surface by a partial absence of Si-H bonds using CPA method, and made a comparison between modulations in the experimental and theoretical SFG spectra of the surface. As the first time of discovery, a theoretical peak shift reproduced the experiment quantitatively, and thus the peak shift was due to the modulation of average polarizability of the Si-H oscillators via dipole coupling. On the other hand, inhomogeneous broadenings of the theoretical peaks in the SFG spectra at lower coverages were much larger than those of the calculated peaks. Understanding the effect of surface temperature and excited e-h pairs on behavior of H-Si bonds is very important for growth of organic and inorganic thin film which is utilized for silicon based devices.

I also investigated the hydrogen desorption from regular step H-Si(111) surfaces with 9.5^{o} miscut toward $[\bar{1}\bar{1}2]$ direction. The regular Si(111) surface was terminated by hydrogen by dosing hydrogen molecules in the UHV chamber. The upstair SFG spectra with *ppp* and *ssp* polarization combination were taken. In both the cases, the terrace mode A (2082cm^{-1}), and step modes C_1 (2094 cm^{-1}) peaks were clearly observed, while C_2 (2101 cm^{-1}) and C_3 (2134 cm^{-1}) were not. Considering that only one group except me has observed this kind of step SFG signal, the result is a very important contribution in this field. The A mode was readily attributed to the in-phase

terrace vibration of the monohydride. The step C_2, C_3 modes could not be detected on the step bunched 9.5° miscut surface because of the decrease in the step mode intensities (step bunches appeared when the Si surface was flashed at 1200 °C). On the other hand, the downstair SFG spectra with *ppp* and *ssp* polarization combination were also observed. The terrace mode A appeared in all spectra while the step C_1 mode appeared in *ssp* only.

The regular step H-Si(111)1x1 surface with miscut toward $[\bar{1}\bar{1}2]$ direction was heated at several high temperatures, and time dependence of the upstair SFG spectra with *ppp* and *ssp* polarization combination were taken. The peak intensity of both terrace and step modes was reduced when the heating time was increased, but the step mode reduction was faster. The reduction was best fit to the 2nd order of hydrogen desorption. The step mode C_1 was shifted by ~2 cm^{-1}. I suggest that it may be related to the dipole-dipole interaction among the H-Si species. However, the theoretical calculation is required to clarify this point. Some phenomena shown in SFG spectra are not understood well. Further experimental and theoretical studies should be done in the future. This study about hydrogen desorption on the step Si surface contributes to fundamental science and opens a new research topic.

Summarizing all the above results, I can confidently say that I have developed a new surface observation tool, and thereby discovered some important fundamental phenomena on the flat and stepped H-Si(111) surfaces.

Chapter 8: Future work

In this report, the pump-probe SFG microscopy was successfully constructed. The time resolved SFG intensity images of the flat H-Si(111)1x1 were clearly observable which indicate that the system had correct operation. However, the resolution of microscopy system now is ~5 μm, so that it is difficult to observe the hydrogen diffusion of ~2 μm. I will try to improve this resolution.

According to the time resolved SFG intensity images of the flat H-Si(111)1x1 surface after visible pump light irradiation, the areas of modulated SFG signals is ~two times larger than the pump spot size. This is not due to the carrier diffusion or surface temperature. Analysis of these images will be carried out.

The second problem is related to isothermal hydrogen desorption from the flat H-Si(111)1x1 surface. The surface was heated at 711 K with each few tens of seconds, then SFG spectra were observed. The hydrogen coverage was reduced as a function of the heating time. The vibrational peak of H-Si bond was shifted to lower frequency and it can be understood via dipole coupling effect. However, the width broadening of vibrational peaks as a function of hydrogen coverage is still not well indentified. Theoretical calculation will be considered in the future.

As I shown in the chapter 6, SFG spectra of the step H-Si(111) surface with 9.45^{o} miscut toward $[\bar{1}\bar{1}2]$ direction present several interesting phenomena. The theoretical calculation about the titled angle of Si-H(1) will be carried out in order to make clear the appearance of C_1 mode in SFG spectra. The ratio of peak intensity between A and C_1 modes will be considered. I suggest that there is energy transfer from A to C_1 mode via dipole coupling. If this suggestion is reasonable, the peak shift of A and C_1 due to hydrogen desorption also can be understood.

Appendix A: The polarization dependence of SFG spectrum on the Si(111) 9.45° miscut toward $[\bar{1}\bar{1}2]$ direction

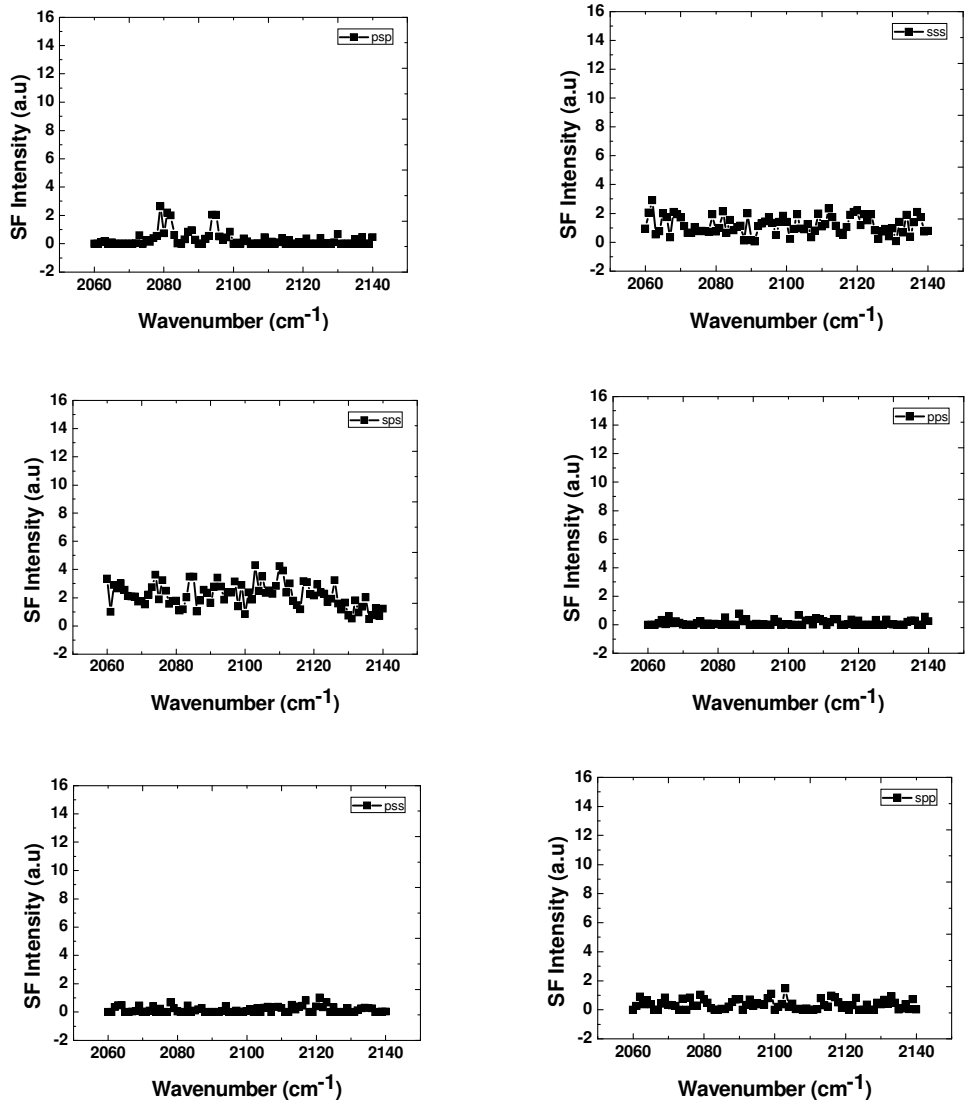

Appendix B: Hydrogen diffusion on the Si(111)1x1 surface

In order to observe the inhomogeneous distribution of hydrogen atoms caused by the existence of rough areas, I observed SFG intensity images of the H-Si(111) surface as a function of heating temperatures from 592 to 752 K, as shown in fig. B. The white dots represent SFG photons. I observed a gradual decrease in SFG intensity

from 592 K to 752 K. An especially dramatic reduction of the SFG photon density was observed between 666 K (fig. B(c)) and 728 K (fig. B(d)); finally, the observed number of photons at 752 K in fig. B(e) was close to the non-resonant background shown in fig. B(f). I interpret the reduction of the SFG signal as simply the result of a deficiency in hydrogen atoms, taking account of the fact that the surface still has a 1x1 structure at temperatures lower than 770 K [1], and thus the molecular orientation has not changed.

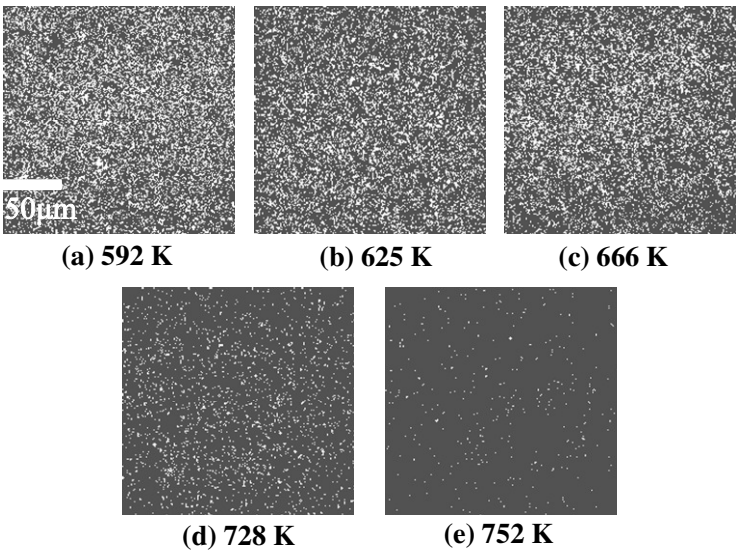

Fig.B: SF intensity images of the H/Si(111) surface after heating in 10s with several temperatures.

Here, it is important to note that the number of SFG photons has been reduced homogeneously at 728 K in fig. B(d). Fourier transform analysis of this image also supports that there are no significant structures. These results suggest that there was no island structure [2] and the hydrogen atoms diffused homogeneously with my microscope's estimated spatial resolution of ~ 5μm. If the size of the rough areas observed by RHEPD has a micron scale, the SFG images should be inhomogeneous. These results, therefore, indicate that the size of the rough areas is at least smaller than 5

μm.

It has been reported that the diffusivity of hydrogen atoms on a Si(111)7 × 7 surface is 5 × 10−14 cm2/s at 740 K [3, 4], which means that a hydrogen atom moves ~20 nm per 10 seconds during heating at 740 K. Moreover, the diffusion barrier of an unreconstructed 1 × 1 surface may be higher than that of a 7 × 7 surface, and thus the diffusivity of the 1 × 1 surface can be presumed to be slower. Thus, the scale of hydrogen diffusion is under the resolution limit of present microscopes. Future development of a microscope with better resolution will enable us to directly observe the change of hydrogen distribution due to the diffusion of hydrogen atoms.

Appendix C:

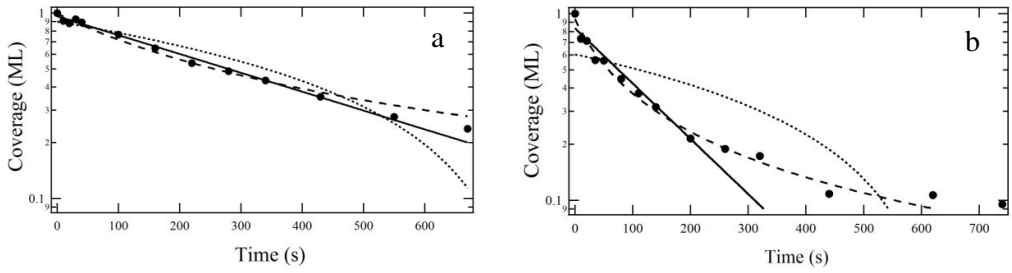

The isothermal hydrogen desorption from the H/Si(111) surface with the surface temperature (a) 711 and (b) 732 K. The points are experimental results. In this case, I assume that the hydrogen coverage N can be estimated from the intensity of SFG peaks with homogeneous width and Lorentzian shape as:

$$N \sim \chi_v \propto \sqrt{I_{SFG}} \times \gamma$$

The dotted curve, solid line, and dashed curve are the zeroth, first, and second order of hydrogen desorption, respectively.

Appendix D [5-7]

Principle of Ultraviolet photoelectron spectroscopy

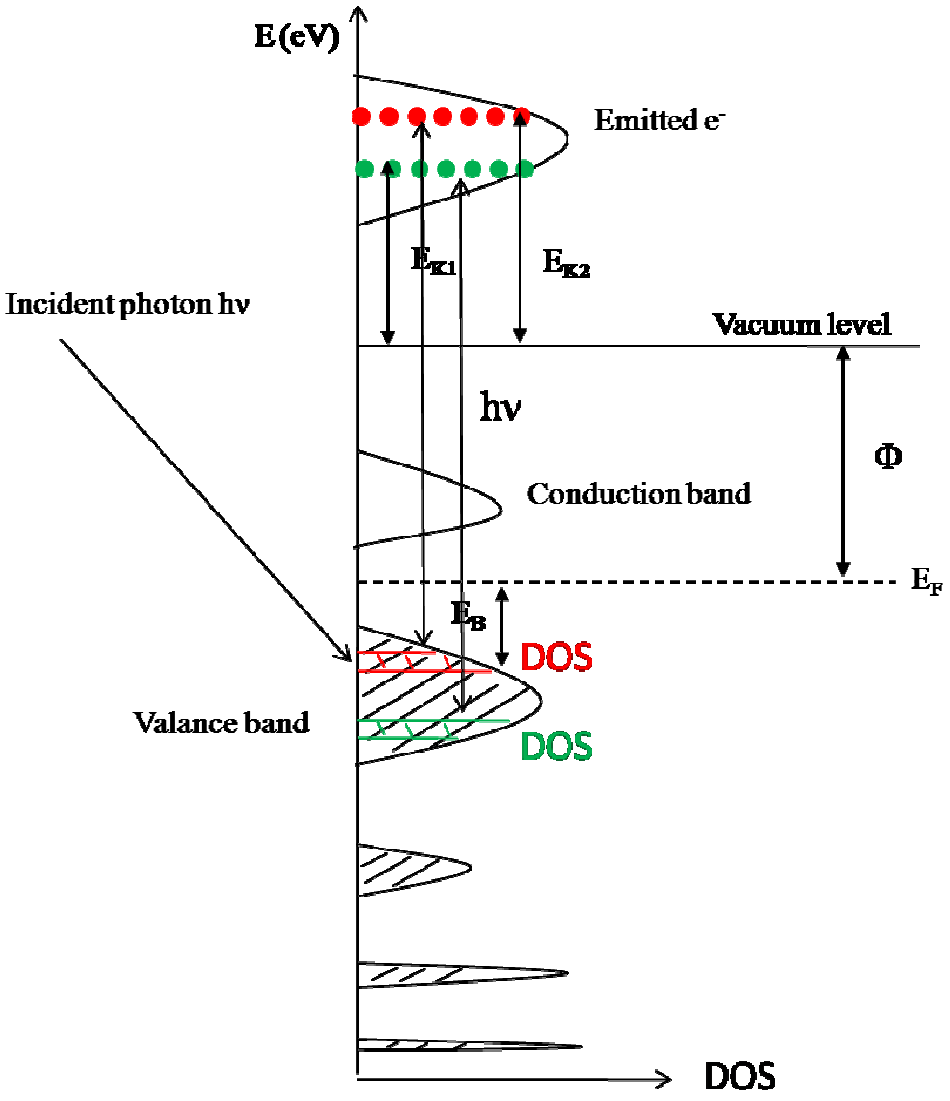

Fig. D1: Energy diagram of a photoemission process in photoelectron spectroscopy

Ultraviolet (UV) photoelectron spectroscopy (PES) is used to study information about occupied electronic states (density of state DOS) of valance-band. When a UV photon comes to the surface, it interacts with atoms or molecules. UV photons with specific energy $\hbar\omega$ are created in a continuous discharge source (typically He) by applying a high voltage. Usually, the photon energy of a typical line (He II) with 40.8 eV is used. This photon energy make the electrons from the valance band go out from the surface

(to the vacuum level) with the kinetic energy E_{kin} and wave vector k^{ex}:

$$E_{kin} = \frac{\hbar^2 (k^{ex})^2}{2m} \qquad (1)$$

here k^{ex} is defined by the emission direction described by the angles ϕ and θ (fig. D2(a)).

From fig. D1, we have the relation:

$E_{kin} = \hbar\omega - \Phi - E_B$ (2)

In semiconductor, the work function depends on the type of doping.

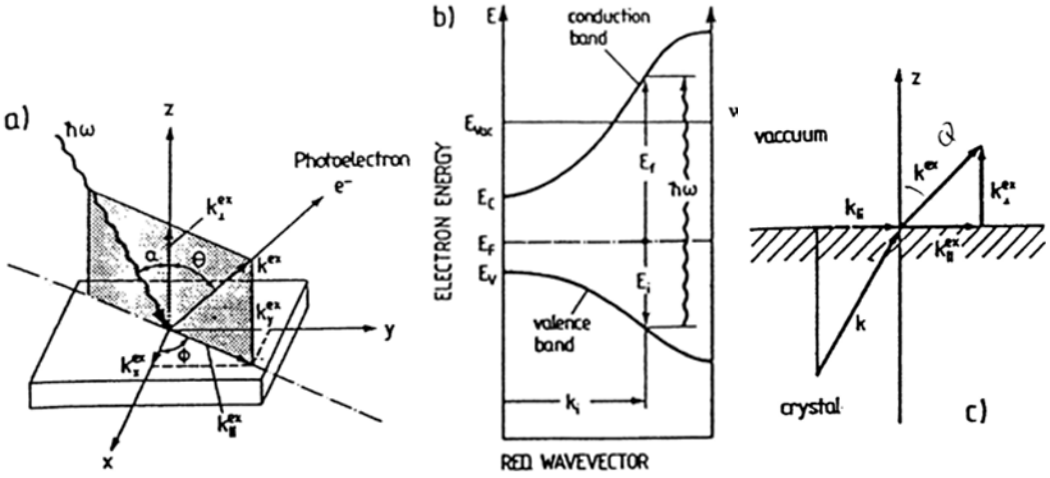

Fig. D2: Description of a photoemission experiment. (a) Definition of the angles and wave vectores of the incident photon (Ħω) and emitted electron (e^-). (b) Representation of the photoexcitation process in the electronic band scheme E(k) of a semiconductor. Only direct transitions with $k_i \sim k_f$ are taken into account. The energies of the initial state (E_i) and final state (E_f) are defined with respect to to the Fermi level E_F. (c) Conservation of the wave vector component $k_{//}$(parallel to the surface) upon transmission of the emitted electron through the surface. (Surfaces and Interfaces of Solid Materials – Third Edition, H. Luth, Springer)

The process of an electron receiving photon energy and remove to vacuum is separated into three parts (three-step model):

i, Optical excitation of an electron from an initial into a final electron state within the crystal (fig. D2(b)).

ii, propagation of the excited electron to the surface.

iii, Emission of the electron from the solid into the vacuum (fig. D2(c)).

The transition probability for optical excitation of an electron in the first step:

$$w_{fi} = \frac{2\pi}{\hbar}|\langle f,k|\mathcal{H}|i,k\rangle|^2 \delta(E_f(k) - E_i(k) - \hbar\omega)$$
$$= (2\pi/\hbar) m_{fi} \delta(E_f - E_i - \hbar\omega) . \quad (3)$$

δ-function in this equation describes energy conservation in the excitation of an electron from a state $E_i(k)$ into a state $E_f(k)$ of electron band structure (fig. D2(b).)

In the step 2, the transition happened between two states with nearly unchanged **k.** The perturbation can be described by dipole approximation:

$$\mathcal{H} = \frac{e}{2m}(\mathbf{A}\cdot\mathbf{p} + \mathbf{p}\cdot\mathbf{A}) \simeq \frac{e}{m}\mathbf{A}\cdot\mathbf{p} \quad (4)$$

The perturbation operator κ is given by the momentum operator p and the vector potential A of the incident electromagnetic wave. Only electrons with $k_\perp > 0$ can go out of surface to be detected, for selected energy E by the analyzer the intensity is:

$$I^{int}(E,\hbar\omega,\mathbf{k}) \propto \sum_{f,i} m_{fi} f(E_i) \delta(E_f(\mathbf{k}) - E_i(\mathbf{k}) - \hbar\omega) \delta(E - E_f(\mathbf{k})) \quad (5)$$

here m_{fi} is the matrix element for the transition between two states and f(Ei) is density of states.

These electrons, however, in the second step will undergo various scattering processes including inelastic ones, which make them lose energy and also gives secondary electrons. The mean free path length D can be used to describe the transport probability λ:

$$D(E,k) \propto \lambda(E,k) \quad (6)$$

λ for UV light is very small between 5 to 20 Å

In the step three, transmission of the photoexcited electron through the surface can be considered as the scattering of a Bloch electron wave (wavefunction places in a periodic potential) from the surface-atom potential with translational symmetry parallel, but not normal to the surface. In any case, because of the 2D translational symmetry, the transmission of the electron through the surface into the vacuum requires conservation of its wave-vector component parallel to the surface (fig. D2(c)):

$$\mathbf{k}_{\parallel}^{ex} = \mathbf{k}_{\parallel} + \mathbf{G}_{\parallel} \quad (7)$$

There are also energy conservation:

$$E_{kin} = \frac{\hbar^2 k^{ex^2}}{2m} = \frac{\hbar^2}{2m}(k_\perp^{ex^2} + k_{\parallel}^{ex^2}) = E_f - E_{vac} \quad (8)$$

From (7) and (8) we have:

$$k_{\perp}^{ex^2} = \frac{2m}{\hbar^2} E_{kin} - (k_{\parallel} + G_{\parallel})^2 \quad (9)$$

According to (7), transmission through the surface, the third step can be described formally by the transmission rate:

$T(E,k)\,\delta\,(k_{//}+G_{//}-k_{\parallel}^{ex})$ (10)

In the simplest and rather naïve approach one might assume that T(E,k) is a constant R≤ 1 with:

$$T(E,k)=0 \text{ for } k_{\perp}^{ex^2} = \frac{2m}{\hbar^2}(E_f - E_{vac}) - (k_{\parallel} + G_{\parallel})^2 < 0 \quad (11)$$

$$T(E,k)=R \text{ for } k_{\perp}^{ex^2} = \frac{2m}{\hbar^2}(E_f - E_{vac}) - (k_{\parallel} + G_{\parallel})^2 > 0 \quad (12)$$

(11) and (12) of T(E,k) takes into account that only electrons with the positive wave-vector component $k_{\perp}^{ex}$ can be observed in the photoemission experiment; all others are unable to reach the vacuum side of the crystal surface and are internally reflected since their kinetic energy is not sufficient to surmount the surface barrier.

Finally, from equations (3, 5, 6, 10, 11, 12) we can get the formula for the observable external emission current in the three step model:

$$I^{ex}(E,\hbar\omega, k_{\parallel}^{ex}) = I^{int}(E,\hbar\omega,k)D(E,k)T(E,k)\ \delta\,(k_{//}+G_{//}-k_{\parallel}^{ex})$$

$$\approx \sum_{fi} m_{fi} f\big(E_i(k)\big)\delta(E_f(k) - E_i(k) - \hbar\omega)\delta\big(E - E_f(k)\big) \times \delta\,(k_{//} + G_{//} - k_{\parallel}^{ex})\, D(E,k)T(E,k)$$

Where $f\big(E_i(k)\big)$ is density of state of the internal electron.

For example, figure D2 shows UPS valance band spectra of a Si(111)-H surface taken as a function of annealing temperature. Let's see the bottom curve of the panel corresponding to the RT clean Si(111)–H surface. It is characterized by two main features at 5.68 eV and 7.7 eV binding energy. They are assigned to bulk backbond (BB) and Si-H state (H), respectively.

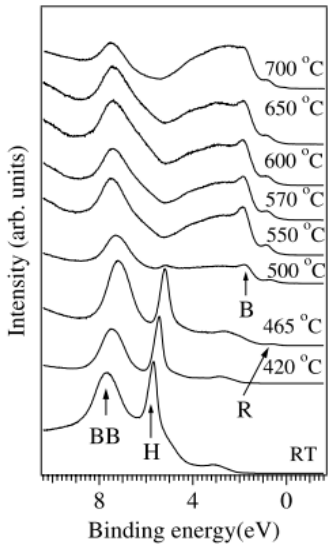

Fig. D2: UPS valance band spectra of a Si(111)-H surface taken as a function of annealing temperature. (V. D. Renzi et al., Surf. Sci. ***497****, 247 (2002).)*

Appendix E: Low electron energy diffraction (LEED)

LEED is a surface analysis technique for the determination of the surface structure of crystalline materials by an electron beam with low energy of 20–200 eV. It may be used in one of two ways. One is the LEED pattern which shows the image of the surface reciprocal net when viewed along the surface normal at a great distance from the crystal. The other way is that the intensities of the various diffracted beams recorded as a function of the incident electron beam energy to generate so-called I-V curves. By comparison with theoretical curves, it may provide accurate information on atomic positions.

In this appendix, let's consider the way of observing LEED patterns. Figure E1 illustrates a typical arrangement of a LEED system. Electrons come from the electron gun and some fraction backscatter towards a hemispherical grid G_1. A retarding potential difference between G_1 and a second grid G_2 allows only the elastically backscattered electrons to reach G_2. A fluorescent screen is held at a large positive potential so that the electrons accelerate and excite the screen phosphors upon impact. The diffraction spot pattern can be seen from this screen.

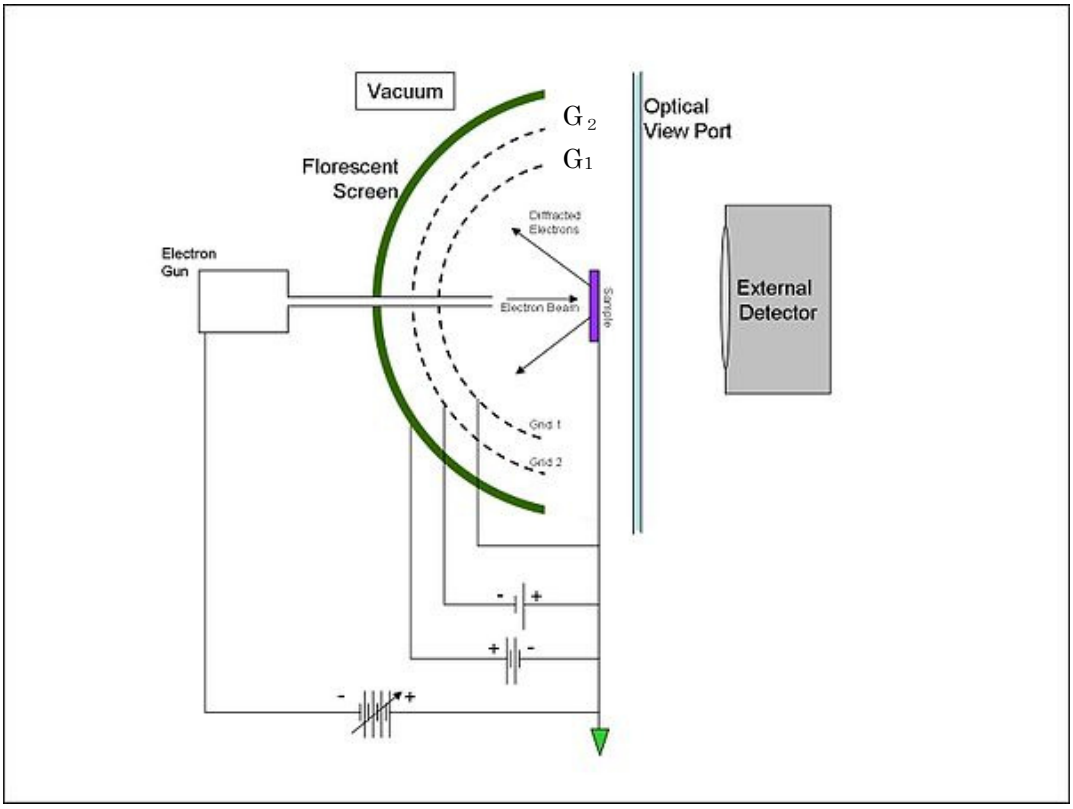

Fig. E1: A display-type LEED system.

In principle, electron diffraction in LEED is similar to that in X-ray. However, the atomic scattering of electrons at LEED energies is in reality always a multiple-scattering process within the individual atom. First, let's see the X-ray diffraction:

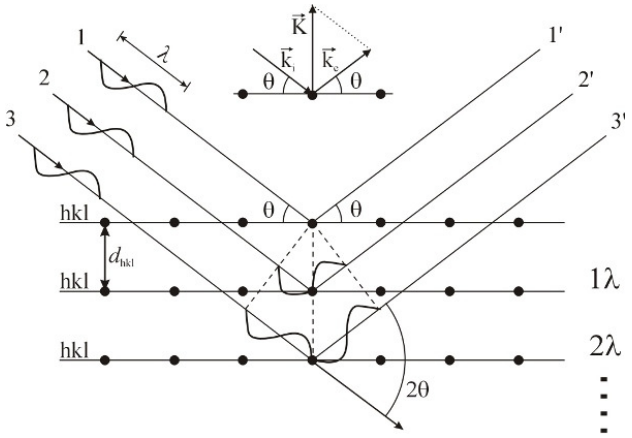

Fig.E2: X-ray diffraction model

The incoming beam (coming from upper left) causes each scaterer to re-radiate a small portion of its intensity as a spherical wave. If scatterers are arranged symmetrically with a separation *d*, these spherical waves will be in sync (add constructively) only in directions where their path-length difference $2d\sin\theta$ equals an integer multiple of the wavelength λ. In that case, part of the incoming beam is deflected by an angle 2θ, producing a *reflection* spot in the diffraction pattern. We have Bragg's law for the conditions for constructive interference:

$$n\lambda = 2d_{hkl}\sin(\theta) \quad (13)$$

Here *d* is the spacing between diffracting planes, θ is the incident angle, *n* is any integer, and λ is the wavelength of the beam. Alternatively, one defines a scattering vector $\mathbf{K} = \mathbf{k_e} - \mathbf{k_i}$ as the difference between the wave vector $\mathbf{k_e}$ of the scattered wave, and the wave vector $\mathbf{k_i}$ of the incident X-ray, as shown in the inset of Fig. E2.

Let's consider a electron beam impinging on the surface. The beam is represented by a plane wave which is described by

$$A_i = A_o \exp(i\vec{k}_i . \vec{r}) \quad (14)$$

Where A_i is the amplitude of the incident wave, A_o is a constant, $\vec{k}_i$ is the incident wave vector, and $\vec{r}$ is a space vector. If multiple scattering is neglected, the amplitude of a diffracted beam is presented by

$$A_s = A_o[\sum_n \alpha f_n(\vec{s})\exp(i\vec{s}.\vec{r}_n)]\exp(i\vec{k}_e.\vec{r}) \quad (15)$$

here $f_n(\vec{s})$ is the atomic scattering factor for the nth atom located at position $\vec{r}_n$, $\vec{s} = \vec{k}_e - \vec{k}_i$ is the momentum transfer.

Now we assume that $f_n \exp(i\vec{s}.\vec{r}_n)$ that appeared in eq.(15) is generally known as the structure factor S in diffraction theory. For three-dimensional cases, the atomic positions $\vec{r}_n$ is represented by

$$\vec{r}_n = \vec{R}_p + m_1\vec{a} + m_2\vec{b} + m_3\vec{c}$$

$(\vec{a}, \vec{b}, \vec{c})$ is the basis vectors of the lattice; m_1, m_2, m_3 are intergers; and $\vec{R}_p$ (p=1,2,..N) are the locations of the atoms within one unit cell. Then, in 3D case, the structure factor is given by

$$S^{(3)} = \left[\sum_p f_p \exp(i\vec{s}.\vec{R}_p)\right]\left\{\sum_{m_1 m_2 m_3} \exp\left[i\vec{s}(m_1\vec{a} + m_2\vec{b} + m_3\vec{c})\right]\right\} \quad (16)$$

The sum over lattice vectors is proportional to the Dirac delta function $\delta\left(\vec{s}-\vec{G}^{(3)}\right)$, where $\vec{G}^{(3)}$ is any of the 3D reciprocal lattice vectors of the given lattice $(\vec{a},\vec{b},\vec{c})$:

$$\vec{G}_{hkl}=h\vec{a}^{*}+k\vec{b}^{*}+l\vec{c}^{*} \quad (17)$$

With

$$\vec{a}^{*}=\frac{2\pi b\times c}{a.(b\times c)},\qquad \vec{b}^{*}=\frac{2\pi c\times a}{b.(c\times a)},\qquad \vec{c}^{*}=\frac{2\pi a\times b}{c.(a\times b)}$$

And (h,k,l) is a set of integers. The delta functions define the Bragg conditions for the existence of diffracted beams: $\vec{s}=\vec{G}_{hkl}=h\vec{a}^{*}+k\vec{b}^{*}+l\vec{c}^{*}$ (18)

In the surface lattice case, the periodicity of the diffracting lattice is drawn in fig. E3. We assume the distance among three atomic layers in the surface normal direction is very far from each other. Then, in the reciprocal lattice, we get the reciprocal lattice rods containing several reciprocal lattice points.

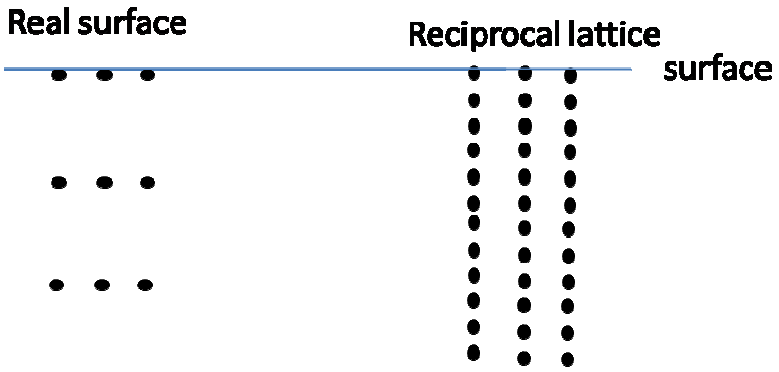

Fig. E3: Formation of the reciprocal lattice rods from surface atomic layers.

For an incident electron with wave vector

$$k_0=2\pi/\lambda_0$$

is used interchangeably with momentum p due to De Broglie relation $p_0=\hbar k_0$.

$$\lambda_0\sim\frac{2\pi\hbar}{\sqrt{2mE}}\sim\sqrt{\frac{150}{E(eV)}}\ (\text{Å}) \quad (19)$$

E is the energy of the incident electron beam. From these two equations, the relation between k_0 and λ_0 can be described:

$$k_0\sim 2\pi\sqrt{\frac{E(eV)}{150}}\ (\text{Å}^{-1}) \quad (20)$$

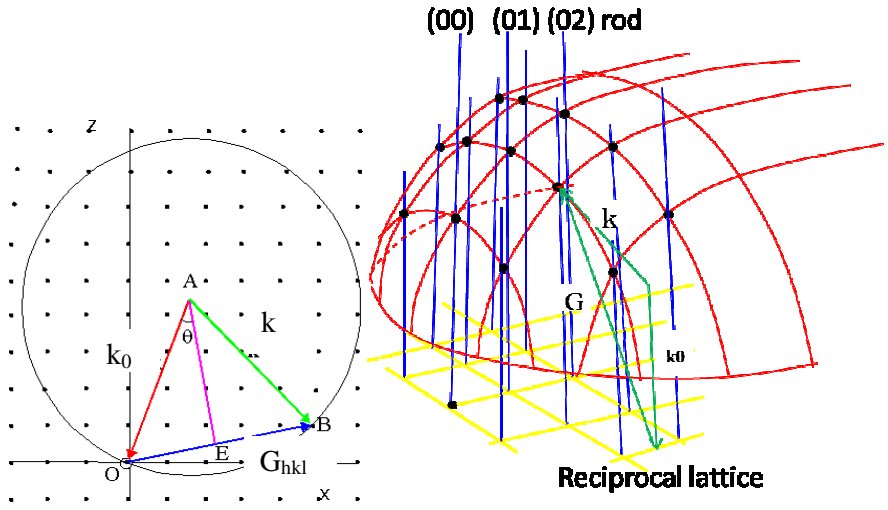

Fig. E4: reciprocal lattice diffraction in 3D.

When the incident beam with wave vector k_0 comes, the vector k_0 is fixed with its top at one of the reciprocal lattice. The condition for constructive interference and hence diffraction of scattered electron waves is given by the Laue condition: (see fig. E4)

$$\vec{k} - \vec{k}_0 = \vec{G}_{hkl}$$

Each point (*hkl*) in the reciprocal lattice corresponds to a set of lattice planes (*hkl*) in the real space lattice. Since the mean free path of low energy electrons in a crystal is only a few angstroms, only the first few atomic layers contribute to the diffraction pattern. This means that there are no diffraction conditions in the depth into the sample surface. As a consequence the reciprocal lattice of a surface is a 2D lattice with rods extending perpendicular from each lattice point (see fig.E4). Therefore in the case of diffraction from a surface, equation (18) reduces to the 2D form:

$$\vec{k}^{\parallel} - \vec{k}_0^{\parallel} = \vec{G}_{hk} = h\vec{a}^{**} + k\vec{b}^{**} \quad (21)$$

Where $\vec{a}^{**}$ and $\vec{b}^{**}$ are the primitive translation vectors of the 2D reciprocal lattice of the surface, and $\vec{k}^{\parallel}, \vec{k}_0^{\parallel}$ denote the component of the incident and reflected wave vector parallel to the sample surface. $\vec{a}^{**}$ and $\vec{b}^{**}$ are related to the real space surface lattice in the following way:

$$\vec{a}^{**} = \frac{2\pi b \times \hat{n}}{|a \times b|}, \quad \vec{b}^{**} = \frac{2\pi \hat{n} \times a}{|a \times b|} \qquad (22)$$

The Laue condition equation (21) can readily be visualized using the Ewald's sphere construction. Figure E5 shows a simple illustration of this principle: The wave vector k_0 of the incident electron beam is drawn such that it terminates at a reciprocal lattice

point. Then, from the origin of wave vector k_0, the Ewald's sphere is drawn with radius k_0 (because only elastic scattering is considered).

In the analysis, every wave vector centered at the origin and terminating at an intersection between a rod and the sphere will satisfy the Laue condition and thus represent an allowed diffracted beam.

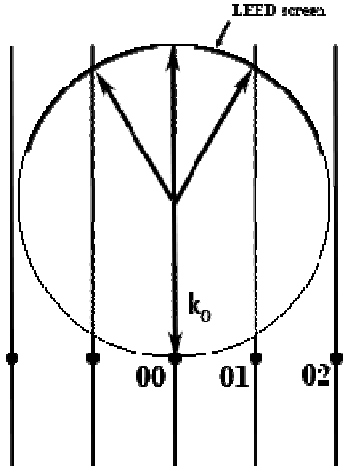

Fig. E5: Ewald's sphere construction for the case of normal incidence of the primary electron beam. The diffracted beams are indexed according to the values of h and k.

When energy of the electron beam is increased, the value of vector k_0 is increased, too (eq.20). This results in enlargement of the Ewald sphere (fig. E5) and the extra number of spots will be seen in the LEED pattern of a Si(111)1x1 surface (fig. E6). Simultaneously, the direction of the certain G vector is changed narrowly (comparing the dashed arrow and vector G' in fig. E7). This change of vector G makes 6 spots in fig. E6(a) move to the center and extra spots of lattice are visible on the screen.

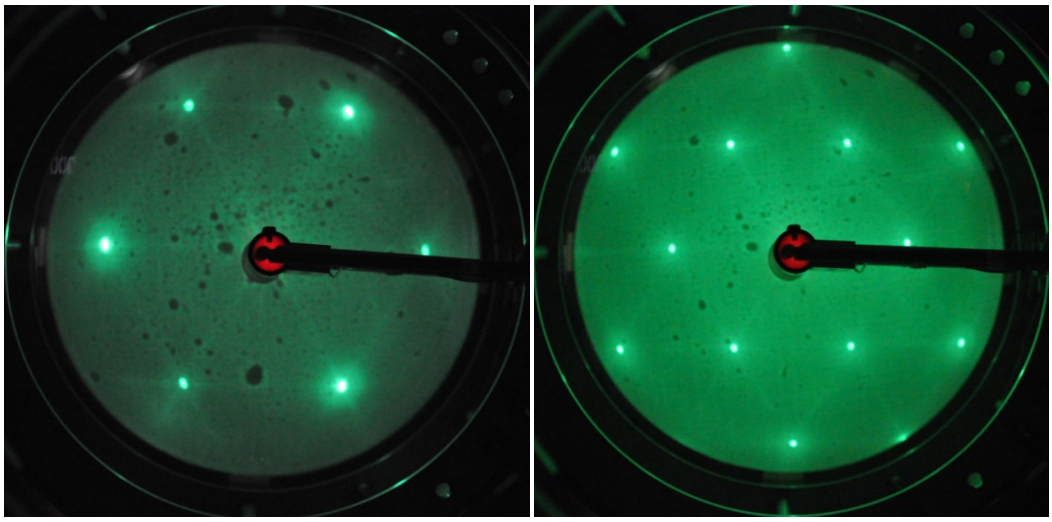

(a) 45 eV (b) 75 eV

Fig. E6: LEED patterns of the Si(111)1x1 surface.

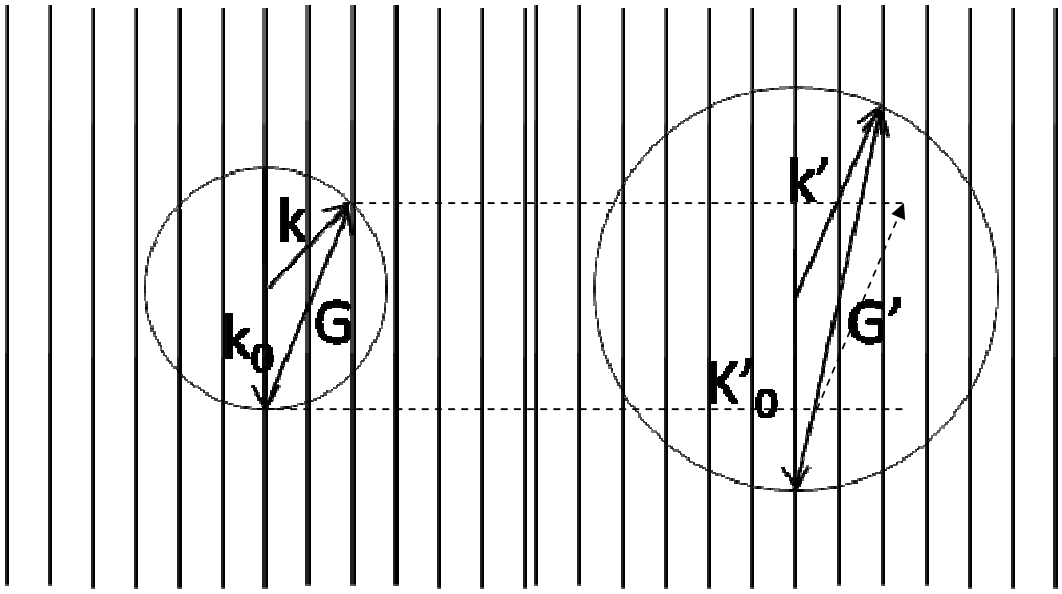

Fig. E7: Ewald spheres with different k vectors.

References

1. De Renzi, V., R. Biagi, and U. del Pennino, *Study of the transition from the ideal Si(1 1 1)–H(1×1) surface to the (7×7) reconstruction by HREELS, UPS and LEED.* Surface Science, 2002. **497**(1–3): p. 247-253.
2. Kawasuso, A., et al., *Rocking curves of reflection high-energy positron diffraction from hydrogen-terminated Si(111) surfaces.* Physical Review B, 2000. **61**(3): p. 2102-2106.
3. Reider, G.A., U. Höfer, and T.F. Heinz, *Surface diffusion of hydrogen on Si(111)7×7.* Physical Review Letters, 1991. **66**(15): p. 1994-1997.
4. Lo, R.-L., et al., *Diffusion of Single Hydrogen Atoms on Si(111)-(7 × 7) Surfaces.* Physical Review Letters, 1998. **80**(25): p. 5584-5587.
5. Luth, H., *Surfaces and Interfaces of Solid Materials* Springer. **Third Edition**.
6. Hufner, S., *Photoelectron spectroscopy. Principles and applications.* Springer. **Third edition**.
7. Wooddruff; and Delchar, *Modern techniques of Surface Science.* Cambridge. **Second edition**.

Publications:

1. **Khuat Thi Thu Hien**, Yoshihiro Miyauchi, Goro Mizutani, “Pump-probe time-resolved sum frequency spectroscopy of the H-Si(111)1x1 surface”, *e-J. Surf. Sci. Nanotech.* **8** (2010) 89-92.

2. **Khuat Thi Thu Hien**, Yoshihiro Miyauchi, Goro Mizutani, "Construction of a pump-probe system for observing time resolved sum frequency images". *Surface and Interface Analysis* **42** (2010), 1671-1674.

3. **Khuat Thi Thu Hien**, Yoshihiro Miyauchi, Masahiro Kikuchi, Goro Mizutani, "Hydrogen desorption from a Si(111)1×1 surface studied by Sum Frequency Generation Spectroscopy and Microscopy", *Surface and Interface Analysis*, Wiley, **44** (6) (2011), 662-665.

4. **Khuat Thi Thu Hien**, Yoshihiro Miyauchi, Goro Mizutani, "Sum frequency generation on a regular step H-Si(111) surface", *in preparation.*

5. **Khuat Thi Thu Hien**, Yoshihiro Miyauchi, Md Abdus Sattar, Goro Mizutani, "Hydrogen desorption on a regular step H-Si(111) surface observed by sum frequency spectroscopy", *in preparation.*

6. Yoshihiro Miyauchi, **Hien Khuat**, Goro Mizutani, “Si-H vibrational mode on a H-Si(111) 1x1 surface with hydrogen deficiency”, Surface Science **614** (2013), 24-29.

Conference Proceedings

1. Yoshihiro Miyauchi, **Khuat Hien Thi Thu**, Goro Mizutani, “Sum Frequency intensity images of the H-Si(111) surface during electron-hole pair excitation and relaxation”, *Conference on Dynamics At Surfaces,* August 9-14, 2009. USA.

2. **Khuat Hien Thi Thu**, Yoshihiro Miyauchi, Goro Mizutani, "Construction of pump-probe time resolved optical sum frequency microscopy”, *The physical Society of Japan 2009 Autumn Meeting* (September 2009), Japan

3. **Khuat Thi Thu Hien**, Yoshihiro Miyauchi, Goro Mizutani, "Construction of a pump-probe system for observing time resolved sum frequency images", *Proceeding of 7th International Symposium on Atomic Level Characterizations for New Materials and Devices,* 2009. Hawaii, USA

4. **Khuat Thi Thu Hien**, Yoshihiro Miyauchi, Goro Mizutani, " Optical sum frequency intensity images of a vicinal H-Si(111)1x1 surface", *7th International Symposium on Advanced Materials in Asia-Pacific and JAIST International Symposium on Nano Technology 2010,* Ishikawa, Japan.

5. **Khuat Thi Thu Hien**, Yoshihiro Miyauchi, Masahiro Kikuchi, Goro Mizutani, “Hydrogen desorption from a flat Si(111)1x1 surface studied by Sum Frequency Microscopy”, *International Symposium on Atomic Level Characterizations for New Materials and Devices,* 2011. Seoul, Korea.